UNIVERSIDAD DE CHILE
FACULTAD DE CIENCIAS FÍSICAS Y MATEMÁTICAS
DEPARTAMENTO DE GEOLOGÍA

GEOCHEMICAL, MINERALOGICAL AND MICROBIAL MODELLING OF AN IOCG TAILINGS DEPOSIT (EL BUITRE, CHILE): IMPLICATIONS FOR ENVIRONMENTAL SAFETY AND ECONOMIC POTENTIAL

TESIS PARA OPTAR AL GRADO DE DOCTORA EN CIENCIAS MENCIÓN GEOLOGIA

ERIKA YELISBETH GONZÁLEZ DÍAZ

PROFESOR GUÍA:

DR. BRIAN KEITH TOWNLEY CALLEJAS

PROFESOR CO-GUÍA:

DR. MANUEL ANTONIO CARABALLO MONJE

MIEMBROS DE LA COMISIÓN:

DRA. KATJA DECKART

DR. JULIO CESAR CASTILLOS HERNÁNDEZ

SANTIAGO DE CHILE

2022

RESUMEN DE LA TESIS PARA OPTAR AL

GRADO DE: Doctora en Ciencias, Mención Geología

POR: Erika Yelisbeth González Díaz

FECHA: 2022

PROF. GUÍA: Brian Keith Townley Callejas

PROF. CO-GUÍA: Manuel Antonio Caraballo Monje

MODELAMIENTO GEOQUÍMICO, MINERALÓGICO Y MICROBIANO DE UN DEPÓSITO DE RELAVES IOCG (EL BUITRE, CHILE): IMPLICACIONES PARA LA SEGURIDAD AMBIENTAL Y SU POTENCIAL ECONÓMICO.

Los tranques de relaves se han convertido en un foco de interés como posibles fuentes alternativas de materias primas para mitigar parcialmente la escasez de elementos críticos estratégicos impuesta por la creciente demanda de aplicaciones tecnológicas y energías verdes. Además, se han convertido en un grave problema ambiental para los ecosistemas que rodean estos depósitos artificiales. Este trabajo reporta los resultados de un estudio de caracterización mineral, geoquímica, microbiana y modelamiento geoestadístico y conceptual de un yacimiento de Óxidos de Hierro-Cobre-Oro con pH neutro, en un clima árido. Se realizó un total de 28 sondajes con perforación sónica, que permitieron recolectar 755 muestras. De la totalidad de las muestras, se seleccionaron 98 para la caracterización de las comunidades microbianas. El tranque de relaves El Buitre presenta una mineralogía primaria caracterizada por un bajo contenido de pirita y calcopirita y un contenido relativamente alto de magnetita y hematita. La ganga está dominada por cuarzo, clorita, feldespato alcalino, plagioclasa y calcita. Las condiciones climáticas limitan la disponibilidad de agua y restringen la movilidad de los metales en el agua intersticial a pH neutro, inhibiendo el desarrollo de frentes de oxidación extensos y zonas de enriquecimiento mineral, y la precipitación de sales eflorescentes en la superficie de los relaves. Por lo tanto, la distribución de la mineralogía y sus elementos asociados están controlados principalmente por la composición mineral del depósito de origen, la tecnología de procesamiento mineral, los procesos de segregación gravitacional y la geometría del depósito. Además, la historia deposicional de los relaves tuvo una gran influencia en la distribución vertical y horizontal de pirita. Sin embargo, las leyes de elementos de interés económico como Fe, Cu y Co se distribuyen de manera relativamente homogénea, lo que podría facilitar la aplicación de tecnologías de reprocesamiento de relaves y podría permitir ajustar el número de pozos requeridos para su evaluación económica. Por otro lado, la estructura y diversidad de las comunidades microbianas estuvo determinada por las ligeras variaciones en la composición química a lo largo del perfil de profundidad y por el establecimiento de una zona oxidada y primaria (no-oxidada) dentro del depósito de relaves. Sin embargo, la biomasa y la riqueza de especies se mantuvo prácticamente constante con la profundidad. Las especies claves en el microbioma del depósito comprenden los phylum *Proteobacteria, Firmicutes, Actinobacteria, Nitrospirae* y *Deinoccocus-Thermus*. Estos microorganismos parecen tener una actividad mutualista, incluso con algunas bacterias no cultivables pertenecientes al phylum *Actinobacteria*. La funcionalidad de las bacterias presentó ligeras variaciones asociadas a la estratificación de la composición química y refleja un alto potencial para la revalorización y restauración de estos ecosistemas. Adicionalmente, las bacterias sulfato reductoras, fueron utilizadas como bioindicadores de las condiciones redox a lo largo del perfil de profundidad del depósito de relaves.

RESUMEN DE LA TESIS PARA OPTAR AL

GRADO DE: Doctora en Ciencias, Mención Geología

POR: Erika Yelisbeth González Díaz

FECHA: 2022

PROF. GUÍA: Brian Keith Townley Callejas

PROF. CO-GUÍA: Manuel Antonio Caraballo Monje

GEOCHEMICAL, MINERALOGICAL AND MICROBIAL MODELLING OF AN IOCG TAILINGS DEPOSIT (EL BUITRE, CHILE): IMPLICATIONS FOR ENVIRONMENTAL SAFETY AND ECONOMIC POTENTIAL

Tailings dams have become a focus of interest as possible alternative sources of raw materials to partially mitigate the shortages on many critical raw elements imposed by the always growing demand of technological applications and green energies. Additionally, they have become a serious environmental problem for the ecosystems that surround these artificial deposits. This work reports the results of a mineral, geochemical and microbial characterization study and geostatistical and conceptual modelling of an Iron Oxides Copper Gold deposit with neutral pH, in an arid climate. Twenty-eight boreholes allowed recovery of 755 samples for analysis. However, 98 were selected for the characterization of microbial communities. The El Buitre tailings dam presents a primary mineralogy characterized by low pyrite and chalcopyrite content with relatively high magnetite and hematite content. Gangue is dominated by quartz, chlorite, alkali-feldspar, plagioclase and calcite. Secondary sulfides such as chalcocite/digenite, enargite/tennantite and malachite/azurite can be considered negligeable. Climatic conditions limit the availability of water and restrict the mobility of metals under neutral pore water pHs, inhibit the development of extensive oxidation fronts and mineral enrichment zones and prevent the appearance of efflorescent salts precipitated on the tailings surface. Therefore, the distribution of the mineralogy and its associated elements are mainly controlled by the source deposit mineral composition, the mineral processing technology, gravitational deposition processes and the geometry of the tailings dam. Therefore, the low mobility of the polluting elements makes these deposits environmentally safe and with low contamination potential. Additionally, the depositional history of the tailings had a great influence on the vertical and horizontal distribution of pyrite. Nevertheless, the grades of economic interest elements such as Fe, Cu and Co are distributed in a relatively homogeneous way, which would facilitate the application of tailings reprocessing technologies and maximize the number of boreholes required for its economic evaluation. On the other hand, the structure and diversity of the microorganisms were determined by the slight variations in the chemical composition and the establishment of an oxidized and non-oxidized zone within the deposit of tailings. However, biomass and species richness remained practically constant with depth. The tailings core microbiome comprised the phylum *Proteobacteria, Firmicutes, Actinobacteria, Nitrospirae* and *Deinoccocus-Thermus*. The networking analysis suggests a mutualistic activity between bacteria and highlights the importance of the microbial dark matter in these complex ecosystems. The predicted functional presented slight variations associated with the stratification of the chemical composition. Finally, based on the functionality, distribution and mutualistic activity among the microorganisms, capabilities can provide a direction for the management of the tailings dam and maximize their potential for revalorization. Additionally, sulfate-reducing bacteria were used as bioindicators of redox conditions throughout the depth profile of the tailings deposit.

A journey of a thousand miles begins with a first step

Lao Tzu

ACKNOWLEDGEMENT

Firstly, I want to thank each of the institutions that allowed the development and financing of this research work. To the companies Codelco Tech and Pucobre for their technical assistance during the sample collection process. For the financing of CORFO and Codelco through project 16PTECME-66524. For the partial financing obtained by the projects CONICYT / PIA Project AFB180004 and UNESCO-IUGS-IGCP-Project 682. For the financing granted to Professor Manuel Caraballo by the Ministry of Science and Innovation of Spain through the Ramón y Cajal 2019 program, Grant RYC2019-026496-I. Finally, to the National Research and Development Agency (ANID) for granting me the scholarship to develop my Doctorate studies during the period 2019-2021.

Secondly, I want to give a special thanks to the Professors Manuel Caraballo, Brian Townley and Julio Castillo for being wonderful tutors, for guiding me step by step in the development of the thesis and for their effort and dedication so that everything flowed quickly and in a timely manner. I appreciate that your concern went beyond the academic student-teacher relationship, always inquiring about my personal well-being. In addition, I thank Sebastián García, Karen Kotthoff and Byron Riquelme for being excellent co-workers and for their great contributions to the development of this thesis project. To Valeria Espinosa for her patience and dedication to teach me each of the steps of microbiological characterization.

Finally, I want to thank my husband, for his great unconditional support in each of the stages of the PhD program and even more so in the mother and student stage, which many times became difficult, but not unattainable thanks to his support. I thank my beautiful son for giving me moments of happiness and relaxation, for inspiring me to achieve this goal, which I hope will pay off in many benefits for his future. I thank all my family in Venezuela who always support me from a distance, giving me encouragement and being attentive to all my progress and achievements. Especially to my mom and dad who are always proud and confident of my abilities, even more than myself.

TABLE OF CONTENT

LIST OF FIGURES

LIST OF TABLES

SUPPLEMENTARY MATERIAL FIGURES

SUPPLEMENTARY MATERIAL TABLES

CHAPTER 1

1. INTRODUCTION

1.1 THEORICAL BACKGROUND

The continuous accumulation of mining tailings on Earth has become a serious environmental problem. In addition, a recent study by Franks et al., (2021) has estimated the presence of more than 8,100 deposit of tailings globally and the generation of 10 billion m^3 of fresh tailings every year. The need to restore these environmental liabilities, together with the growing demand for many critical raw elements, has made deposit of tailings a focus of interest. Therefore, various studies have focused on the mineralogical, geochemical, hydrological, and microbiological characterization of these systems. In order to understand the various factors that control the dynamics, evolution and distribution of chemical elements within the depth profile of deposit of tailings. They can be summarized as deposit of origin, climatic conditions, mineral processing technology, tailings disposal and storage and microbial communities.

1) Origin of tailings

The type of ore deposit will determine the mineralogy associated with the deposit of tailings. Due to the heterogeneity of deposits, mineralogy can frequently change during the life of a mine, influencing the mining techniques selected and the sequence of mining operations (European Commission, 2017).

Chilean tailings deposits are the result of the processing of different ore deposits, or they are simply abandoned deposits with unknown origins (Sernageomin, 2020). However, the adequate environmental management of the deposit of tailings, acidity generation control treatments and the possibility of extraction of chemical elements and raw materials of economic importance require a clear understanding of the mineralogy of the deposit of tailings (European Commission, 2017).

The geochemical processes that occur in a deposit of tailings consist of a combination of geochemical reactions that include the oxidation sulfides, acid neutralization, precipitation and dissolution of secondary minerals, ion exchange, adsorption / desorption reactions and complex formation. These reactions are conditioned by mineralogical and water/rock interaction processes, which regulate the physical-chemical conditions of the system (Bea et al., 2010; Blowes et al., 1998; Dold and Fontboté, 2001; Dold and Spangenberg, 2005; Kovács et al., 2006).

In the closed deposit of tailings, a drop in the water table occurs, which allows the diffusion of O_2 from the atmospheric air into the unsaturated zone, causing the oxidation of sulfide minerals. The most common sulfides are iron sulfides (Pyrite (FeS_2 and pyrrhotite (Fe (1-x) S)) (1). These sulfides often coexist with other sulfides of higher economic value such as chalcopyrite ($FeCuS_2$); galena (PbS); sphalerite (ZnS), pentlandite ($(Ni, Fe)_9S_8$) among others, or with sulfides of very little economic value such as arsenopyrite ($FeAsS_2$). Pyrite and pyrrhotite oxidation, are the main

reason for the formation of acid rock drainage (ARD). These heavy metal loaded acid effluents are the principal environmental problem facing the mining industry today (Dold and Fonboté, 2001).

$FeS_2 + \frac{7}{2O_2} + H_2O \rightarrow Fe^{2+} + 2SO_4^{2-} + 2H^+$ (1)

$Fe^{2+} + 1/4O_2 + H^+ \leftrightarrow Fe^{3+} + 1/2H_2O$ (2)

$FeS_2 + 14Fe^{3+} + 8H_2O \rightarrow 15Fe^{2+} + 2SO_4^{2-} + 16H^+$ (3)

Ferrous iron is oxidized by oxygen in the oxidation zone (2). However, this reaction can be catalyzed by the presence of Fe oxidizing bacteria and ferric iron may take over the role of the principal sulfide oxidant (3). Because ferric oxidation of sulfides is more efficient in releasing protons to the medium. Sulfide oxidation leads to the liberation of bivalent cations as for example $Fe^{2+}, Cu^{2+}, Zn^{2+}, Mn^{2+}$ oxyanions as $HMoO_4^-, H_2AsO_4^-$ and SO_4^{2-}, as well as protons ($2H^+$). Furthermore, ferric iron can be hydrolyzed and precipitated as crystalline or amorphous Fe oxy-hydroxide mineral phases and ferric sulfate mineral phases such as jarosite (4), schwertmannite (5), ferrihydrite (6), goethite (7) or others Fe (III) hydroxides (8), depending on pH-Eh conditions and activity of Fe, SO_4, Cl, Al, Na and K (Dold and Fonboté, 2001).

$3Fe^{3+} + K^+ + 2SO_4^{2-} + 6H_2O \leftrightarrow KFe_3(SO_4)_2(OH)_6 + 6H^+$ pH ~ 2 Jarosite (4)

$16Fe^{3+} + 3SO_4^{2-} + 26H_2O \leftrightarrow Fe_{16}O_{16}(OH)_{10}(SO_4)_3 + 42H^+$ pH~2,8-3,5 Schwertmannite (5)

$10Fe^{3+} + 60H_2O \leftrightarrow 5Fe_2O_3 + 9H_2O + 30H^+$ pH ~ 2,8 Ferrihydrite (6)

$Fe^{3+} + 2H_2O \leftrightarrow FeOOH + 3H^+$ pH 3-4 Goethite (7)

$Fe^{3+} + 3H_2O \rightarrow Fe(OH)_{3(S)} + 3H^+$ pH ~ 3 (8)

The ferric hydroxide sulfates jarosite and schwertmannite are metastable in respect to goethite, this transformation (9-11) is a source for future proton liberation (Dold and Fonboté, 2001).

$KFe_3(SO_4)_2(OH)_6 \rightarrow 3FeO(OH) + K^+ + 2SO_4^{2-} + 3H^+$ Jarosite → Goethite (9)

$Fe_{16}O_{16}(OH)_{10}(SO_4) + 6H_2O \rightarrow 16FeO(OH) + 3SO_4^{2-} + 6H^+$ Schwertmannite → Goethite (10)

$Fe_8O_8(OH)_6(SO_4) + 2H_2O \rightarrow 8FeO(OH) + SO_4^{2-} + 2H^+$ Schwertmannite → Goethite (11)

However, the presence of minerals such as calcite (12-14), dolomite and, to a lesser extent, some aluminosilicates, can effectively neutralize the acidity generated and maintain circum-neutral pH conditions (Blowes et al., 1998; Lindsay et al., 2009a). These reactions involve the exchange of H^+ for cation bases. The initially acidic fluid remains enriched in base metals.

$CaCO_3(s) + 2H^+ \longrightarrow Ca^{+2} + H_2CO_3(ac)$ (12)

Carbonic acid is unstable and breaks down.

$H_2CO_3(ac) \longrightarrow H^+ + H\,CO_3^-$ pH> 6 (13)

$H_2CO_3(ac) \longrightarrow H_2O + CO_2(ac)$ pH<6 (14)

Depending on the composition of the gangue mineralogy, a specific neutralization sequence can be observed through the stratigraphy of the tailings, which is controlled by the different mineral buffers. Successive buffer chains have been determined as: successive dissolution of calcite ($CaCO_3$) at pH 6.5, siderite ($FeCO_3$) at pH 5.5, aluminum hydroxide Al $(OH)_3$ at pH 4 and ferrihydrite at pH 2.8 (Blowes et al., 1991) The dissolution of carbonates containing Fe such as siderite and ankerite are not a potential source of neutralization, because the Fe (II) released generates acidity once it is oxidized and precipitates as ferric oxyhydroxide phases (Blowes et al., 1991; Dold and Fontboté, 2001).

Several characterization studies have been carried out on tailings from sulfide-rich mineral deposits, such as copper porphyry, skarn, volcanogenic massive sulfide, among others (Dold and Fontboté, 2001; Hällström et al., 2018; Lindsay et al., 2009a; Lindsay et al., 2009b). Dold and Fontboté (2001) determined that the deposit of tailings generated from copper porphyry deposits have a low neutralization potential associated with the low carbonate content and the relatively high content of minerals derived from supergene enrichment. These characteristics, together with favorable climatic conditions and long exposure time of the tailings typically lead to the development of acid mine drainage (Smuda et al., 2014). Skarn-type deposit materials are considered high in carbonates, sulfides, and fluorite. As a result, their deposit of tailings frequently exhibit high mobility of metals due to the pH decrease induced by iron-sulfides oxidative dissolution (Blowes et al., 2003) and complexation with F ions keeping metals mobile (Petrunic and Al, 2005). On the other hand, the deposit of tailings with low-sulfur and high-iron (Henne et al., 2020), like the impoundments generated after the mineral processing of Iron Oxides Copper Gold (IOCG) or Iron Oxide-Apatite (IOA) type deposits have been barely studied (Dold and Fontboté, 2002; Henne et al., 2019; Medina et al., 2019) and their weathering and evolution in arid and semi-arid climates is poorly understood.

IOCG-type ore deposits are globally distributed, grouping different styles of mineralization. Only eleven IOCG provinces “sense strict” have been recognized worldwide, including the Central Andean Coastal Belt, spanning from Southern Peru to Northern Chile (Sillitoe, 2003). In recent decades they have been considered profitable exploration targets due to the economic recovery of copper, gold and other by-products such as uranium (Barton, 2014). These deposits may also contain high concentrations of rare earth group elements (REEs), silver, molybdenum, nickel, cobalt, barium, fluorine, and phosphorus (Barton, 2014). Most of these elements are on the European Commission’s list of critical raw materials due to their economic importance and supply risk (European Commission, 2017). Therefore, the mining wastes derived from the processing of IOCG ore deposits, especially the tailings deposits, have gained great significance in recent years (Henne et al., 2019, 2020; Karimi et al., 2019; Medina et al., 2019).

2) Climate condition

Climatic conditions can control the mobility of chemical elements within the tailing dam (Anawar, 2015; Dold, 2007; Dold et al., 2005; Dold and Fontboté, 2001). Under arid climate conditions, high temperatures and low relative humidity during the summer cause evaporation, causing the water to flow upward via capillary forces. Solute concentrations in rising water increase dramatically, with saturation giving rise to some salts that form an efflorescent crust. As evaporation proceeds, the pore water content is reduced, preventing the flow of liquid from rising

to the surface. Therefore, the evaporation front shifts slightly downward, and efflorescence continues to grow within the pore volume. This causes the upper part of the tailings to become more and more cemented by salts in acid tailings. The availability of the mobilized metals in acid tailings as water-soluble phases represent a latent source of pollution, even in arid climates with sporadic rainfall events. Nevertheless, the availability of metals in water soluble form at the top of the tailings is an economic metal recovering methods for revalorization of the tailings under arid condition. Secondary sulfide enrichment processes are less important, and in acid oxidation zone mobile elements may substitute into secondary phases. In contrast, in neutral and alkaline tailings the mobility of metals is more restricted due to the dominance of sorption processes (cementation zone), limiting the development of efflorescent salts on the surface (Dold and Fonboté, 2002).

In addition, in hyper-arid climates, the lack of water decreases the oxidation speed of sulfides, for this reason their oxidation is limited to fine-grained horizons, due to their greater water retention capacity. In general, thin horizons are poorer in sulfides compared to thicker layers, due to gravitational segregation processes. Therefore, layers with lower sulfur content are available for oxidation (Dold and Fonboté, 2002).

In the presence of humid climates, the metals released by the oxidation and neutralization reactions of sulfides are transported down to more reducing conditions (below groundwater level). This often results in the retention of these elements through sorption processes, controlled by pH and/or precipitation of secondary minerals (for example, Fe oxides and Cu sulfides) (Dold and Fontboté, 2001; Bea et al., 2010). In addition, the coarse-grained horizons of the oxidation zones show stronger oxidation and mobilization of sulfide compared to the horizons with finer grain size. Because thick horizons have a higher sulfur content and allow greater transport of water and oxygen (Dold and Fontboté, 2001).

In general terms, climatic conditions control the availability of water, the transport of the products of oxidation reactions, and the interaction of the effluent with natural waters or with other effluents, producing the concentration or dilution of their constituents. On the other hand, temperature can have various effects, such as promoting evaporation at high temperatures or inhibiting effluent transport in freezing conditions (European Commission, 2017).

The climate also determines the dispersion of the tailings towards the environment. In rainy areas, the generation of AMD is favored and its dispersion through surface runoff, while in arid areas, the dispersion of tailings caused by the wind is favored as suspended particles (Romero et al. 2008).

3) Mineral processing technology

Mineral processing is carried out in order to concentrate the ore, which must be transported and subjected to subsequent processes, using methods to separate the valuable minerals from the gangue. Mineral processing techniques include comminution techniques such as crushing, grinding, screening, etc. Also, they include beneficiation techniques such as sorting, gravity concentration, magnetic separation, electrostatic separation, flotation, leaching, etc. The procedures are based on the physical characteristics of the mineral (particle size, density, magnetic

properties, color) or physical-chemical properties (surface tension, hydrophobicity, wear resistance) (European Commission, 2017).

Some processing techniques influence AMD, especially those that alter the accessibility of sulfides (crushing and milling) or change the sulfide content in tailings. For instance, the electrostatic separation can eliminate part of the pyrite. Similarly, the flotation process can remove the sulfides to the concentrate or remove other minerals while the sulfides remain in the tailings (European Commission, 2017). On the other hand, the reduction of the particle size by crushing and grinding, has the effect of making the sulfide minerals more accessible (increase of the surface area). Additionally, all the processes in which reagents are added (for example the flotation process), also influence the surface properties of minerals and may influence negatively the environment (European Commission, 2017).

4) Tailings disposal and storage

There are different types of tailings disposal methods, which are a function of different factors: the physical properties and chemical nature of the tailings, the site topography, climatic conditions, environmental regulations and restrictions, and the socioeconomic context of the mining operations and processing plants (Management, 2016). The most common forms of deposit of tailings are slurry (to over 50 % solids for hard rock metalliferous tailings), thickened (> 20 % water), paste (10 to 25 % water) and filter cake (less than 20 % of water) (Management, 2016). Therefore, tailings with higher water content are more likely to generate AMD (according to mineralogical composition, climatic conditions, type of mineral deposit of origin and presence of microorganisms).

The thickened tailings show some segregation, settling and infiltrating the deposit. While paste tailings have a non-segregating, non-sedimentation consistency, releasing only small amounts of water after deposition. Filtered tailings have the lowest water content, therefore, losses due to infiltration and evaporation are lower compared to thickened and paste tailings (Management, 2016).

Fig. 1 Tailings disposal methods. a) Paste tailings, b) Filter cake, c) Thickened tailings and d) Slurry tailings (Management, 2016)

On the other hand, the deposit of tailings in the form of slurry, favors the stratification of the material due to its high-water content. The coarser particles with a higher specific gravity are deposited on the upper beach, while the supernatant water transports finer particles with a lower specific gravity to more distal areas (Pan et al., 2014). In addition, tailing stratification is also a function of deposit of tailings geometry and location of material discharge points. This factor determines the possibility of both lateral and vertical stratification of the particles. Additionally, stratification will occur depending on whether the discharge is continuous or intermittent over time. Also, the specific weight of the mineral particles and the effluent concentration are factors that causes tailings stratification.

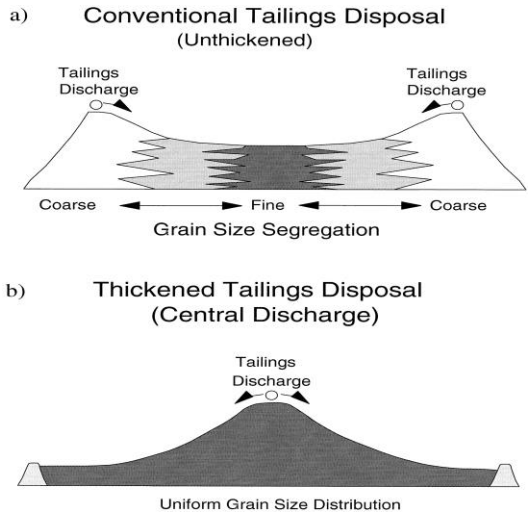

Fig. 2. A) Grain size segregation of conventional tailings disposal. B) Uniform grain size distribution of thickened tailings disposal (Al and Blowes, 1999)

Al and Blowes (1999) reported that paste tailings and dry stacking recover the water before final deposition and increase the geotechnical safety of the deposit. However, sulfur oxidation is enhanced as tailings are never fully saturated with water, but they are wet, and oxygen can more easily get into sulfides compared to traditional water-saturated tailings dam.

Finally, the construction of new tailings impoundment upstream of the old deposits are generated when an erroneous planning of the dimensions of the deposit occurs, with respect to the tailings generation capacity by the flotation plant. As a result, seepage from the new to the older tailings could occur (Dold and Fonboté, 2002).

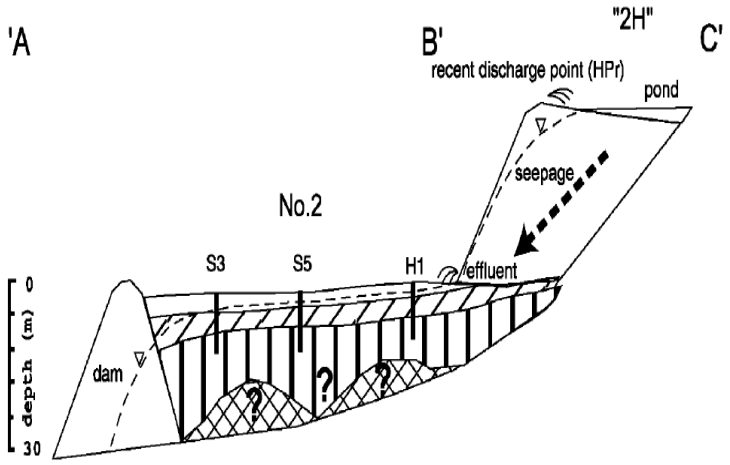

Fig. 3. Seepage of fresh tailings over old deposit of tailings (Dold and Fonboté, 2002)

Microbial communities

Microorganisms can control the dynamics of metals along the depth profile of deposits through two processes 1) metals mobilization or microbial leaching 2) metals immobilization (Hennebel et al., 2015). This process has application in the field of biohydrometallurgy for the extraction and processing of valuable metals. Biomining procedures are generally more environmentally friendly compared to conventional processes and allow to use low grade ores that are nor exploitable by conventional technologies.

Metal mobilization

The process of metals solubilization catalyzed by microorganisms is called bioleaching. This process refers to the direct action of some microorganisms in nature or the indirect action of their metabolites to produce oxidation, reduction, complexation, adsorption, or dissolution, by which heavy metals or value elements are separated from the solid phase. This biotechnology is widely used for the metals recovery from low-grade ores and concentrates that cannot be processed economically by conventional methods (Bosecker, 1997). The low cost of this technology with respect to conventional processes has allowed its application to expand to the recovery of metals from mining tailings. Since the early 1950s, Fe/S oxidizing bacteria have been used in industrial scale processes to extract metals from sulfide ores. The microorganisms most widely used are *Acidithiobacillus ferrooxidans, Acidithiobacillus thiooxidans* and *Leptospirillum ferrooxidans.* In the case of bioleaching in mining tailings, the indigenous microorganisms show better adaptability

and have a higher leaching rate. Furthermore, the presence of complex microbial consortia of autotrophic and heterotrophic bacteria has been determined to be more efficient in bioleaching processes. However, its application in deposit of tailings present difficulties due to the inhomogeneous distribution of the leachate bacteria along the depth profile and the possible temperature variations inside the deposit. On the other hand, in the case of fresh tailings, the presence of surfactants from the flotation process could inhibit the leaching activity of bacteria. Organic reagents can also influence certain nutritional or growth processes by being adsorbed on the bacterial envelope or by changing the growth environment of bacteria (Gao et al., 2021). Finally, in tailings iron/sulfur oxidizing bacteria are more likely to undergo redox reactions under acidic conditions. However, the presence of iron/sulfur oxidizing neutrophilic bacteria such as *Gallionella ferruginea, Leptothrix ochracea, Meiothermus* and *Thiobacillus* has been reported under neutral or alkaline conditions (Blowes et al., 1998; Gupta et al., 2020; Hallberg and Johnson, 2003; Johnson and Hallberg, 2003; Sun et al., 2018).

Two sulfide leaching mechanisms have been proposed direct and indirect mechanisms (Tributsch, 2001). In the direct mechanisms the microorganisms oxidize sulfide minerals through direct attack on the mineral surface. The mineral is oxidized by an enzymatic system with oxygen to sulfate and metal cations. The remaining sulfur in the mineral is biologically oxidized to sulfate without producing any detectable intermediate. Bacteria adhering to the surface of the mineral oxidize the sulfide phase by biological means directly, without any requirement for ferrous or ferrous ions. Hydrogen ions are produced simultaneously, resulting in a decrease in the pH of the environmental system and an increase in the redox potential and thus the formation of soluble sulphates. This process can be represented by the pyrite oxidation.

$$4FeS_2 + 14O_2 + 4H_2O \xrightarrow{bacteria} 4FeSO_4 + 4H_2S\ . \qquad 15$$

$$4FeSO_4 + O_2 + 2H_2SO_4 \xrightarrow{bacteria} 2Fe_2(SO_4)_3 + 2H_2O \qquad 16$$

$$4FeS_2 + 15O_2 + 2H_2O \xrightarrow{bacteria} 2Fe(SO_4)_3 + 2H_2SO_4 \qquad 17$$

The acid produced in 15 reacts with ferrous iron and dissolved oxygen to produce ferric sulfate (16-17) which is vital for the oxidation reactions that occur in the indirect mechanism. Whereas in the indirect mechanism metabolites of Fe/S oxidizing bacteria are used in redox reactions that occur with sulfide minerals, and finally, a redox circulatory system is formed. In this mechanism, bacteria oxidize ferrous ions to ferric ions in solution, and ferric ions oxidize metal sulfides (Figure 3). The bacteria generate a leaching agent which chemically oxidizes the surface of the mineral. In acid solutions, this leaching agent is ferric iron and the solubilization of the metal can be described according to the following reaction:

$$MeS + Fe_2(SO_4)_3 \rightarrow MeSO_4 + 2FeSO_4 + S^0 \qquad 18$$

To keep enough iron in solution, oxidation of the metal sulfide must occur in an acidic environment below pH 5.0. Ferrous iron originated in this reaction can be re-oxidized to ferric iron by *Thiobacillus ferrooxidans* or *Leptospirillum ferrooxidans* and can take part in the oxidation process again. Bacteria have a catalytic function because they accelerate the re-oxidation of ferrous iron (19).

$$2Fe^{2+} + 0{,}5O_2 + 2H^+ \xrightarrow{bacteria} 2Fe^{3+} + 2H_2O \quad 19$$

Sulfide can simultaneously be oxidized to sulfuric acid (20) by *Thiobacillus ferrooxidans* (Bosecker, 1997).

$$2S^0 + 3O_2 + 2H_2O \xrightarrow{bacteria} 2H_2SO_4 \quad 20$$

The role of *Thiobacillus thiooxidans* in bioleaching is to create favorable acidic conditions for the growth of ferrous iron oxidizing bacteria such as *Thiobacillus ferrooxidans* and *Leptospirillum ferrooxidans*.

A third sub-mechanism is cooperative leaching where the dissolution of colloidal sulfides, intermediate sulfides, and mineral fragments occurs through the joint cooperation of platonic cells (freely suspended) and cells attached to metal sulfides.

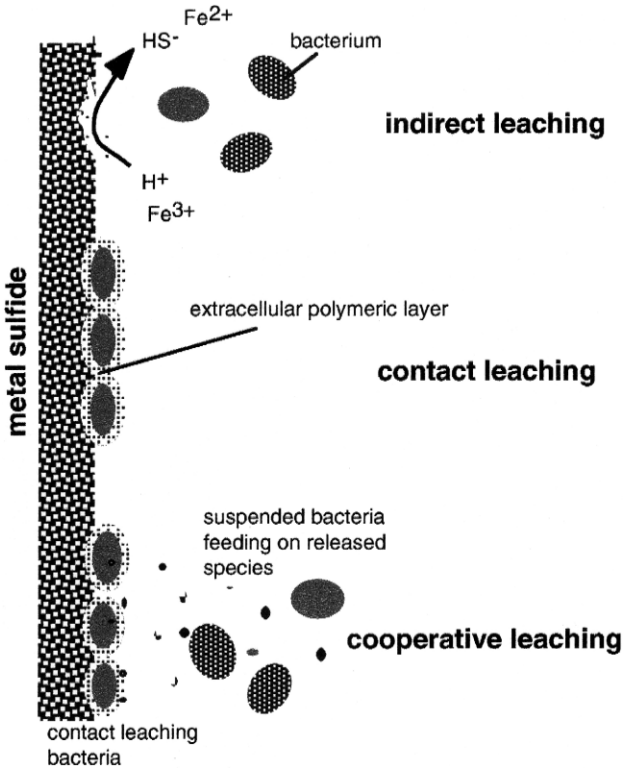

Fig. 4. Mechanism of indirect leaching, contact leaching and cooperative leaching by Tributsch 2001

Metal immobilization

There are various mechanisms by which metal immobilization processes by microorganisms occur, among these we have: biosorption, bioaccumulation, biomineralization and biotransformation.

Biosorption: is metabolically passive process and is performed by material of biological origin, not by living biomass (Chojnacka, 2010). It is characterized by metal retention through a physicochemical interaction with ligands belonging to the cell surface. This interaction occurs with functional groups exposed to the outside of the cell belonging to parts of component molecules of

the cell walls, such as carboxyl, amino, hydroxyl, phosphate and sulfhydryl. It is a fast kinetic mechanism that does not have a high dependence on temperature. Microorganisms can reach very high specific surface areas, due to their small size and different surface structures (> 100 m2 g-1 biomass), providing many sorption sites for metal ions (Fein et al., 1997). In addition, microorganisms can grow in complex structures such as biofilms and granules where molecules such as polysaccharides, alginates and other biopolymers function as binding molecules (Flemming and Wingender, 2010; Gao et al., 2011). Additionally, these biomolecules provide functional groups in their structure that increase the sorption sites for metals (Hennebel et al., 2015).

Bioaccumulation: is metabolically active and is performed by living cells. This process is defined as intracellular accumulation of sorbate, which occurs in two-stages: a quick stage identical to biosorption and the second is a slower stage which includes transport of sorbate into inside of cells by the most frequently active transport system (Chojnacka, 2010). In contrast to biomineralization process, bioaccumulation is generally highly controlled, producing uniform particles with defined crystallinity and particle morphology (Frankel, 2003). Generally, these particles may be difficult to separate from the residual biomass. However, if combined with pyrometallurgical processes even biomass enriched in intracellular metals can represent a valuable resource. In addition, some bacteria that can accumulate metals to amounts exceeding their own cellular weight on their surface (Schultze-Lam et al., 1996). On the other hand, the process of bioremoval of pollutants include intracellular accumulation and oxidation or reduction reactions. It is highly affected by the operational conditions, in particular by the concentration of pollutants in the growth medium which can inhibit the growth of cells and also bioaccumulation itself (Chojnacka, 2010).

Biomineralization: the microorganisms can form extracellular minerals and metals product of a bio-induced process (Frankel, 2003). These extracellular phases are of particular interest for recovery, because no downstream processing (e.g. ultrasonic rapture, treatment with surfactants) is needed to separate materials from the cells (Narayanan and Sakthivel, 2010). Sulphate reducing bacteria play a crucial role in metal mobility in the environment by precipitating metals through their metabolic end product, sulfide. One major advantage of biogenic sulfide is that it can be produced on site from wastes using an electron donor that can be a waste product itself. Critic (Co) and economically important metals (Fe, Zn, Ni and Mn) have been recovered by selective precipitation (Jandová et al., 2005; Tokuda et al., 2008). In addition, this strategic can be use in bioremediation needs, for instance in the treatment of acid mine drainage (Hennebel et al., 2015).

Biotransformation: heavy metals cannot be degraded, but they can be transformed from one oxidation state to another inorganic complex. Therefore, it is a process that involves a chemical change on the metal, such as in the oxidation or methylation state. This biological transformation results in compounds that are poorly soluble in water or low toxic state; thus, the metal precipitates and becomes less bioavailable. Then, they are removed from the contaminated site or volatilized and removed from the polluted area . Heavy metal removal through microbial remediation can be achieved through several approaches, such as bioaugmentation, biostimulation and bioattenuation (Emenike et al. 2018). Bioaugmentation involves the application of indigenous bacteria to contaminated sites to accelerate the removal of undesired compounds or value elements. Whereas biostimulation is a process where the environment is modified to stimulate the existing bacteria,

for instance by adding water, electron donors or acceptors and nutrients, such as phosphorous, nitrogen, oxygen or carbon. Nutrient addition increases the population or activity of naturally occurring microorganisms available for bioremediation. In contrast, bioattenuation (or natural attenuation) depends on natural process of degradation. The environmental contaminants remain undisturbed to provide an opportunity for natural degradation, reduction or transformation of the contaminant (Emenike et al. 2018).

Characterization of microbial communities in deposit of tailings

Several studies have been carried out on the characterization of the microbial communities that inhabit mining tailings dam. Most of the studies focus on tailing dams with high potential for generating acid mine drainage. It has been reported that the extreme conditions found in the tailings dam with acid mine drainage are the product of the metabolic activity of acidophile and chemolithotrophic microorganisms, mostly iron- and sulfur-oxidizing bacteria. The most dominant bacteria in AMD with extremely low pH (<2) are *Acidithiobacillus ferrooxidans, Acidithiobacillus thiooxidans, Leptospirillum ferrooxidans, Alicyclobacillus, Ferrithrix, Ferrimicrobium* and *Ferroplasma spp*. The increase in temperature makes the moderate thermophilies dominate in microbial populations, such as *Bacillus spp.* and *Sulfobacillus acidophilus* (Yuan et al., 2013). In contrast, in many low temperature AMD waters, *Acidithiobacillus ferrivorans* tends to dominate over *Acidithiobacillus ferrooxidans* and *Leptospirillum ferrooxidans*. If the pH conditions are not so extreme (pH 3-6) the moderate acidophilus, such as *Tumebacillus, Thiobacillus* and *Thiomonas* are the dominants genus (Gupta et al., 2020; Korehi et al., 2014; Xiao et al., 2016).

Diaby et al. (2007) proposed a geochemical and microbiological conceptual model of an acidic deposit of tailings. They indicate that as the water level fall, the oxygen promotes the oxidative dissolution of pyrite and other sulfide minerals, mainly by *Leptospirillum spp*. Other iron and sulfur acidophilus (*Sulfobacillus sp*p. and *Acidithiobacillus Ferrooxidans*) contribute to this process by generating sulfuric acid and oxidizing ferrous iron. Lysates and exudates (dissolved organic carbon) of autotrophic acidophilus support the growth of heterotrophic acidophilus (iron-reducing bacteria: *Acidiphilium,* and sulfate-reducing bacteria: *Acidobacterium*). While the oxidation products (ferric iron and sulfate) act as electron acceptor terminals for heterotrophic organisms where oxygen is limited or absent. Below the oxidation front, dissimilatory reduction of ferric iron and sulfate are considered to be the dominant geochemical processes, both of which are limited by the availability of these oxidized species or by electron donors. The oxidation front will continue to migrate downward, depending on the rate at which the tailings water table falls. Ultimately, when the reservoir is fully drained, the tailings could become completely oxidized, leading to the dissolution of large amounts of sulfide minerals and the generation of acidic and metal-rich effluents.

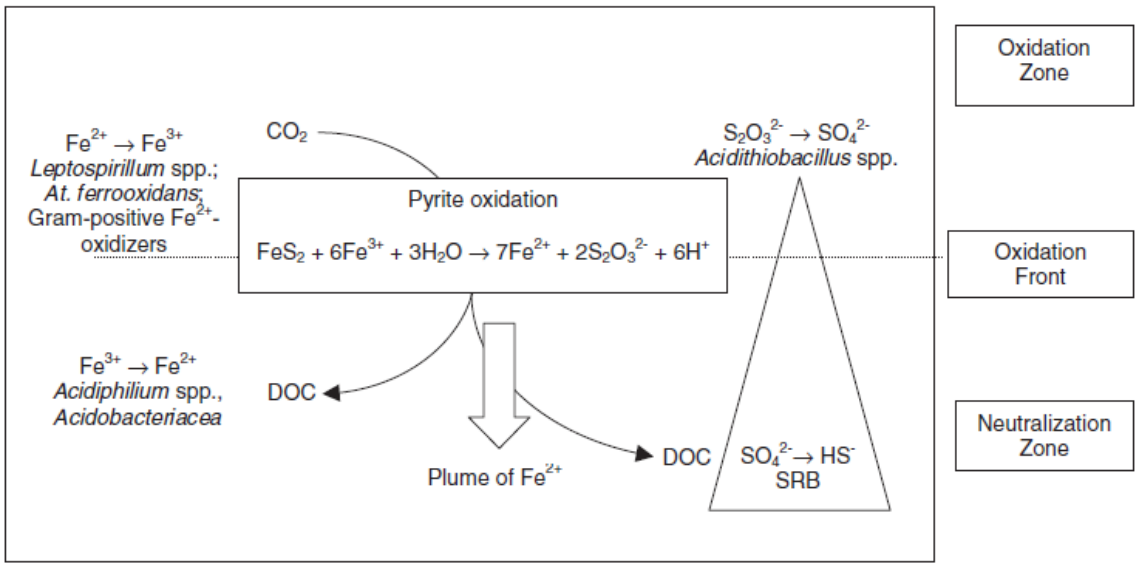

Fig. 5. Model of the microbial impact on geochemical dynamics observed in a copper porphyry tailings impoundment (Diaby et al. 2007). DOC, dissolved organic carbon.

On the other hand, microbial communities belonging to fresh, neutral or alkaline tailings have been less studied. Nevertheless, previous works have been determined that microorganisms such as *Thiobacillus, Meiothermus, Sphingomonas, Hydrogenophaga, Acidiferrobacteraceae* and *Sulfurifustis* are the dominants genus that control the Fe and S cycle in the early stages of the tailings acidification processes (Chung et al., 2019; Gupta et al., 2020; Sun et al., 2018).

1.2 RESEARCH PROBLEM

In Chile there are more than 757 tailing dams, of which 173 are abandoned and 467 are inactive. More than 80 % are located in the north of the country where the climatic conditions are arid and semi-arid and where the main IOCG deposits are located (e.g., Manto Verde, Punta del Cobre, Cerro Negro, El Espino and Candelaria; (Sernageomin, 2020). The growing demand for strategic chemical elements associated with deposits of the IOCG type has opened the interest to study the deposit of tailings derived from their processing. Additionally, the restoration studies of these ecosystems require a detailed knowledge of the dynamics of the chemical elements along the depth profile and the different factors that control their mobility. Nevertheless, due to the difficulties and costs of drilling these deposits and the low economic potential they are thought to represent, most tailings studies in Chile (and around the world) are usually limited to near surface samples, depths of 10 m or less. However, there are plenty of reasons that justify obtaining a better knowledge of the deeper sections of these deposits, among others:

1) In almost all cases there is a complete absence of historical record of the mineralogical, geochemical, and microbiological characteristics of the deposit of tailings during the years and decades of production, being impossible to anticipate the existence and extent of sedimentation layers with different mineralogical, geochemical and microbiological characteristics within the different depths of the tailings.

2) Old deposit of tailings (with many years and even decades after their closure) typically generate alteration fronts (e.g., leaching, enrichment and/or depletion of certain elements) that may evolve deep into the tailing impoundment.

3) Depending on the geometry of the deposit of tailings, during its deposition the accumulation of heavy minerals in the deeper layers can be favored by gravitational processes, being relatively enriched in heavy metals with respect to the shallower layers. Therefore, a detailed understanding of the deeper sections of the deposit of tailings is essential to understand their geochemical, mineralogical, and microbiological evolution, to generate realistic environmental assessments and to create acceptable economic evaluations for a future revalorization or restoration of these secondary deposits.

1.3 HYPOTHESIS AND OBJECTIVES

1.3.1 Research questions and hypothesis

From the above background, the following research questions arise:

- Is there any stratification within the deposit of tailings? If it exists, which are the factors that control these processes?
- Are there alteration fronts within the deposit of tailings? If they exist, what is its extension within the depth profile and what factors control it?
- What aspects could favor the restoration of the deposit of tailings?
- Does the deposit of tailings show any potential for revalorization?
- Could microbial communities be of interest for the revalorization and restoration of the deposit of tailings?

Due to the absence of information on the historical record of the tailings dam, it is possible to assume that the tailings material may present heterogeneities typical of the reservoir of origin, such as sulfide veins, hydrothermal alteration zone, among others. Another option is that it comes from different deposits located near the flotation plant. Based on the aforementioned, it is possible to find slight stratifications along the depth profile. Which may be more evident at the bottom of the tailing dam, where the pond geometry favors the gravitational segregation processes of minerals with high specific weight such as sulfides and iron oxides during the initial stage of tailings discharge in the form of slurry, creating zones slightly enriched. Another factor that could influence is the use of increasingly efficient extraction technologies over time. On the other hand, due to the arid climatic conditions, alkaline tailings, and low sulfur content, it is expected to find alteration fronts of little extension, almost total absence of efflorescent salts on the surface and low concentrations of heavy metals in the soluble fraction. All these aspects can be considered as positive for future restoration processes of the deposit of tailings. The dominant microbial communities must be mainly neutrophilic, chemolithotrophs, and highly resistant to heavy metals. Their structure and composition must be defined mainly by pH and redox conditions (oxidation zone and primary zone). On the other hand, despite the low sulfide content of the deposit of tailings from the processing of IOCG reservoirs, its possible revaluation could focus on obtaining iron, cobalt, and elements of the rare earth group. Finally, the study of microbial communities could yield favorable results on the presence of microorganisms capable of leaching or immobilizing

elements of interest within the deposit of tailings. In this way, biotechnologies could be proposed for in situ / ex situ value metals recovery or for restoring the deposit, for instance by Phyto-stabilization (use of plants to limit the mobility and bioavailability of pollutants by prevention mechanisms by migration and immobilization).

1.3.2 Objectives

The main objective of this study is to develop geostatistical (using interpolation by co-kriging) and conceptual models, allowing to decipher its geochemical, mineralogical, and microbiological spatial-temporal evolution as well as the most relevant physical and chemical parameters controlling this evolution.

To this end, the following specific objectives were raised:

-Perform a geochemical, mineralogical, and microbiological characterization based on detailed and systematic sampling of an IOCG deposit of tailings. Together with other relevant physical and chemical parameters (e.g., paste pH, hydraulic conductivity, and particle size distribution).

-Evaluate the possible presence of alteration fronts and their possible vertical and horizontal extensions. In addition, the different factors that promote the alteration of sulfide minerals under arid climate conditions.

- Determine the influence of the impoundment geometry and the possible sediments depositional history on the geochemical and mineralogical composition.

-Characterize microbial communities using 16S rRNA gene sequencing and statistical analyzes.

-Analyzer the bacterial diversity and community inhabiting the tailing dam and their correlation with the geochemical composition of the deposit.

-Predict the metabolic potential of the most dominant microorganisms using Pycrust2 software.

-Evaluate the environmental and economic implications of the deposit based on critical raw elements such as Co, Cu and Fe and the most dominant microbial communities.

CHAPTER 2

2. STUDY AREA: EL BUITRE TAILING DAM

2.1 ORE GEOLOGY

The Punta del Cobre district includes the Candelaria deposit, and several medium and small sized mines such as Alcaparrosa, Carola, Las Pintadas, Socavón and Santos, all hosted within volcanic rocks of the Punta del Cobre Formation. These rocks of a pre-upper Valanginian age (Marschik and Fontboté 2001). Rocks of this formation are subdivided from bottom to top into the Geraldo-Negro Member (> 300 m) and Algarrobo Member (up to >800 m) comprised mainly of altered sub-aquatic volcanic and volcanoclastic rocks. Mineralization occurs in a diversity of styles including veins, stratiform orebodies, stockworks and hydrothermal breccias, hosted by andesite volcanic, volcanoclastic and volcanic breccia rocks, locally termed an albitophire facies of the Punta del Cobre Formation (Marschik and Fontboté 2001). Five main alteration types are identified and associated with mineralization as well as a regional contact metamorphism caused by the Coastal Batholith in the western sector. An early episode of hydrothermal alteration generated extensive albitization (albite–quartz–chlorite, ±sericite ±calcite) which was locally superimposed by potassic alteration (K-feldspar–quartz–chlorite/biotite ±sericite ±calcite ±tourmaline). The rest of the alterations are associated with the batholith and are characterized by the following mineral assemblage (from contact, west to east): Ca-amphibole ± biotite ± sericite, biotite ± chlorite ± sericite ± epidote and epidote chlorite ± quartz ± calcite (Marschik and Fontboté, 2001). Main hypogene minerals in the Punta del Cobre District are chalcopyrite, pyrite, magnetite and hematite (Oyarzun et al., 1999).

2.2. DESCRIPTION OF THE STUDIED MINE TAILINGS

El Buitre tailings deposit is located in the province of Copiapó, in the community of Tierra Amarilla. The General Directorate of Water of Chile has reported the presence of an unconfined aquifer consisting mainly of an alluvial deposit. The aquifer has been subdivided into 6 sectors to facilitate management of its resources (Fig. S1). El Buitre tailings deposit is located in the vicinity of sector IV, in the lower part of the sub-basin of the Middle Copiapó River, specifically in Los Buitres and Los Diques sub-basins (Compañía Contractual Minera Candelaria, 2013). This region is characterized by an arid climate with an annual average temperature of 18.2 °C and an average annual accumulated rainfall of 22.5 mm/year for the period of 1998-2019. The months of June, July and August present the highest rainfall during the year. The record value in 24 hours was 92.3 mm during the month of December 1997, with a return period of 200 years. However, there is a considerable number of years with null precipitation, or that the totality of the annual precipitation was concentrated in one or two days of the year. The averages of maximum, and minimum absolute temperature values in the same period were -0.4 °C and 40 °C (Ministerio de Obras Públicas de Chile, 2020). Evaporation rates strongly exceed rainfall (Sistema de información integral de Riego, 2020).

At present El Buitre tailings deposit is closed, having been in operation from 1997 to 2005 and it has a total authorized tonnage of 6.6 Mt. After its closure, it was used until 2010 as an emergency dam, in case the active Las Cruces tailings dam, currently active and belonging to the Pucobre company, presented any inconvenience. Tailings in this deposit are the result of an alkaline flotation circuit (~ pH 10.5-11) designed for the recovery of copper ore concentrates. The plant processed ore deposits from the Punta del Cobre, Mantos del Cobre and Granate Mines, however there are no reliable records regarding which specific mines the ore rock came from. The Punta del Cobre mine extracts copper sulfides and oxides, while the Granate and Mantos del Cobre mines extract copper sulfides. The deposit of tailings was built by the downstream method, and the tailings were deposited in the form of slurry. According to the historical image of the deposit of tailings (Fig 6a), multiple outfall deposition (spigots) was the deposition method used. At least 3 discharge points are observed along the dam wall in the eastern and central sector of the deposit. In addition, the tailings were not treated with amendments or any remediation technology. However, it has a 30 cm thick layer of coarser tailings fraction (separated by hydrocyclones) on the surface to avoid its dispersion by wind.

CHAPTER 3

3 SAMPLES AND METHODS

3.1 SAMPLING AND FIELDWORKS

All samples were collected in two campaigns during the summer to reduce any heterogeneity caused by climatic conditions. Eight cores up to depths of 4 m were taken with a hand auger, and twenty-four cores at different depths (1-49 m) were taken by sonic drilling. The depth in each core depended on the geometry of the deposit of tailings. Undisturbed samples were obtained by sonic drilling, and color, moisture, grading and degree of alteration and oxidation, with emphasis on sulfide contents were recorded in situ (Fig. 6a). A total of 755 samples were obtained from 1 m sample composites obtained from 755 m of core. These were sealed in plastic bags and stored in ice-packed cooler boxes (8 °C), for later analysis. For the geochemical analysis samples were oven-dried at 30 °C and homogenized in the Mining Sustainability Laboratory of the Chile University.

Of the twenty-four cores collected for the geochemical and mineralogical characterization study of El Buitre tailings deposit, five cores were selected near the material discharge area (Sector 1), four cores from the central area (Sector 2) and three cores from the most distal area of the dam wall (Sector 3) (Fig. 6b), for the microbiological analysis. A total of 98 samples were analyzed through the depth profile, which were distributed as follows: 52 samples in the oxidized zone (< 5 m) and 41 samples in the non-oxidized zone (including the pyrite and apatite enriched zone) within the different sectors (> 5 m). The samples were collected using sterile zip-lock plastic bags and transported in a cooler box at 4 °C for further analysis.

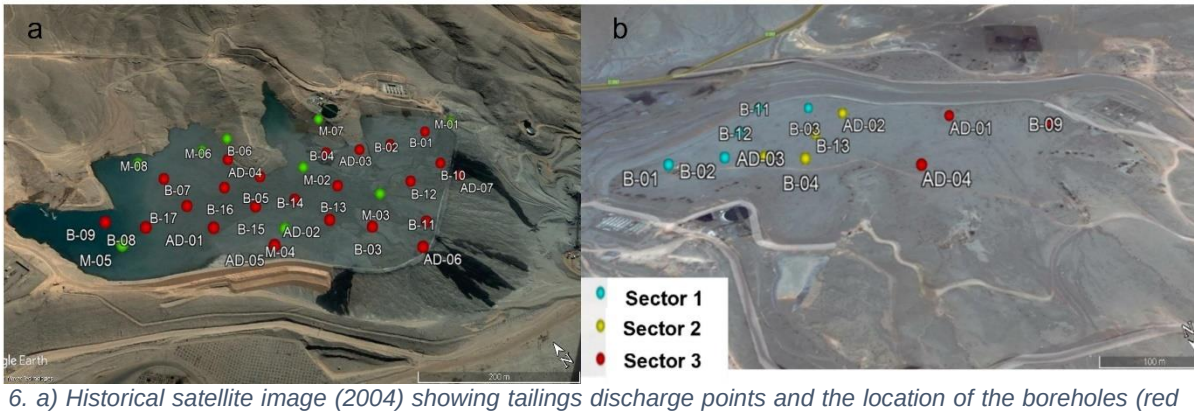

Fig. 6. a) Historical satellite image (2004) showing tailings discharge points and the location of the boreholes (red spots = sonic drilling and green spots = hand auger); b) Satellite image showing the location of the boreholes for microbiological analysis (red spots = samples located in sector 3 (far from dam), yellow spots = samples located in sector 2 (central sector) and cyan spots = samples located in sector 1 (discharged point).

3.2 PHYSICOCHEMICAL PARAMETERS

Paste pH was measured according to (Tremblay and Hogan, 2000) using a HI-5222 Hanna pH meter, equipped with a HI-1053B electrode. The pH meter was calibrated every 30 samples with certified standard reference solutions (HI7004L/C and HI7007L/C). In addition, duplicates were analyzed every 10 samples. In addition, particle size distribution of a representative sample composite was performed by Cisa Ro-Tap sieve shaker at ASMIN industrial laboratory, Santiago, Chile. The hydraulic conductivity was measured by a constant-head method for the laminar flow of water through granular soils following the ASTM D2434 procedure. The visual inspection of the drill cores allowed to qualitatively differentiate between the dry and wet tailings samples. This information was used to define a "moisture horizon" that could be defined by the depth at which wet tailings samples are unequivocally identified in each drill core.

3.3 GEOCHEMICAL METHODS

3.3.1 Total digestion

The 755 samples collected from 1 m sample composites were completely digested using a 4 acids digestion procedure (HNO_3+HF+$HClO_4$+HCl). A total of 59 elements were measured by ICP/MS (Perkin Elmer Elan, 9000) with detection limits as indicated in Supplementary material, Table S1. One blank was run for every 40 samples, and an in-house control was run every 20 samples. For every 15 samples, a digestion duplicate was analyzed. In addition, digested standards and instrument recalibration were run every 80 samples. All the sample digestions and analyses were performed by Actlabs, an accredited laboratory at Coquimbo, Chile.

3.3.2 Sequential extraction

The sequential extraction was performed by AGQ Laboratories, Santiago, Chile, following the procedure defined by Dold and Fontboté (2001) with the objective to study element speciation in the deposit of tailings. Three boreholes (B-04, B-13 and AD-02) located in the eastern and central sectors were selected with the objective of studying element speciation to the deepest zones of the deposit. A total of 17 composite samples every 2 m were selected from the most superficial, intermediate, and deep zones of the deposit. The depth ranges were selected, taking as criteria mineralogical changes detected from the detailed analysis of the boreholes core and variations in the geochemical data with depth. The first four extractions allowed to separate the mobilized elements and secondary minerals. The last three stages allowed to separate organic material, secondary and primary sulfides, and silicates. For more details on the physical and chemical treatment of the samples and the main dissolved minerals in each step, see Table S2. The solutions were analyzed by Inductively Coupled Plasma Atomic Emission Spectroscopy (ICP-OES) with detection limits indicated in Table S3. Saturation index (SI = logIAP – logK; IAP = ion activity product) of gypsum with respect to water soluble fraction element concentrations were calculated using PHREEQC version 3.6.2-15100 and the paste pH value was used as a reference.

3.3.3 Geochemical characterization of the soluble fraction

The paste pH of the solid samples was measured following the protocol describe by (Tremblay and Hogan, 2000) and using a HI-5222 Hanna pH meter equipped with a HI-1053B electrode.

Before the elemental composition analysis, tailings samples were oven-dried at 30 °C and homogenized. The soluble fraction (bioavailable) of the tailings samples was extracted using deionized water. It was used 1.0 g sample into 50 ml deionized water and shake for 1 h. A total of 63 elements (Ca, K, Mg, Na, S, Fe, Al, P, Sr, Ba Br, Cu, Li, Mn, Se, Mo, Zn, Ce, Co, Cs, Ga, Ge, La, Nb, Nd, Ni, Pb, Pr, Rb, Re, Sb, U, Ti, Tl, Zr, Au, Ag, As, Er, Eu, Gd, Hf, Hg, Ho, In, Li, Lu, Sc, Sm, Sn, Ta, Tb, Te, Th, Tm, Be, Bi, Cd, Dy, V, W, Y, Yb) from the soluble fraction of each sample were analyzed by Inductively Coupled Plasma Atomic Mass Spectroscopy (ICP-MS). Commercial analytical package (LH101 analysis for geochemical selective or sequential leaches) with detection limits as indicated in Supplementary material, Table S4. For quality control a blank and an in-house control was running every 15 samples and every 20 samples, respectively. All samples were analyzed in Bureau Veritas Laboratories, Vancouver, Canada.

3.4 MINERAL CHARACTERIZATION METHODS

A total of 340 composite samples every 1 m were analyzed by X-ray diffraction (XRD). Samples located in the closest and most distal zone of the dam wall, and in the central zone of the deposit of tailings were analyzed. In addition, samples belonging to different depth ranges were selected, taking as criteria mineralogical changes detected from the detailed analysis of the boreholes core and variations in the geochemical data with depth. These selection criteria were also used for all other mineralogical analyzes. Homogenization and micronisation of the tailing's particles were carried out to obtain grain sizes of less than 10 microns. The mineralogical composition was determined using a Bruker® D8 Endeavor X-ray diffractometer with a tube with cobalt radiation. Diffractometer settings were: 35 kV, 40 mA and a scan range of 3–70° 2θ, 0.02° 2θ step size, and 5 s counting time per step. The obtained diffractograms were analyzed using the software DIFFRAC. EVA® version 4.2 and DIFFRAC.TOPAS® version 5.0. The Powder Diffraction File™ (PDF-2 2001) database was used for phase identification. Spectra standard of corundum was used for semi-quantification of mineral phases. Besides, QA/QC was performed by analysis of duplicates and X-ray fluorescence. In addition, clay minerals from 202 composite samples every 1 m were characterized following USGS protocol (U. S Geological Survey Open-File report OFR01-041 2000). The < 2 µm fraction was separated by centrifugation and the samples were analyzed by XRD before and after heat treatment. The semi-quantification of clays was carried out with spectra standards of montmorillonite, kaolinite and illite. XRD analyzes were performed by Geomaq Limitada, an accredited laboratory at Antofagasta, Chile.

A total of 100 composite samples every 1 m were prepared in polished thin sections of tailings and analyzed by optical microscopy Olympus model BX51, using reflected-light mode to identify opaque minerals in the tailings assemblage. The mineral composition was determined by the count point method at 350 equally spaced points across the thin sections. In addition, photomicrographs were obtained to complement the observations. This analysis was made in the Minerals Laboratory of the Mining Department of the Chile University. In addition, semi-quantitative element

composition was studied by Quantitative Evaluation of Materials by Scanning Electron Microscopy (QEMSCAN) combining information generated by the retro dispersed electrons (for imaging) and X-ray dispersive energy spectra (EDS) for chemical composition. A total of 150 composite samples every 1 m were analyzed. The Bulk Mineral Analysis (BMA) measurement method was used to provide statistically abundant data for mineral identification, speciation, distribution, and quantification. This analysis was performed by SGS minerals, Chile.

3.5 BIOLOGICALS ANALYSIS

3.4.1 Cell counting

A suspension was prepared by adding 100g of tailings in 100 ml of 0.06M EDTA buffer and sonicated for 2 min. This process was repeated two times to release the adsorbed cells on the mineral surfaces and to dilute and eliminate by chelation of metal(loid)s (Liu et al., 2019). Subsequently, the same procedure was repeated adding 20 mL acidic water / 0.05M ascorbic acid. The suspension was used for cell counting. The number of cells in the solution was counted in a Petroff-Hausser counting chamber (Hausser Scientific, Horsham, PA, USA) with a microscope (CX31, Olympus, Japan). The cell counting procedure is illustrated in Fig. S1 of the supplementary material.

3.4.2 DNA extraction

The DNA extraction process was carried out in several stages. The first stage consisted of separating the cells adhering to the mineral surface using two reagents, 0.06 M EDTA buffer and a solution of acid water/0.05 M ascorbic acid. Each selected tailings sample (100g) was suspended using 100 ml and 20 ml of the reagent (buffer or acid, respectively) and sonicated for 2 min. Subsequently, the suspension was transferred to a sterile filtration unit, with a 0.22 µm Durapore membrane to concentrate the cells. This step was performed twice to ensure the maximum possible cell extraction and concentration.

The second stage describe the DNA extraction: 1) 2 ml of buffer STE was added to the membrane and 0.5 g of chitosan was added to the tube and the mixture was vortexed. 2) A 1 ml aliquot was removed from the falcon tube and transferred to an Eppendorf tube and centrifuged at 17,000 G for 7 minutes at 23 °C. 3) Thereafter, the supernatant was eliminated, and the pellet was treated adding 2 ml Buffer STE and steps 2 and 3 were repeated 3 times. 4) The cells were then resuspended in a mixture of 200 µL of STE buffer, 10 % PEG, 5 % SDS and 20 % Sucrose. Then, Proteinase K and lysozyme were added up to a concentration of 1mg/mL and of 5mg/ml, respectively. The mixture was incubated at 37 °C and vortexed every 10 minutes for 1 hour. 5) The samples were frozen at -80 ° C for 15 minutes and thawed in a thermoregulated bath at 37 °C for 1.5 minutes, this procedure was repeated 2 times. Then, 200 µL of phenol was added, vortexed vigorously for 2 minutes and centrifuged at 17,000 G for 5 minutes at 4 °C. Thereafter, 250 µL of aqueous phase were transferred to a 1.5 ml Eppendorf tube and 30 µL of 3 M sodium acetate (pH 5.2), 50 µL of TE buffer and 125 µL of chloroform-isoamyl alcohol were added and shake by

inversion and centrifuged at 17,000 G for 5 minutes at 4 °C. The aqueous phase was transferred to a clean tube and, once more, 50 µl of TE buffer and 125 µl of chloroform-isoamyl alcohol were added and shake by inverting 6 times and centrifuge at 17,000 G for 5 minutes at 4 °C. 6) Promega Wizard® Genomic DNA Purification Kit was used to purify the DNA and the products were quantified using Picogreen dsDNA reagent by fluorimeter.

3.4.3 16 RNA amplicon sequencing

Amplification of the 16S rRNA gene region V3 and V4 was performed using the following primers: PCR forward 515F (5'-TCG TCG GCA GCG TCA GAT GTG TAT AAG AGA CAG CCT ACG GGN GGC WGC AG- 3') and 806R (5'-GTC TCG TGG GCT CGG AGA TGT GTA TAA GAG ACA GGA CTA CHV GGG TAT CTA ATC C-3') (Caporaso et al., 2011).

The sample preparation for PCR was performed following the protocol described by (Caporaso et al., 2011). The PCR program included an initial denaturation step of 94°C for 3 min, with amplification proceeding for 35 cycles at 94 °C for 45 s, 50 °C for 60 s, and 72 °C for 90 s; followed by a final extension of 10 min at 72 °C. Purified amplicons were quantified using Picogreen dsDNA reagent in 10 mM Tris buffer (pH 8.0). Then, a composite sample for sequencing was created by combining equimolar ratios of amplicons from the individual samples, followed by the removal of contaminants (Caporaso et al., 2011). Additionally, we used PhiX, FC-110-3001 library as a calibration control to examine the overall performance of sequencing. Finally, sequencing was performed on an Illumina MiSeq, using a 300 cycles paired-end approach at Codelcotech (Santiago, Chile).

3.6 STATISTICAL ANALYSIS

3.6.1 Statistics applied to geochemical, mineralogical analysis and geostatistical modeling

The database of total digestion and sequential extraction was filtered and adjusted according to the following criteria. 1) All the values below the detection limit (LOD) were changed according to the values resulting from dividing the specific detection limit value by the square root of 2 (Hites 2019). 2) Variables with more than 50 % of data under the LOD was not suitable to be included in any statistical analysis and was eliminated. 3) The normality of the data was evaluated by the Kolmogorov-Smirnov tests. Due to the non-normal distribution of the dataset, the transformation to normal logarithm was performed. 4) Alpha was set at 0.05 for interactions. The mean value of chemical data (as the dependent variable) concerning different depths was analyzed using one-way factorial ANOVA and Welch t-test. Tukey's and Dunnett T3's multiple comparisons procedures by homogeneous and non-homogeneous variables were performed.

A Principal component analysis (PCA) was carried out by means of a Pearson's correlation matrix (0.05 significance level, 2-tailed test) on all validated variables in order to define the main element associations and the reflected mineralogical variations, for the interpretation of processes such as weathering or to characterize variations of origin. This analysis is also used to interpret these associations in terms of geochemical processes by comparing their patterns with other analytical determinations (sequential extraction, mineralogical characterization, and geostatistical

model). PCA discovers linear combinations of the variables based on measures of association and, it allows the reduction of dimensions for a complex multi-element dataset. The results are graphed in a biplot. It is a plot of the PC loadings for each variable with the loadings of each sample along two sets of PC axes (Abraitis et al., 2004). Evaluation of the chemical data, PCA analysis and one-way ANOVA was performed using ioGAS 7.3 and IBM SPSS Statistics 25 software, respectively.

The estimation of the grades in the deposit of tailings was carried out using interpolation by co-kriging. This method allows modelling the grades in the deposit based on drill core depths and considering together all the grades of the study and the spatial continuity through variographic analysis. Due to the lack of information of the previous underlying topography the tailings, the tailings bottom surface was modeled by kriging the length of the drill cores at the studied domain. The estimation of the bottom surface was performed as follows: 1. the bottom surface was defined to estimate the total volume of the restricted modeled area (Kokkola, 1986); 2. the bottom surface of the whole the deposit of tailings was restricted by the dam structure, to estimate the total volume of the deposit (Parviainen, 2009). The total resources of Co, Cu, light rare earth elements (LREE), heavy rare earth elements (HREE), Fe, S, Ca, P and Al were estimated using a 3D block model and a discretization cell of 3 m x 3 m x 2 m (Deutsch and Journal, 1997). This model was arranged according to a sampling grid with horizontal distances of five meters and depth intervals of one meter (block size of 5 m x 5 m x 1 m) resulting in a total of 1,800,000 blocks. The validation of the models was carried out by cross validation with the chemical data. The modelling workflow was performed by the method proposed in (Parviainen et al., 2020). This methodology takes into consideration the difficulties in defining the topography of the abandoned tailings and the anisotropy generated by the greater length of the horizontal direction than the vertical direction. Multivariate modelling was performed using the ANDES software (Soto et al., 2017).

3.6.2 Statistics applied to microbiological analysis

The taxonomy assignment of the sequences generated by Illumina MiSeq amplicon sequencing of the V3-V4 region of the 16S rRNA gene were done using R version 4.1. Operational taxonomic units (OTUs) were obtained as follows: the QIIME software was used for the identification and filtering of chimera sequences (Usearch 61). Then, the sequences were clustered with 97 % similarity (Uclust). The choice of the most abundant sequences of each cluster was made. Finally, the taxonomic assignment of representative sequence was performed against the Silva version 128 database (https://www.arb-silva.de). The resulting taxonomy and read-count tables constructed in QIIME were imported into phyloseq for downstream analysis.

.

3.6.1 Bacterial α-diversity

The taxonomy, OUT table and chemical data (metadata include the sample ID) were merged and converted into a phyloseq object. The unassigned, mitochondria and chloroplast were eliminated. Then, in order to standardize the samples and facilitate comparisons of alpha diversity, rarefraction was performed. Rarefaction curves were created using the rare curve function ggrare (CRAN.R-project.org/package=ggplot2). Chao1, Observed and Shannon diversity index were measure using

the function “trans_alpha class” and the differences along the depth profile were tested using the Kruskal Wallis test and ANOVA test with multiple comparisons. The relative abundance of the high abundant genera was analyzed using the function trans_abund and the unique and shared OTUs between the studied depth ranges were analyzed by Veen diagram using the function trans_venn class. All these functions were within the “microeco package” and “file2meco package”. In addition, the abundance-prevalence relationship were determined using the package “ggrepel”.

3.6.2 Bacterial β-diversity

Bacterial β-diversity was also analyzed using the microeco and file2meco packages. The distance matrix of beta diversity can be transformed and plotted using trans_beta class. The compositional dissimilarity between different sites were measured using Bray-Curtis dissimilarity based on the relative abundance of OTUs. Adonis function in the R package vegan was used to perform a PERMANOVA test, which allows assessing differences in composition between groups. While permutational tests of homogeneity of multivariate dispersions (PERMDISP) was used to measure differences within each group, with betadisper function from the R package vegan v2.4-1. The structure of the bacterial community in the deposit of tailings was visualized using principal coordinate analysis. Differential abundance test was used to determine the significant taxa and the community differences across groups. DESeq2 v1.24.0 package was used to test whether bacterial taxa were differentially abundant along the depth profile. Finally, the function trans_diff class can calculate random forest (Beck et al., 2014) by bootstrapping using the significant features. MeanDecreaseGini was selected as the indicator value in the analysis. The correlations (Pearson correlation) between environmental variables and significant taxa (determined by the differential abundance test and random forest analysis) were analyzed inferring the factors affecting community structure. The correlation results were visualized using heatmap (package microbiomeSeq).

3.6.3 Chemical data

Differences in physicochemical data were visualized using one way ANOVA with Welch's correction (Welch test) for non-homogeneous samples. In addition, Tukey’s and Dunnett T3’s multiple comparisons procedures by homogeneous and non-homogeneous variables were performed.

3.6.4 Prediction of the functional potential

Phylogenetic Investigation of Communities by Reconstruction of Unobserved States 2 (PICRUSt2) (https://github.com/picrust/picrust2) software, was used to predict the metagenome functional content from the sequence data.

CHAPTER 4

4 RESULTS AND DISCUSSION

4.1 GEOCHEMICAL, MINERALOGICAL AND GEOSTATISTICAL MODELLING OF AN IOCG TAILINGS DEPOSIT (EL BUITRE, CHILE): IMPLICATIONS FOR ENVIRONMENTAL SAFETY AND ECONOMIC POTENTIAL

4.1.1 Tailings morphology and physical and hydraulic main characteristics

Modelling the tailings' depth and current surface topography is very important to properly estimate the tailings precise volume for future revalorization and reprocessing studies. It is also important to control the physical stability of a future operation because it will control the formation of a ditch network eroding the tailings surface (Parviainen et al., 2020). The thickness of the deposit of tailings was determined from the drill holes, taking into consideration that the surface topography was quite regular, and the deepest areas were delimited by coarse sand and gravel and by a waterproof membrane of high-density polyethylene in the area the dam wall. The deposit's thickness varies from one to 49 m. The deepest parts of the tailings are in the eastern and central parts of the deposit of tailings (Fig. 7b), following the original shape of the valley basin where the tailings were deposited. In the western area, the depth tends to decrease, ranging from 1 to 25 m (Fig. 7b). From a sedimentary perspective, visual field observations showed that the tailings deposit is comprised by alternating fine sandy to clayey-silty layers. Particle size analyses of a composite sample from one drill hole showed that the cumulative passing curve is ranging from 1 to 300 µm, and d*80* is 40 µm (Fig. S2 a and b). This distribution of particle size is in agreement with the milling stages required for the flotation process in tailings with similar characteristics (Medina et al., 2019). Please notice that, although this grain size distribution curve can be useful for a general understanding of the tailings deposit, it does not provide detailed information about the grain size distribution within the specific horizontal layers observed along the tailings depth profile. The proportion of sand and clay changes with borehole depths and with their locations respect the dam wall. The first five meters of depth are typically more sandy, whereas the intermediate zone (5-17 m) presents intercalations of sand-clay-sized material, and the deepest zone (> 17 m) is mainly clayey (Fig. 7c). This particle size distribution has a direct impact on the hydraulic conductivity of the deposit of tailings (Fig. 7c), resulting on low hydraulic conductivity $K = 1.3 \times 10^{-6}$ cm/s for the deepest layer and higher hydraulic conductivities (in the order of 10^{-4} cm/s) for the more surficial layers (0-17 m). To illustrate the distribution of the moisture horizon within the deposit of tailings, an iso-piezometric map was made. It shows how this horizon is deeper towards the central sector of the deposit of tailings, in the area more distal to the streams located northeast and northwest of the deposit of tailings (Fig. S3). On the other hand, the moisture content within the deposit of tailings appears not to be influenced by the presence of groundwater. According to groundwater level monitoring and quality control wells located in El Buitre sector (Fig. S4), the confined aquifer is found at a depth greater than 125 m (the maximum tailings depth is 49 m). Besides, the Alcaparrosa well located in the vicinity of El Buitre sector, has diminished

by 40 m in the period 1998-2008, as a result of agricultural activities in the area. Additionally, the recharge of the aquifer by natural processes is complex, since the potential evaporation considerably exceeds the precipitation, causing the net recharge to tend to zero. Therefore, groundwater recharge occurs during wet years. According to the record of the last 40 years of the Copiapó Weather Station (1971-2011), it is estimated that the recharge is between 5 to 12 mm/year (considering a recharge rate of 10 %) (Compañía Contractual Minera Candelaria, 2013).

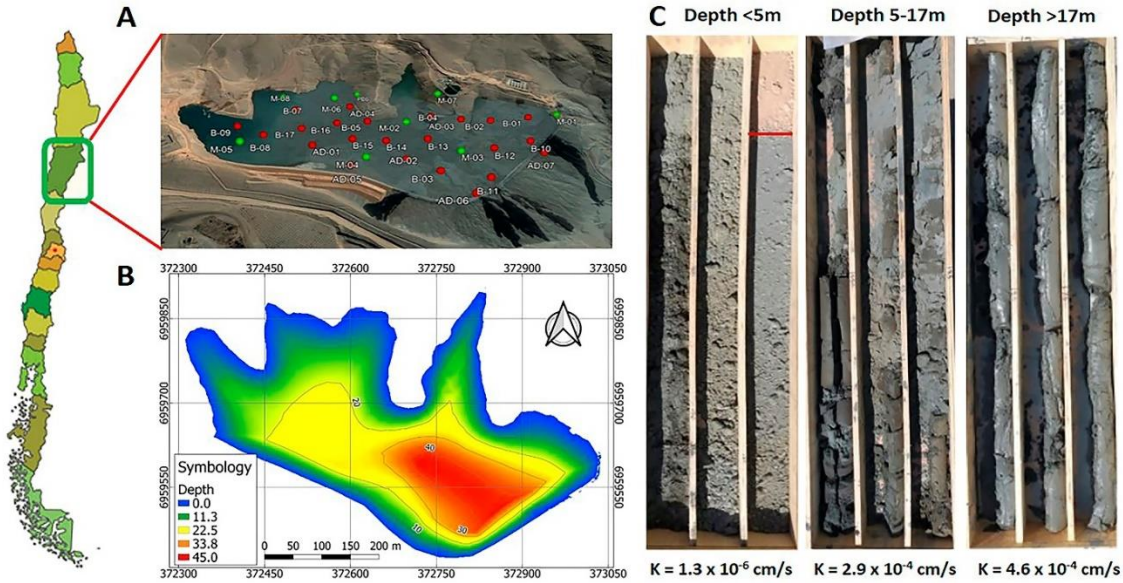

Fig. 7. a) Historical satellite image (2004) showing tailings discharge points and the location of the boreholes (red spots = sonic drilling and green spots = hand auger); b) depth spatial variation within the deposit of tailings; c) representative tailings core sample boxes of different depth ranges. The first box on the right shows a light brown layer that corresponds to coarse tailings fractions used to avoid wind borne dispersion.

4.1.2 Mineralogical characterization

The mineralogical composition of the tailings is quite homogeneous, most samples are similar in mineral composition and abundance. XRD shows that quartz, chlorite, alkali-feldspar (microcline and orthoclase), plagioclase and magnetite are the main mineral constituents, whereas other minerals like hematite, calcite, pyrite, and gypsum-anhydrite appears as minor mineral constituents of the deposit of tailings (Fig. 8 and Fig. S5). Illite, chlorite, and kaolinite were the typical minerals in the clay fraction < 2 µm. Additionally, QEMSCAN analyses (more reliable than XRD analyses for minerals with wt % lower than 1 %) show that muscovite, biotite, tourmaline, rutile, apatite, amphibole, sphene, pyroxenes, ilmenite, epidote, dolomite/ankerite and garnet could be considered as trace constituents (Table S5). Also, the QEMSCAN study revealed that chalcopyrite is the main Cu-bearing mineral (ranging from 0.163 wt % to 0.02 wt %), whereas other minerals like chalcocite/digenite, enargite/tennantite and malachite/azurite can be considered negligeable, with and abundance lower than 0,0001 wt % (Fig. S6).

The relative abundance of magnetite (Fig. 8b), orthoclase and microcline (Fig. S5 c and h) do not significantly change with depth. Therefore, they are homogeneously distributed in the deposit of tailings and alkaline-feldspar probably does not act as neutralizing agent. In contrast, pyrite and calcite (Fig. 8a and e) progressively increase their abundance with depth, moving from values around 1.5 wt % and 2.5 wt % on the tailings surface to values around 3.5 wt % and 7.5 wt % in the deepest layer, respectively. This trend might be the result of pyrite oxidative leaching and acidity generation at the most surficial part of the tailings (where scarce rainwater reaches) followed by calcite dissolution and leaching solution neutralization. In accordance with that, the tailings showed a mean paste pH of 7.9, with values consistently ranging from 7.78 to 7.95 (Fig. S2c). On the other hand, the gypsum content remains practically constant with depth, however, it decreases significantly in the depth range of 12-14 m. (Fig. 8d). This gypsum distribution is in accordance with aforementioned pyrite oxidation and leaching process and neutralization of acid solutions by calcite. Apatite shows relative abundances significatively higher for the deeper samples (in the range of depths of 6-10 m and 12-14 m) than the shallower samples (Fig. 8c). This distribution could be attributed to the gravitational deposition of apatite particles in the deposit of tailings.

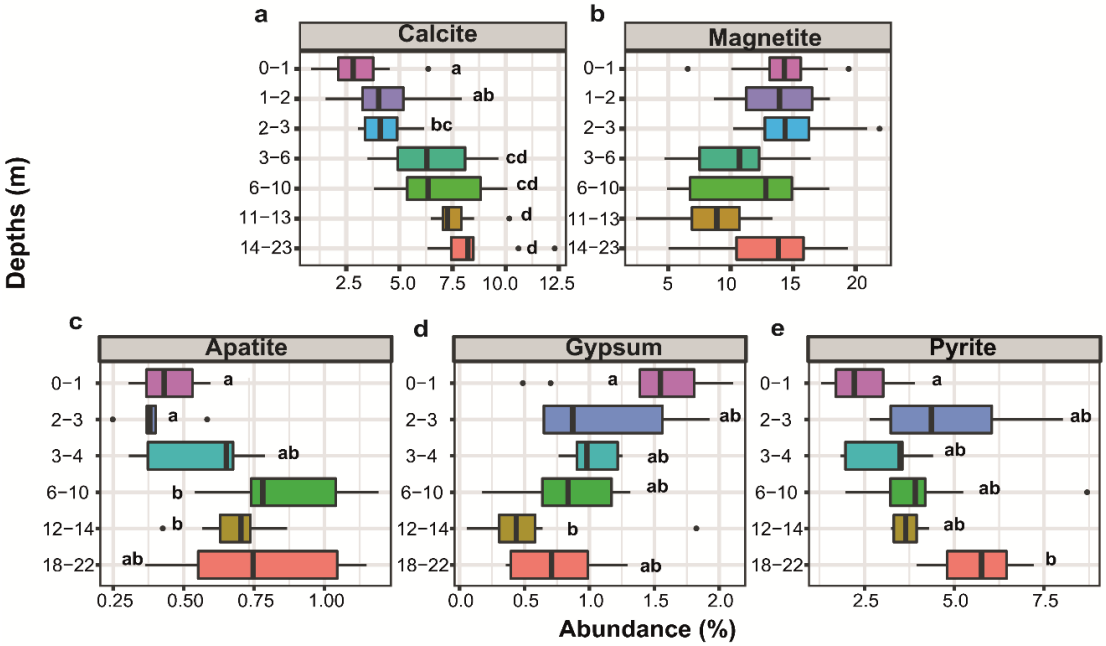

Fig. 8. Mineralogical characterization of major minerals (calcite and magnetite) by XRD (340 samples) and minority minerals (pyrite, gypsum, and apatite) by QEMSCAN (150 samples) in samples at different depths. The lowercase letters on the graph represent a one-way ANOVA analysis. Different letters indicate that there is a significant difference between the relative abundance of the mineral at a certain depth. On the contrary, the same letters indicate that there are no significant differences. Minerals without letters indicate that the relative abundance of the mineral does not present significant differences in any of the analyzed depths.

Complementary to the XRD study, the examination of polished sections showed that the sulfide assemblage is dominated by pyrite (ranging from 1.2 to 8.7 wt %), which is little fractured and disturbed in the oxidation zone, not showing Fe (III) oxyhydroxides rims or coatings (Fig. 9a). Low alteration of the sulfide assemblage in neutral tailings has been reported by Dold and Fontboté 2002; Lindsay et al., 2009b. Chalcopyrite and sphalerite are present as trace minerals and do not show replacements. Chalcopyrite is associated with magnetite, sphalerite, and pyrite (Fig. 9a and

f). Supergene Cu-sulfide were not identified by petrographic microscopy and QEMSCAN analysis indicated that these minerals are below 0.0001 % in abundance. The oxide assemblage is dominated by magnetite and hematite, and trace amounts of specularite, goethite, and ilmenite. Hematite in the form of specularite has been described by Marschik and Fontboté (2001). Magnetite is partially replaced by hematite (Fig. 9c) and goethite at the edges and fractures, and hematite is partly replaced by goethite. In addition, magnetite is commonly associated with ilmenite, hematite, and chalcopyrite (Fig. 9b, e, and f). The replacement of magnetite and hematite by goethite at the edges can occur for oxidation reactions in the deposit of tailings. On the contrary, the pervasive magnetite alteration to hematite and magnetite and hematite alteration to goethite (Fig. 9c and d) can be attributed to hydrothermal alteration processes within the deposit of origin.

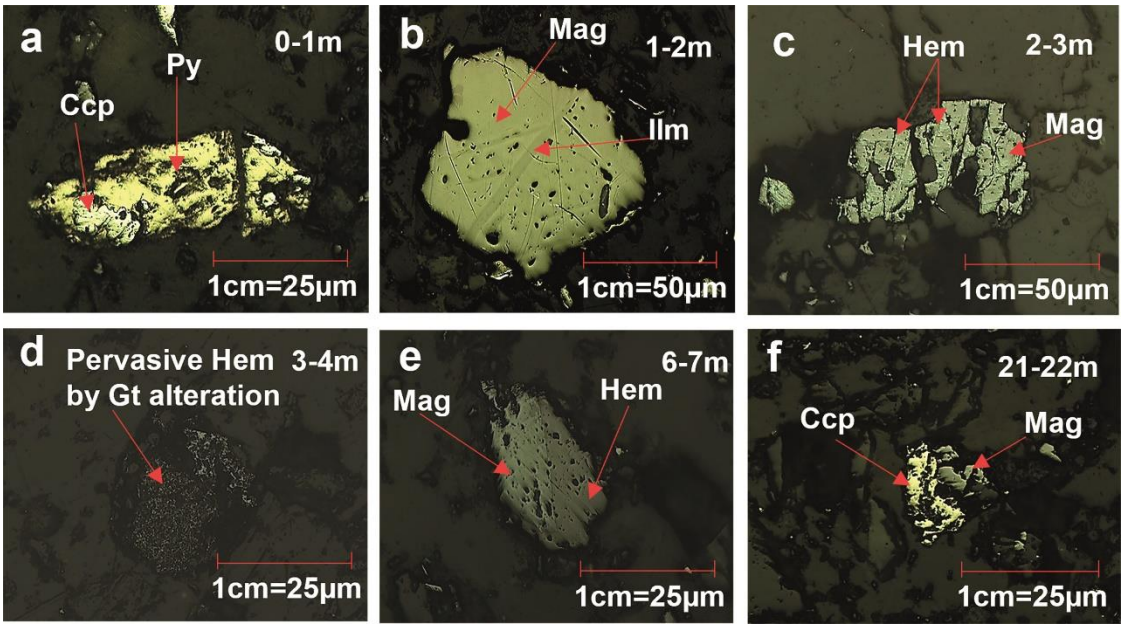

Fig. 9. Mineralogical characterization by petrographic microscope in samples with different depths. A) Pyrite-Chalcopyrite (Py-CCp) association, b) Magnetite (Mag) with ilmenite (Ilm) bands, c) Mag partially replaced by Hematite (Hem) at the edges and fractures, d) Pervasive Hem by Goethite (Gt) alteration, e) Mag-Hem association and f) CCp-Mag association.

4.1.3 Geochemical and Geostatistical characterization

The original database of 59 elements (Table S6) was reduced to the 31 elements presented in Table 1. In addition to the previous filters carried out before the statistical analysis, some immobile elements with very low concentrations were eliminated (Ba, Cd, Cr, Hg, Hf, Nb, Rb, Sb, Se, Sr, Ta, Te, Tl, Zr). REEs was divided into LREE and HREE to improve the visualization of the data distribution patterns and because of the very different commercial value of both groups. Table 1 summarizes the geochemical composition and the univariate statistics of the tailings. As expected from its mineralogical composition, the bulk chemistry of the tailings is mainly comprised of Fe, Si, Al, Ca, S and P, which is in accordance with the geochemical analyses of similar IOCG deposits in this region (Medina et al., 2019; Sernageomin, 2020b).

Taking as reference grades reported for ore deposits and deposits of tailings worldwide, it is possible to indicate a significant content of some value elements e.g., Co (103 ± 32 mg/kg), Cu (795 ± 514 mg/kg), and REEs (337 ± 118 mg/kg). In addition, it is necessary to take into consideration that due to the energy and infrastructure savings associated with the reprocessing of tailings, it is possible to exploit lower elemental ore grades (Parviainen et al., 2020). Mud and Jowitt (2018) reported Cu grades from 0.18 to 1.5 wt % in ore deposits around the World. While economic recovery of Cu has been reported in Minera Valle Central (Rancagua, Chile), a company that reprocesses fresh tailings from El Teniente mine and old mine tailings from the Cauquenes tailings deposit with Cu grades from 0.1 wt % - 0.25 wt % (Henderson, 2018). Regarding Co grades of ore deposits around the World, Mudd et al., (2013) reported values ranging from 0.019 to 0.24 wt %. While in the case of REEs, deposits ion adsorption clays contain REOs from 0.02-1 % (Su, 2009). On the other hand, some pollutants elements e.g., As (38 ± 12 mg/kg) and Pb (12 ± 6 mg/kg) are present in considerable concentrations in the solid fraction and their solubilization could represent an environmental risk.

A geostatistical model (using a 5 m x 5 m x 1 m block model, a total of 1,800,000 blocks) was made to facilitate the interpretation and visualization (3D) of the bulk chemistry spatial variations within the tailings (Fig. 10 and Fig. S7). In addition, it allowed to evaluate the tailings as a "secondary ore deposit", by modeling some critical elements, e.g., Cu, LREE, HREE and Co (Fig. 10). Variographic analysis and validations of the model can be found in Fig. S8 and Fig. S9.

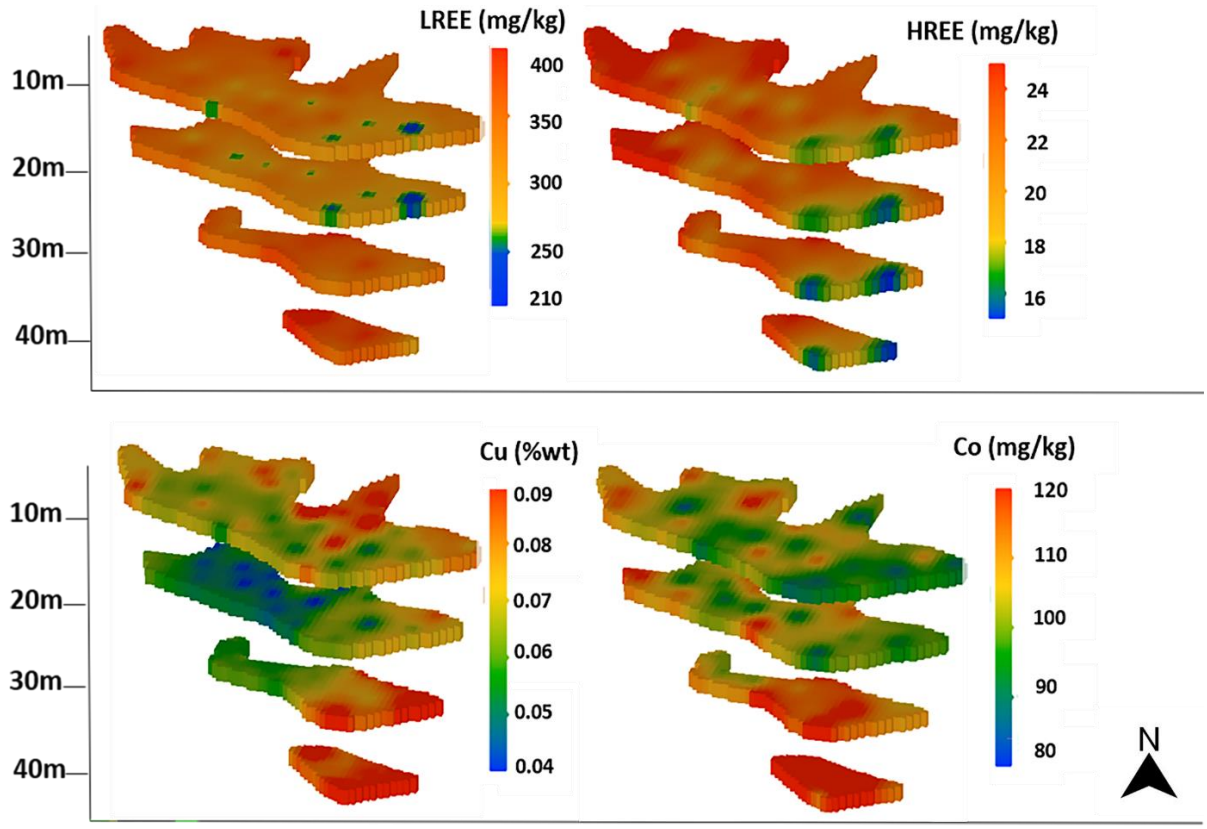

Fig. 10. Spatial distribution of LREE, HREE, Cu and Co grades in the deposit of tailings according to the block model. All 3D views were separated into sections at every 10 m depths to facilitate data visualization.

Table 1 Univariate statistics for selected elements of the tailings with Min., Max., Mean, Median, standard deviation (SD) and percentiles (25, 50, 75 and 95). Major elements in wt.-% and minor and trace elements in mg/kg [ppm]. The concentrations correspond to the total digestion analysis (N= 755 samples).

	Min.	Max.	Mean	Median	SD	Percentiles			
Major						25.0	50.0	75.0	95.0
Fe	9	26	16	15	2	14	15	17	20
Al	1	10	5	5	2	4	5	6	8
Ca	2	6	3	3	1	2	3	3	4
Mg	1	5	2	2	1	2	2	3	3
Si* (XRF)	0.2	3	2	2	0.4	1	2	2	2
K	0.7	5	2	2	0.4	2	2	3	3
S	0.2	3	2	2	0.4	1	2	2	2
Na	0.3	2	0.9	0.9	0.3	0.7	0.9	1	2
Ti	0.1	1	0.3	0.3	0.1	0.2	0.3	0.3	0.3
P	0.1	0.2	0.1	0.1	0.0	0.1	0.1	0.1	0.2
Minor									
Cu	227	4290	795	647	514	433	647	990	1790
LREE	67	800	315	306	110	234	306	373	520
V	62	579	108	105	29	91	106	121	150
Co	25	303	103	100	32	83	100	120	158
Trace									
Ni	28	178	79	76	22	63	76	93	121
Zn	35	196	63	60	18	50	60	71	93
As	1	107	38	37	12	30	37	43	59
Li	14	79	30	26	10	22	26	33	52
Ga	14	41	24	25	5	19	25	28	32
HREE	10	44	22	22	5	18	22	25	30
Pb	2	38	12	11	6	8	11	16	24
W	0	101	7	6	6	4	6	8	12
Th	1	9	3	3	1	3	3	4	5
Sn	1	18	3	2	2	2	2	3	5
Cs	1	7	2	2	1	1	2	2	3
U	1	3	2	2	0.3	2	2	2	2
Ag	0.1	4	1	1	1	1	1	1	2
Mo	0.1	4	1	1	1	1	1	1	2
Be	1	3	1	1	0.3	1	1	1	2
Ge	0.1	2	1	1	0.4	0.3	1	1	1
Bi	0.1	4	1	1	0.3	0.4	1	1	1

Based on the block model, some general trends for the mineral forming elements can be observed. The Fe concentrations distinctly increases from West to East and from top to bottom (Fig. S7). On the other hand, Al and Ca concentrations tend to decrease from West to East in all depths, clearly displaying the lowest concentrations at the dam wall proximity (Fig. S7). Sulfur, and phosphate to a lower extent, show a tendency to increase with depth (Fig. S7). Regarding the modelled grades for some selected critical elements (Fig. 10), a modelled mean grade for LREE of 324 mg/kg (ranging from 209.1 to 524.2 mg/kg) was obtained. Some enriched layers (> 350 mg/kg) can be observed in the central and western sectors at all depths. However, the tailing's LREE concentration can be considered relatively homogeneous. On the other hand, HREE modelled mean grade is 21.5 mg/kg, ranging from 14.6 to 29.1 mg/kg, showing more significant grades increase on an east-western direction in all depths. Modelled Cu mean grade is 0.069 wt %, ranging from 0.037 to 0.157 wt %. The highest concentrations are found in the eastern sector at 30 m and at the bottom of the tailings (depth > 40 m, Fig.10). Finally, the modelled Co mean grade is 105 mg/kg (Fig. 10), ranging from 79 mg/ kg to 171 mg/kg, and clearly showing higher grades in the deepest levels (> 30 m).

It is important to take into account that the present geostatistical model is based on chemical data obtained from a high density sampling campaign (32 boreholes) that were drilled to the bottom of the deposit. This allows a reliable estimation of the grades and geometry of the deposit. Therefore, the results of the present study can be considered an excellent exploratory model to evaluate the economic potential of this waste. Based on the mean grades of the elements of interest and the lowest reported cut-off grades for tailings and deposits worldwide, a rough estimation of the total remaining resources for Cu, Co and REEs (Table 2) using the volume of the whole the deposit of tailings was made. It was considered a tonnage of 6.6 Mt (Sernageomin, 2021a). Additionally, Fe was included, because currently the Compañía Minera del Pacífico (Copiapó, Chile) produces pellet feed with tailings from the copper concentrator plant of the Compañía Contractual Minera Candelaria, with average Fe grades of 11.4 % (Compañía Minera del Pacífico, 2020). According to this estimate, the modeled mean concentrations of Fe and REEs present 100 % of the blocks above the cut-off grade (11.4 wt % and 0.02 wt %) and they represent 1.023 Mt and 0.00132 Mt of the reserve (Fig. S10). The modeled mean concentrations of Cu present an estimated 2.1 % of the blocks are profitable, with grades above the cut-off grade (0.10 wt %). While the average modeled concentrations of Co show 100 % of the blocks below the cut-off grade (0.19 wt %) (Fig S10). On the other hand, economic potential was calculated as the fraction of each value element in the tailings multiplied by the mass of the deposit and the metal price (Table 2). The price of REEs was 4,651,315 US/ton and it corresponds to the average of Eu_2O_3, Gd, Tb, Dy, Er, Y, La, Ce, Pr, Nd, Sm.

The results indicate a high economic potential for iron and REEs. In contrast, Cu and Co represent a low potential, because the modeled average grades are below the reference cut-off grades (Table 2). Parviainen et al, (2020) suggest considering tailings deposits as polymetallic deposits to increase their economic potential. However, the revaluation of tailings depends on other factors like metal price, element-bearing mineralogy for elements of interest, metallurgical recovery technologies, dimensions of the deposit of tailings (allowing scale economy), OPEX and CAPEX costs (Araya et al., 2020, Parviainen et al., 2020; Araya et al., 2021), among many other considerations. El Buitre tailings deposit can be considered small (6.6 Mt), which could limit its profitability. Nevertheless, adjacent to its location, there are other tailings deposits belonging to

the Pucobre company, with similar characteristics, that could be reprocessed together. Currently, the Compañía Minera del Pacífico extracts 3.5 Mton/year of Fe by magnetic separation from the deposit of tailings belonging to the Compañía Contractual Minera Candelaria. It has the potential to reprocess deposits of tailings located nearby, including El Buitre tailings deposit. Additionally, during the cleaning process and concentration of magnetic Fe could concentrate pyrite, chalcopyrite and apatite, therefore the extraction of Cu, Co and REEs as secondary products could be favored. The Compañía Minera Valle Central extracts Cu from tailings by froth flotation. Meanwhile, the Co associated with pyrite has been extracted by bioxidation-flotation and bioleaching of sulfidic tailings of iron mines (Ahmadi et al., 2015; Parbhakar-Fox et al., 2018). On the other hand, the possible association of REEs at different mineral phases e.g., phyllosilicates and apatites, could hinder their extraction. Araya et al., (2020) conducted a techno-economic feasibility study of industrial-scale REEs recovery from copper industry tailings, proposing chloride-based hydrometallurgical extraction technology processes as a potential alternative to traditional capital intensive hydrometallurgical processes based on high temperature and pressure (Onyedika et al., 2012). The study was carried out in Chilean tailings deposits with characteristics similar to El Buitre. They determined a net present value (NPV) to 20 years (income that an investment will generate in the future) of 672,987 USD, exceeding the initial investment cost taken as a reference (342,514,448 US$). In addition, the internal rate of return (IRR) that refers to the discount rate at which the NPV of future cash flows is equal to the initial investment, was 10.03 %. It was almost the same as the discount rate chosen for the project (10 %), indicating that the project was not highly profitable. Nevertheless, these calculations considered the average price of REEs of 22 US/kg for the year 2018, including cerium, lanthanum, samarium, gadolinium, praseodymium, dysprosium, and yttrium oxides. Additionally, they projected for the year 2022 an increase of 23 US/kg. However, currently the average price of REEs in element form is 4651.31 US/kg, including Eu, Tb and Nd. Therefore, the extraction of REEs can currently be considered viable taking as a reference the COPEX, OPEX, production capacity and discount rate proposed by Araya et al., 2020.

Table 2. Rough estimation of potential resources of El Buitre tailings deposit

Elements	Cut-off	Mean grade	Percentage (%)	Reserves (Mt)	Metal prices[a] (US$/ton)	Economic potential (MUS$)
REEs	200 mg/kg	337 mg/kg	100	0.0022	4651315	10232.9
Co	190 mg/kg	103 mg/kg	0	0	72780	-
Cu	0.10 wt%	0.07 wt%	2.1	0.00009	9929	0.9
Fe	11.4 wt%	15.50 wt%	100	1.023	141.1	144345.3

[a] Sources: (LME, 2022), Daily metal prices (2022) and Mineralprices.com (2022)

4.1.4 Multivariate Statistical Analyses

Total digestion geochemistry results were studied using the PCA statistical method to define elemental and mineralogical associations as well as to observe possible weathering/ alteration/ depositional processes. Samples were split into the HREE groups (< 5 m, 5-17 m and > 17 m depth) and submitted to the PCA study. This differentiation was made based on the trends of the concentrations obtained by total digestion of Cu, Co, S and Fe, and changes in the mineralogical composition (pyrite, apatite and calcite) along the depth profile (Fig. S12 and Fig. 8). As can be observed in Fig. 11 (left panel) 43.8 % of the variance of the samples from 0 to 5 m depth are explained by two components. The first principal component (PC1) is by far the predominant one and accounts for 28.33 % of the variance, while the second one (PC2) only explains 15.47 %. PC1 is related to silicate minerals, mainly aluminosilicate of Mg, Ca, and Mn, as well as to immobile elements like Cs, Ga, Be, Li, Sn, U, Ag, Co, Ni, Th, Zn and HREE. A Pearson's correlation matrix (Fig. S12) shows that Al exhibits a good positive correlation with HREE (0.651) but no correlation with LREE (0.319). This could be attributed to the adsorption of HREE on micas under the neutral or low pH conditions of the tailings deposit. Yang et al., (2019) indicate that at low ionic strength the adsorption of REEs on kaolinite and halloysite increases with increasing pH conditions. The second principal component could be attributed to the higher presence of sulfide minerals in these surficial samples, as shown by the high loading shown for S (-0.844). The cluster of elements close to Fe (i.e., As, Bi, Co and Ni) are clearly related to the presence of pyrite in the deposit of tailings. A Pearson's correlation matrix shows that S exhibits a strong positive correlation with Ni (0.709) and Co (0.817) and a good positive correlation (> 0.5) with Fe, Ag, As, and Bi, supporting the previous interpretation (Fig. S12). Pyrite is the most abundant sulfide in the deposit of tailings, a mineral that can incorporate these elements within its crystal structure (Abraitis et al., 2004; Moncur et al., 2005; Paktunc et al., 2006; Deditius et al., 2011).

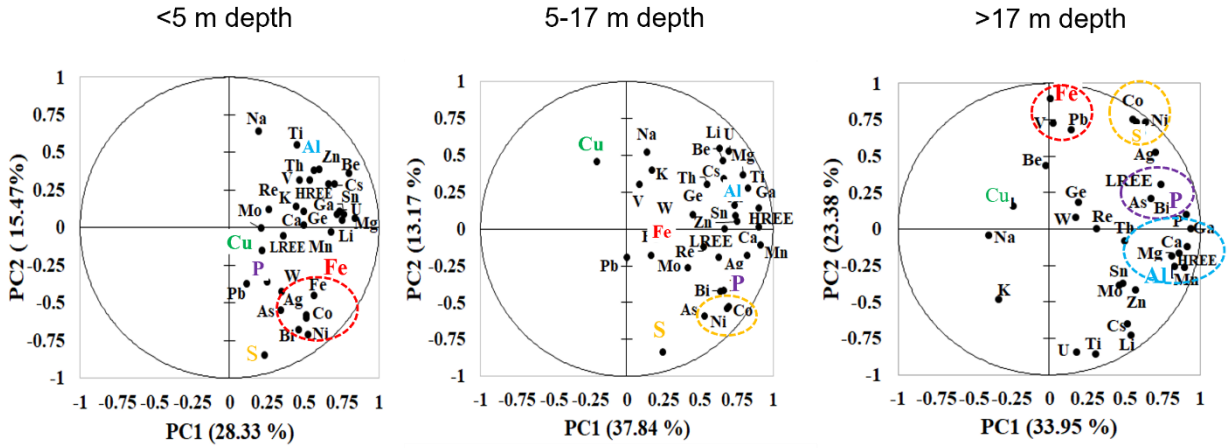

Fig. 11. Principal Component Analyses for tailings samples with depths <5 m, between 5-17 m and > 17 m.

The PCA from samples with depths in the range of 5-17 m are shown in Fig. 11 second panel. As can be observed, 51.01 % of the sample's variance can be represented by two components (PC1 37.84 % and PC2 13.17 %). As in the most surficial samples, the first principal component could be related to Mg, Ca, and Mn aluminum-silicate minerals, as well as associated to immobile

elements whereas the second main component could be attributed to the presence of sulfide minerals, mainly pyrite. However, the elements clustering and the interpretations assigned to this second set of samples are not as evident and robust as for the most surficial samples. Finally, the PCA from samples with depths higher than 17 m are shown in Fig. 10 third panel. As can be observed, 57.3 % of variance can be represented by two components (PC1 33.95 % and PC2 23.38 %). At least four different element clusters were identified in this PCA. The first principal component is associated with elements that cluster around P and LREE (attributed to the presence of apatite in the tailings) and a cluster that associates with Al (Ca, Mg, Mn and HREE) that likely reflect the silicate minerals in the tailings. A Pearson's correlation matrix shows that P exhibits a strong positive correlation with HREE (0.800) and LREE (0.697) (Fig. S12). However, HREE also show a very good Pearson's correlation with Al (0.834). Therefore, in the deeper samples the HREE and LREE could be incorporated into the crystalline structure of apatite as well as in other silicate minerals. The association of elements in the second principal component determines a cluster around S (Ni and Co), most probably reflecting the presence of pyrite. A Pearson's correlation matrix (Fig. S12) shows that S exhibits a strong positive correlation with Co (0.921), Ni (0.919) as well as with Ag (0.824). A second cluster around Fe is also evident for PC2, with V and Pb showing high positive loadings. According to a Pearson's correlation matrix, Fe exhibits a strong positive correlation with V (0.740) and a good correlation with Pb (0.507). This cluster can be attributed to the presence of magnetite and hematite within the tailings deposit. The positive correlation with Pb and V could be attributed to the adsorption of these metals on Fe (III) oxides (Liang et al., 2017).

Based on the main elements grouped by the PCA, one-way ANOVA and Welch test analyses were carried out in order to determine significant differences among the element concentrations in the three studied depth ranges (i.e., < 5 m, 5-17 m and > 17 m; Fig. S13). The results from this study are clearly in good agreement with previous mineralogical and geochemical observations:

1) Al (linked to the presence of aluminosilicates) and HREE concentrations are significantly lower in the deeper levels (> 17 m);
2) P concentrations are significantly lower in surficial samples (< 5 m depth), however, the lowest concentrations of LREE correspond to the samples located between 5-17 m depth;
3) S and Cu concentrations are significantly higher in the deeper levels (> 17 m depth) in accordance with the higher relative abundance of pyrite in deeper samples;
4) Fe (and V) concentrations do not show any significant difference among the three depth groups, as it would be expected from the homogeneous distribution of the major oxides (magnetite and hematite, Fig.8) in the deposit of tailings.

One way ANOVA and Welch test analysis were also used to determine statistically significant differences among the horizontal elemental concentrations. To this end, the samples were grouped according to their presence in the eastern, central, and western sectors of the deposit of tailings (Fig. S14). The results can be summarized as follows: 1) Al, REEs, P and Ca concentrations are significantly higher in samples located in the western sector; 2) Fe, Cu, and Pb concentrations are significantly higher in samples located in the eastern sector. The concentrations of the second group of elements increase in the opposite direction than the first group. These trends are in accordance with the mineralogical characterization, and they could be attributed to a gravitational segregation process during deposition and accumulation. As it occurs in most mine tailings

deposits (Pan et al., 2014) minerals with higher specific gravities (like sulfides and Fe-oxides) tend to settle down in the area closest to the dam wall (where the tailings discharge is produced) whereas minerals with lower specific gravities (like aluminosilicates) typically reach the most distal areas of the deposit.

4.1.5 Sequential extraction

A mineral sequential extraction procedure (SEP) was implemented as an additional tool linking the observed mineralogy and bulk chemistry and to generate a better understanding of elemental mobility within the tailings profile. The methodology of seven steps developed by Dold and Fontboté (2001) was used. This procedure was optimized for IOCG-type tailings deposits located in the vicinity of the study area and with similar mineralogical composition to El Buitre tailings deposit.

The SEP results obtained from three selected boreholes (i.e., B-04, B-13, and AD-02) were averaged to have a representative value for each depth (Table 3). These boreholes are located in the easter sector of the deposit of tailings. Taking into consideration the mineralogical and geochemical information previously presented, as well as the multivariate statistical analysis, the following elements were selected to study the selective dissolution of the most relevant minerals in the tailings deposit: 1) Al and Mg, as indicators of primary silicate minerals; 2) Ca, as indicator of carbonates and gypsum; 3) S, as indicator of sulfide and sulfate minerals, 4) Cu, as indicators of chalcopyrite and 5) Fe, as indicator of Fe (III) oxides, Fe (III) oxyhydroxide and sulfides. Other elements were also studied to characterize the mobility of potential pollutants (i.e., As, Mn, Cr and Ni) and critical raw elements (i.e., V and Co) within the tailings deposit.

The aluminosilicates (marked by the combined presence of Al and Mg) are mostly dissolved in the very last step of the SEP (i.e., Step 7: residual fraction), and they did not show any discernible trend along the depth profile. Gypsum distribution, marked by Ca and S release during the first step of the SEP (Ca/S molar = 1 in Step 1), did not show significant differences through the depth profile (Table 3). In addition, the saturation index calculated using PHREEQC corroborates the precipitation of gypsum by saturation, product of pyrite and calcite dissolution in oxidizing conditions (Table S8). Calcite dissolution can be traced by Ca release, mostly limited to the second step of the SEP (exchangeable fraction and carbonates). As shown in Table 3, calcite concentration progressively increases with depth. Mn is also predominantly released during Step 2, following a similar distribution as the one described for Ca. In addition, a Pearson ‘correlation (Fig. S12) shows a strong correlation between Mn and Ca for samples <5 m (0.803), in the range from 5-17 m (0.909) and >17 m (0.915). Regarding the sulfide minerals, it can be observed how sulfur is predominantly released in step 5, and to a lesser extent in step 6, as opposed to what could be expected from the optical mineralogical study that presented secondary Cu sulfide as a minor sulfide and pyrite as major sulfide phase. Dold and Fontboté (2001) already observed this type of inconsistencies in other mine tailings and they attributed it to the presence of unstable pyrite minerals from the oxidation zone that may partially dissolved in the fifth step of the SEP. Notwithstanding, almost no S reached Step 7, so sulfide selective dissolution was achieved between Steps 5 and 6. Combining Steps 5 and 6, it can be observed how sulfide concentrations slightly increases with depth (Table 3), in accordance with previous mineralogical observations (Fig. 8). Cu concentration (adding all the steps) decreases from the surface to the center of the

tailings deposit to finally increase again in the deepest levels, in accordance with previous observations (Fig. 10). Finally, Fe (III) oxyhydroxides and Fe (III) oxides should be selectively dissolved in the third and fourth step of the SEP. However, most of the Fe and its associated elements (V and Cr) were predominantly released (Table 3 and S7) in the last step of the SEP (residual fraction). This discrepancy could be explained because the solubility of Fe oxides is highly dependent on crystallinity. Highly crystalline Fe (III) oxides remain practically unchanged (and their Fe is not released) until the last step of the SEP (Caraballo et al., 2018).

According to the Chilean Norm 46/2002 for the emission of liquid waste into groundwater in highly vulnerable environments, the concentrations of As and Ni were found in low concentrations (Ministerio Secretaría General de la Presidencia de Chile, 2002). In addition, these elements remain mostly immobile until the last steps of the SEP (Table S7), when pyrite is dissolved. On the other hand, Mn is more mobile, and it is significantly released in step 2, during the neutralization reactions induced by calcite dissolution (Table S7). Finally, V and Cr show very limited mobility (Table S7) that is coupled to the dissolution of the Fe oxides (i.e., hematite and magnetite).

Table 3. Results of the sequential extraction corresponding to the average of boreholes Ad2, B-04 and B-13. The values are expressed in mmol/kg. Elements below the detection limit are indicated as <DL. Step 1: Water soluble fraction. Step 2: Exchangeable fraction, Step 3: Fe (III) oxyhydroxides, Step 4: Fe (III) oxides, Step 5: Organics and secondary Cu-sulfides, Step 6: Primary sulfides and Step 7: Residual fraction. Different letters indicate that there is a significant difference between the concentration of the elements at a certain depth. On the contrary, the same letters indicate that there are no significant differences.

Steps	1	2	3	4	5	6	7
Aluminum				Mean ±SD			
Depth (m)							Silicates
1	<DL	18 ± 5	54 ± 5	43 ±2	12 ± 1	246 ± 12	1633 ± 10 a
3	<DL	26 ± 5	64 ± 3	44 ±3	14 ± 0	233 ± 10	1620 ± 3 a
9	<DL	18± 5	55 ± 11	45 ± 10	13 ± 3	259 ± 82	1415 ± 162 a
15	<DL	17 ± 1	68 ± 2	52 ± 1	15 ± 0	315 ± 62	1612 ± 37 a
21	<DL	18 ± 4	68 ± 5	45 ± 7	15 ± 1	310 ± 38	1456 ± 38 a
35	<DL	19 ± 0	82 ± 11	57 ± 2	20 ± 5	408 ± 48	1425 ± 100 a
Calcium	Gypsum	Carbonates					
1	137 ± 31 a	297 ± 84 a	<DL	<DL	52 ± 5	21 ± 0	53 ± 44
3	108 ± 32 a	411 ± 114 ab	<DL	<DL	69 ± 11	23 ± 5	22 ± 4
9	107 ± 16 a	564 ± 26 b	<DL	<DL	91 ± 15	34 ± 5	<DL
15	99 ± 1 a	616 ± 43 b	<DL	<DL	109 ± 6	31 ± 1	<DL
21	138 ± 69 a	625 ± 61 b	<DL	<DL	105 ± 3	33 ± 1	19 ± 6
35	128 ± 25 a	806 ± 83 c	<DL	<DL	140 ± 24	38 ± 1	<DL
Sulphur	Gypsum				Secondary sulfide	Primary sulfide	
1	134 ± 33 a	<DL	<DL	<DL	274 ± 7 a	68 ± 12 a	<DL
3	120 ± 7 a	<DL	<DL	<DL	324 ± 33 ab	146 ± 5 b	40 ± 6
9	83 ± 5 a	<DL	<DL	<DL	404 ± 27 ab	137 ± 69 b	33 ± 1
15	96 ± 1 a	<DL	<DL	<DL	418 ± 14 ab	78 ± 7 a	<DL
21	140 ± 76 a	<DL	<DL	<DL	432 ± 16 ab	159 ± 18 b	16 ± 9
35	128 ± 27 a	<DL	<DL	<DL	497 ± 13 b	164 ± 62 b	12 ± 1
Copper					Secondary sulfide	Primary sulfide	
1	<DL	6 ± 1	5 ± 1	0.6 ± 0	5 ± 0.3 a	1 ± 0.1 a	0.3 ± 0.1
3	<DL	4 ± 0	2 ± 0	0.3 ± 0	10 ± 2 b	2 ± 1 a	0.3 ± 0
9	<DL	2 ± 0	2 ± 0	0.3 ± 0	4 ± 0.1 a	1 ± 0.1 a	0.3 ± 0.1
15	<DL	2 ± 0	1 ± 0	0.3 ± 0	3 ± 0.1 a	0.7 ± 0.1 a	0.2 ± 0
21	<DL	2 ± 0	2 ± 1	0.3 ± 0	5 ± 1 a	1 ± 0.1 a	0.1 ± 0
35	<DL	5 ± 1	3 ± 1	0.5 ± 0	13 ± 0.1 b	2 ± 0 b	0.3 ± 0.1
Iron			Fe (III) Oxyhydroxides	Fe (III) Oxides			Silicates
1	<DL	31 ± 9	289± 24 a	178 ± 24 a	74 ± 1	538 ± 10	1637 ± 3
3	<DL	44 ± 6	258± 2 a	192 ± 9 a	85 ± 3	583 ± 13	1716 ± 188
9	<DL	38 ± 8	291 ±10 a	195 ± 19 a	116 ± 17	626 ± 60	1902 ± 139
15	<DL	43 ± 1	270±18 a	193 ± 18 a	136 ± 14	664 ± 84	1492 ± 216
21	<DL	38 ± 9	320±79 a	201 ± 11 a	127 ± 15	706 ± 103	1570 ± 234
35	<DL	41 ± 1	302±17 a	206 ± 18 a	151 ± 18	825 ± 38	1155 ± 0

4.1.6 Conceptual model

In the deposit of tailings it is possible to distinguish geochemical and mineralogical variations with increasing depth and in the area distal to the wall dam or the waste discharge zone. The presence of multiple discharge points and the geometry of the deposit, favor the stratification of the tailings due to coarse particle segregation and settling near the spigotting points. Additionally, tailings stratification may be associated with mineralogical changes, and process parameters such as variation grinding size during the production period of the deposit of tailings (Mulenshi et al., 2019, 2021; Pan et al., 2014). Therefore, if certain minerals occur in a particular particle size, they may segregate and accumulate in specific zones of the deposit (Lottermoser, 2010). This trend was evidenced in section 4.1.3, where Al, HREE, P, Ca, Fe, Cu and Pb concentrations presented lateral stratifications. Elements such as Fe, Cu, and Pb could have been associated with coarse particles and tended to settle near discharge points. While Al, HREE, P and Ca could have been associated with finer and lighter particle sizes and were settling further away.

On the other hand, in order to delimit the possible alteration fronts along the depth profile of the deposit of tailings, the distribution patterns of pyrite, chalcopyrite and calcite were analyzed, as they represent the most reactive minerals. In addition, we analyzed the Co (representative of the trends of Cu, S and Fe) and LREE (representative of the trends of REEs) concentrations obtained by total digestion, the geostatistical distribution model, and the results of the different sequential extraction steps. An oxidation zone with an extension between 3-5 m in depth was determined, characterized by a lesser relative abundance of pyrite, chalcopyrite, and calcite with respect to the deeper levels. In this layer, the sulfide minerals present low degrees of alteration and the absence of Fe (III) oxyhydroxides rims or coatings. Below the oxidation zone, the sulfides remain unchanged, with constant relative abundance percentages, up to the depth range between 17-18 m. This layer was defined as the primary zone. Subsequently, towards the deeper layers (> 17 m) a significant increase in pyrite and S concentrations occur, which are reflected in the one-way ANOVA and Welch test analysis performed in section 4.4, and in steps 5 and 6 of the SEP. In addition, elements associated with pyrite such as Co, Cu and Fe, and elements associated with apatite such as P, are slightly enriched at the bottom of the deposit of tailings, mainly in the depth range 30 – 40 m (Fig. 10 and Fig. S7). This last layer was present in the deepest sectors, specifically in the central and eastern sectors of the deposit of tailings (Fig. 12). It was considered as a primary zone enriched in pyrite and apatite. The highest proportion of these minerals in depth was attributed to the combination of three factors: 1) the tailings dam geometry and the gravitational deposition of heavier mineral particles in the tailings slurry that promote the relative enrichment of pyrite and apatite in the deep zone; 2) limited oxygen diffusion at the bottom of the deposit of tailings. Therefore, the biotic oxidation reactions are dominant, and they could be restricted by the low availability of Fe (III) in solution, due to neutral pH conditions and low water flow, preserving pyrite; 3) there is little information about the mine that gave rise to the mine wastes, so it is possible that the older tailings represent a more pyrite-enriched portion of the ore deposit respect more recent materials, or could even correspond to materials from a different mine nearby the flotation plant.

According to the conceptual model proposed in Fig. 12, it is observed that the concentrations of the LREE (present in greater proportion than the HREE) represented in the section of the central-eastern area of the deposit of tailings, do not present enrichment in the areas deeper of the deposit.

This trend corresponds to the observations made in the geostatistical model and it is probably associated with the double association of REEs with aluminosilicates and apatite minerals.

Regarding pH conditions within the tailings deposit, paste pH values remain relatively constant (around 7.9) along the depth profile which indicates a relative homogeneous distribution of calcite. The neutral pH values, low water content of the mine residue and high evaporation in arid climates diminish the mobility of the elements liberated from the oxidation zone and limit the oxidation reactions to fine-grained horizons (relatively poor in sulfide minerals) due to their higher water retention capacity (Dold and Fontboté, 2002). In addition, the low-sulfides characteristic of tailings from IOCG reservoirs together with the restriction of the mobility of their oxidation products, explains the absence of secondary efflorescent salts on the surface and the development of a secondary mineral enrichment zone. The above indicates that the deposit of tailings is environmentally safe, due to the restricted mobility of potential polluting elements.

On the other hand, some important aspects to highlight for future revalorization studies are: 1. The economic recovery of the REEs from the reprocessing of the tailings is improbable, because they are associated with both aluminosilicates and apatite minerals. Which makes it difficult to concentrate these elements as by-products. 2. The high content of magnetite could allow economic recovery of Fe by magnetic separation. This method is currently being applied profitably by CAP's subsidiary Compañía Minera del Pacífico (CMP), located near of El Buitre tailings deposit. CMP produces pellet feed with tailings from the copper concentrator plant of Compañía Contractual Minera Candelaria, with average Fe grades of 11.4 % (Compañía Minera del Pacífico, 2020). 3. The elimination of impurities from the Fe concentrate could favor the concentration of Cu and its possible economic recovery. In addition, it would allow to concentrate pyrite and recover the Co associated with its crystalline structure.

Taking into consideration all the above-mentioned characteristics, a 3D conceptual model was drawn using Leapfrog. To facilitate the model visualization, it was decided to highlight several representative 2D sections (Fig.12a) of the Co concentrations along the deposit of tailings. Additionally, two detailed representative section of the Co and LREE concentrations of the central-eastern area of the deposit of tailings are shown. These sections were contrasted with the geostatistical modeling.

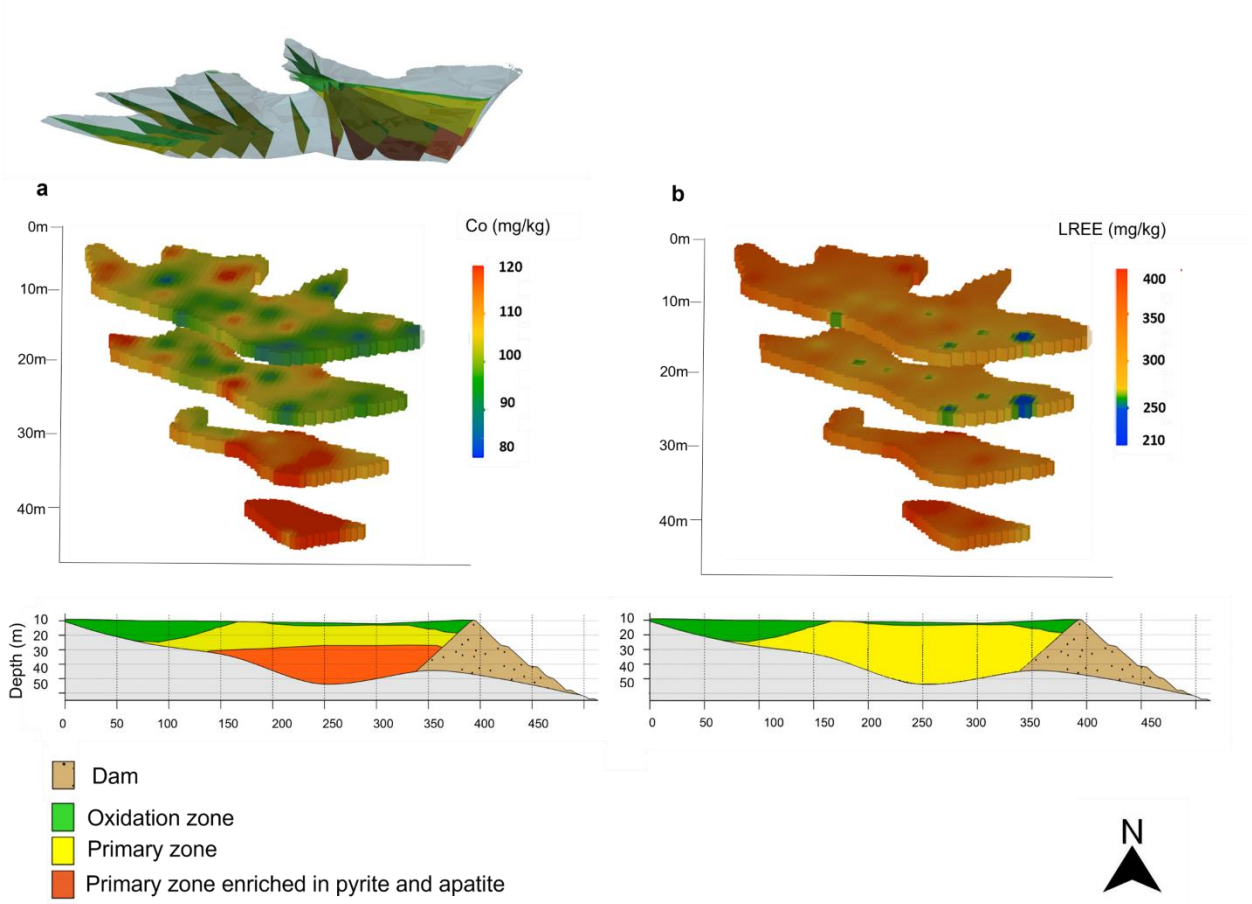

Fig. 12. a. Modeled Co concentration and cross-section of the distribution of the alteration fronts in the central-eastern area of the deposit of tailings. Additionally, the upper left figure shows different sections along the geometry of the deposit of tailings, indicating the absence of the layer enriched in sulfides and apatite, in the western sector of the deposit. b. Modeled LREE concentration and cross-section of the distribution of the alteration fronts in the central-eastern area of the deposit of tailings. This trend is representative of the distribution of REEs in the deposit of tailings.

4.2 GENOMIC AND GEOCHEMICAL CHARACTERIZATION OF ALKALINE TAILINGS DEPOSIT (EL BUITRE, CHILE): IMPLICATIONS FOR TAILINGS RESTORATION AND REVALORIZATION

4.2.1 Geochemistry of the soluble fractions of the tailings

The results of the paste pH indicated that the tailings samples have alkaline pH ranging from 7.9 to 8.1 (Table 3). It is well known that these pH values favor the immobilization of most metals as metals hydroxides and the co-precipitation of metals within carbonate minerals (Hou et al., 2013;Li et al., 2020). Therefore, pH could be one of the main factors controlling the mobility of metals in the deposit of tailings in an eventual leaching process.

The elemental composition analysis shows only 34 elements above the detection limit. The bulk chemistry of the soluble fraction was mainly comprised by Ca, Mg, Na, SO_4^{2-}, P, Fe, Al, and Sr. The high concentrations of these elements are associated with the geochemistry of tailings enriched in carbonates, aluminosilicates, sulfides and iron oxides-oxyhydroxides (González-Díaz et al., 2022). Trace concentrations of Ba, Cu, Li, Mn, Se, Mo, Zn, Co, As, Pb, Cd, Cu, Hg, U and Ni were also detected in the soluble fraction. The elements of the rare earth elements (REEs) with concentrations above the detection limit (Ce, Gd, La, Nd and Pr) were grouped into light rare earth elements (LREE) and heavy rare earth elements (HREE).

In the soluble fraction, only Fe, Mn and Se were above the limit stablished by the Chilean norm for the emission of liquid waste into groundwater in highly vulnerable environments (Norm 46/2002, Ministerio Secretaría General de la Presidencia de Chile, 2002). Sulfate concentrations varied greatly from 600 mg L-1 to 5,880 mg L-1 throughout the sampling area. Fe, Mn and Se have similar trend varying from 0.05mg L-1 to 31 mg L-1, from 0.08 to 7 mg L-1 and from 0.006 to 0.1 mg L-1, respectively.

One way ANOVA with Welch correction (Welch test) for non-homogeneous samples were carried out in order to determine significant differences among the elemental concentrations through the depths profile (i.e., oxidized zone (0-5 m) and non-oxidized zone (> 5 m); Fig.S15 and Fig.S16). In the case of major elements, Ca, S and Na were significantly higher at 0-5 m. In addition, Pearson correlation matrix (Fig. S17) showed an excellent correlation between Ca and S (0.991). It can be attributed to the alteration of sulfide and secondary gypsum minerals in the oxidized zone (González-Díaz et al., 2022). In contrast, Al, Fe, P, Ba, Mn, Sb and U concentration were significantly higher at > 5 m, while there were no differences in the concentrations of Mg and K and some minor elements like Co, Cu, HREE, LREE, Li, Mo, Se, Zn and Zr between the oxidized and non-oxidized zone. Therefore, the geochemical composition in the deposit of tailings presents lightly stratifications through the depths profile which were attributed to the ore deposit mineral composition, the mineral processing technology, gravitational deposition processes, depositional history, and the geometry of the deposit of tailings (González-Díaz et al., 2022).

Table 3. Bioavailable fraction of the deposit of tailings showing the mean, the standard deviation (DS), minimum and maximum concentration in the oxidized zone (0-5 m) and non-oxidized zone (> 5 m).

Depth	0-5m				> 5 m			
Elements (mg/L)	Mean	DS	Minimum	Maximum	Mean	DS	Minimum	Maximum
pH	7.9	0.2	7.5	8.4	7.9	0.2	7.6	8.4
Major elements								
Ca	3634	1409	667	6569	3317	1253	1261	6397
S	3323	1202	600	5880	3081	1096	1137	5532
Mg	143	54	47	378	142	54	47	378
Na	79	38	15	225	75	35	15	225
K	59	16	26	109	58	16	26	109
Fe	8	7	0.1	31	9	7	0.1	31
Al	4	3	1	13	5	3	1	13
Sr	3	1	1	8	3	1	1	8
Minor elements								
Mn	0.8	0.8	0.1	7	0.9	0.9	0.1	7
P	0.2	0.2	0.1	1.2	0.2	0.2	0.1	1
Ba	0.2	0.1	0.1	0.4	0.2	0.1	0.1	0.4
Cu	0.2	0.1	0.03	0.6	0.2	0.1	0.03	0.6
Li	0.1	0.04	0.03	0.3	0.1	0.04	0.03	0.3
Rb	0.1	0.03	0.1	0.2	0.1	0.03	0.1	0.2
Mo	0.05	0.02	0.01	0.1	0.05	0.02	0.01	0.13
Se	0.03	0.01	0.01	0.1	0.02	0.01	0.01	0.07
Zn	0.03	0.01	0.01	0.05	0.02	0.01	0.01	0.04
LREE	0.02	0.04	0.002	0.36	0.02	0.04	0.002	0.36
REEs	0.02	0.04	0.002	0.37	0.02	0.04	0.002	0.37
Co	0.01	0.01	0.001	0.1	0.01	0.01	0.00	0.07
Sb	0.01	0.01	0.004	0.04	0.01	0.01	0.004	0.04
Zr	0.01	0.01	0.001	0.09	0.01	0.01	0.001	0.09
Ga	0.004	0.003	0.001	0.014	0.005	0.003	0.001	0.01
Tl	0.002	0.001	0.001	0.005	0.002	0.001	0.001	0.005
U	0.001	0.001	0.0001	0.004	0.001	0.001	0.0001	0.004

4.2.2 Microbial diversity and community composition

The phenotypic characterization of the tailings shows that the biomass presents in the oxidized (0-5 m) and non-oxidized (> 5 m) zones was very similar (number of bacteria ranging between 2.4 x 10^5 cells g^{-1} up to 9.1 x10^7 cells g^{-1}, Table 4). These results are also in the same range of the biomass described in mines of magnesite (4.4 x 10^6 cells g^{-1}), bauxite (3.8 x 10^5 cells g^{-1}) and sulfide rich tailings (10^7 cell g^{-1}) (Lindsay et al., 2009; Narayanan et al., 2020).

Table 4. Bacterial number in cell per grams of tailings showing descriptive statistics of each depth range (0-5 m and > 5 m) P value > 0.05

Depth	Mean	DS	Max	Min
0-5m	2.9E+07	2.3E+07	9.1E+07	9.4E+05
> 5 m	2.4E+07	2.1E+07	9.1E+07	2.4E+05

The genotypic characterization of samples indicates that a total of 106,050 reads were generated from Illumina Miseq sequencing of the 16S rRNA genes. After quality control, removal of chloroplast and mitochondria, and rarefaction, 91,510 high-quality sequences were obtained. Clustering of these sequences at a 97% identity level resulted in 2,097 operational taxonomic units (OTUs), which were used to assess the bacterial community structure and composition. Despite the low number of OTUs, the rarefaction curve suggests that the sampling was adequate to capture most of the bacterial diversity in the deposit of tailings (Fig. S18). In addition, the indexes of diversity Shannon, Chao 1 and observed showed that there were no differences in the diversity indicating that the evenness and species diversity richness were homogeneous through the depth profile (Fig. S19). The homogeneity of the diversity in the profile was confirmed by Kruskal test ($p > 0.17$). Similarly, Chung et al., (2019) did not observe significant differences in the diversity indexes through the depth profile of two tungsten tailings deposits.

The PCoA plot at the OUT level indicate that the bacterial composition is different between the oxidized and non-oxidized zones (Fig. 13). Adonis test confirmed these observations ($P = 0.001$), as well as the PERMDISP analysis revealed heterogeneous dispersions ($P = 0.002$) within the groups. Therefore, it can be said that the species diversity richness is homogeneous but bacterial composition is heterogeneous comparing these two specific sections of the depth profile. Nevertheless, the Venn diagram reveals that the majority of OTUs (361 OTUs representing 82.1 %) were shared between 0-5 m and > 5 m. Interesting 0-5 m host more unique OTUs (10.9 % of the OTUs) than > 5 m (7 % of the OTUs) (Fig. S20).

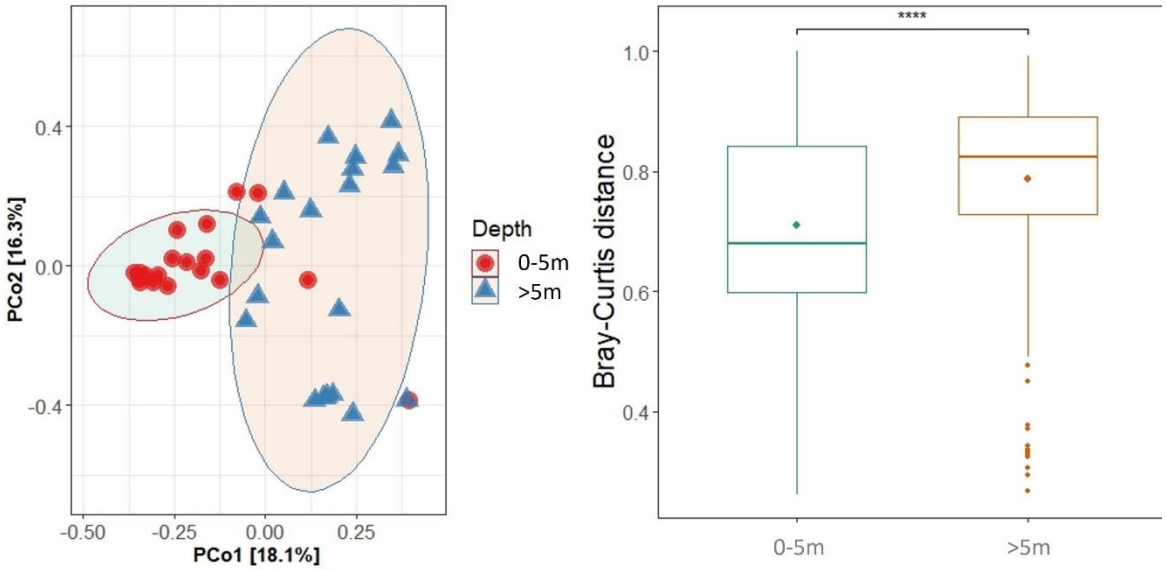

Fig. 13. The left shows a PCoA plot (based on Bray Curtis dissimilarities) at the OUT level in the oxidation (0-5 m) and non-oxidized zone (> 5 m) of the deposit of tailings. The right panel shows the PERMDISP analysis. The PCoA data revealed that the first two PCoA components explained 18.1 % and 16.2 % of the variation, respectively.

A total of 13 phyla were taxonomically identified, but only six of them accounted for more than 1 % of total reads. Bacterial communities were dominated (in the both sections) by *Proteobacteria* (42.4 % on average of total reads), followed by *Deinococcus-Thermus* (20.9 %), *Actinobacteria* (16.2 %), *Nitrospirae* (9.8 %), *Firmicutes* (8.7 %) and *Gemmatimonadetes* (1.1 %) (Fig. 14a). *Proteobacteria* was the most dominant phylum both in the oxidized and non-oxidized zone. While *Deinococcus-Thermus, Actinobacteria* and *Gemmatimonadetes* dominated in the oxidized zone. In contrast, *Nitrospirae* and *Firmicutes* were more abundant in the non-oxidized zone. In accordance to these observations, previous works have also reported *Proteobacteria* as the dominant phylum in circum-neutral pH tailings as they are able to survive under oligotrophic conditions and in high metal concentrations (Blowes et al., 1998; Pereira et al., 2014; Sun et al., 2018; Xiao et al., 2016). Similarly, *Gemmatimonadetes, Actinobacteria* and *Deinococcus-Thermus* have also been reported in neutral and fresh tailings (Pereira et al.,2014; Sun et al., 2018; Gupta et al., 2020).

At the genus level, the more abundant genus in the deposit of tailings was *Meiothermus* (20.8 % on average of total reads) followed by *Thermithiobacillus* (11,7 %), *Thiobacillus* (9.2 %), *Leptospirillum* (9.1 %), *Quadrisphaera* (9.0 %), *Desulfosporosinus* (3.5 %), *Nocardioides* (1.3 %), *Bacillus* (1.3 %), *Spingomonas* (1.2 %), *Rhizobium* (1.0 %), *Acidithiobacillus* (0.9 %) and *Gemmatimonas* (0.9 %) (Fig.14b). *Meiothermus, Thermithiobacillus, Quadrisphaera* and in less proportion *Spingomonas* were the most dominant genera in the oxidized zone. While *Leptospirillum* and *Desulfosporosinus* were dominant in the first meters of depth of the non-oxidized zone. On the contrary, *Thiobacillus* was the most abundant genus in the deepest zone of the deposit of tailings.

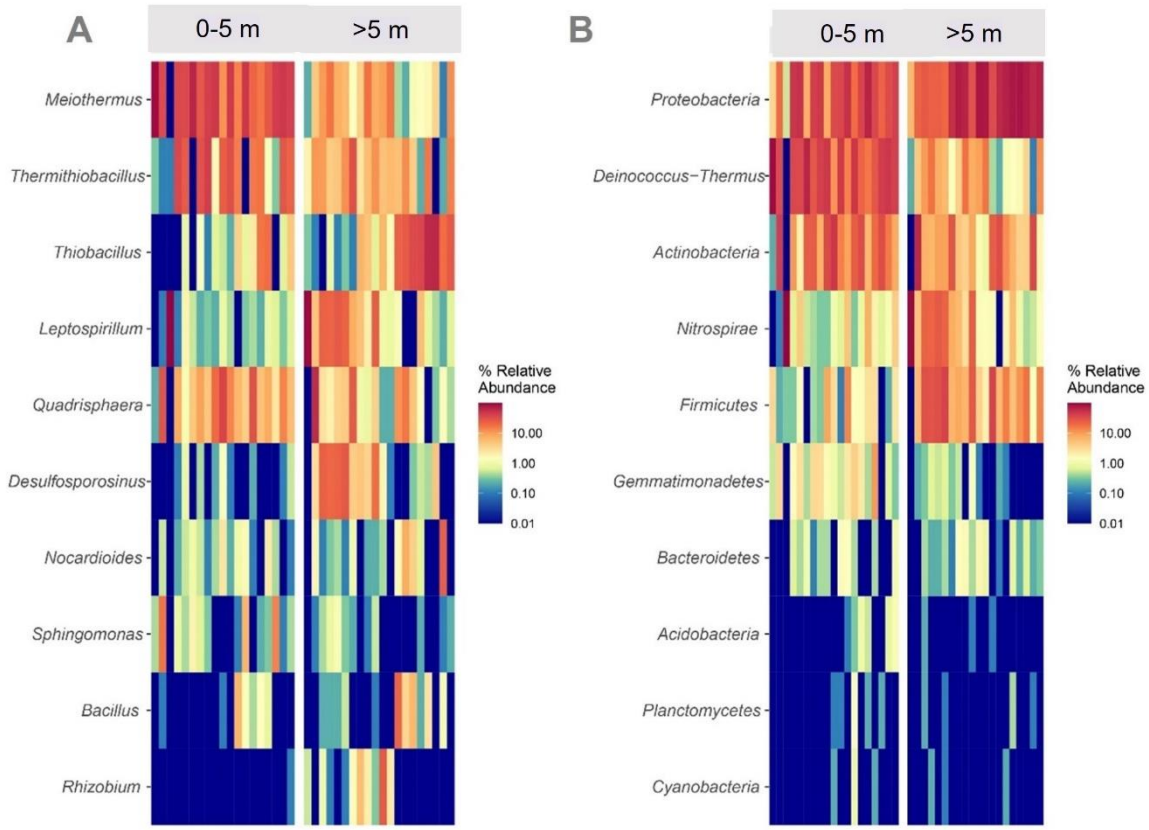

Fig. 14 Heatmap depicting the relative abundance of the dominant phyla (a) and genera (b) in the oxidized (0-5 m) and non-oxidized (> 5 m) zone of the deposit of tailings. Only the top 10 abundant genera and phyla are shown in this figure. The shift of the bacterial community compositions is depicted by the color intensity ranged from 10 to 0.01 percent of relative abundance.

The relative abundance analysis offers an idea of the microbial composition; however, due to the heterogeneity at genus level, it cannot be determined the core genera that might control the biogeochemical cycles of metals in this system. Because of that, it was decided to use DESeq2, and networking analysis get a better understanding of the most influential genera. DESeq2 (Fig. 15) allows to find the significant taxa by determining the community differences between the oxidized (0-5 m) and non-oxidized zones (> 5 m).

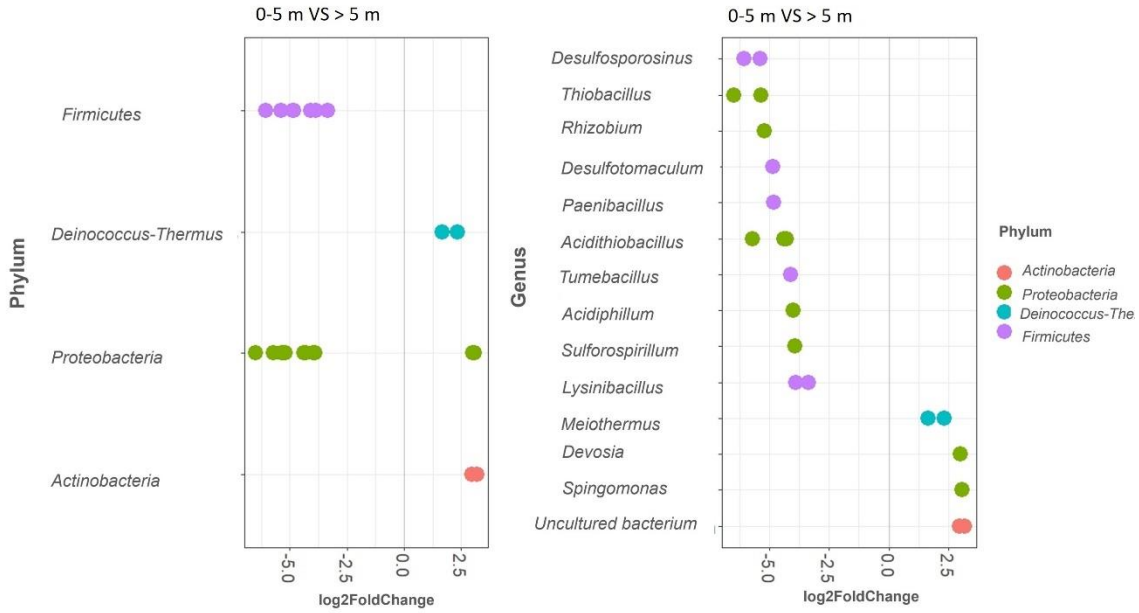

Fig. 15 Differential abundance of bacterial taxa (OUT level) using DESeq2. Points with positive log2FoldChange values represent bacterial taxa with increased abundance in the oxidation zone to the reductive zone.

Of the 2,097 OTUs found through the profile of the deposit of tailings, 16 OTUs were enriched (adjusted P <0.01) in the non-oxidized zone compared to the oxidized zone (6 OTUs) (Fig. 15). The majority of these OTUs were highly prevalent and abundant (Fig. S21). In the oxidized zone the dominant phyla were *Deinoccocus-Thermus, Proteobacteria* and *Actinobacteria*. At the genus level, the core OTUs were mainly identified as *Meiothermus* (2 OTUs), *Devosia* (1 OTUs) and *Spingomonas* (1 OTUs). In the non-oxidized zone, the dominant phyla were *Protobacteria* and *Firmicutes*. At the genus level, *Desulfosporosinus* (2 OTUs), *Thiobacillus* (2 OTUs), *Rhizobium* (1 OTUs), *Desulfotomaculum* (1 OTUs), *Paenibacillus* (1 OTUs), *Acidithiobacillus* (4 OTUs), *Tumebacillus* (1 OTUs), *Acidiphillum* (1 OTUs), *Sulforospirillum* (1 OTUs), *Lysinibacillus* (2 OTUs) were dominant.

c

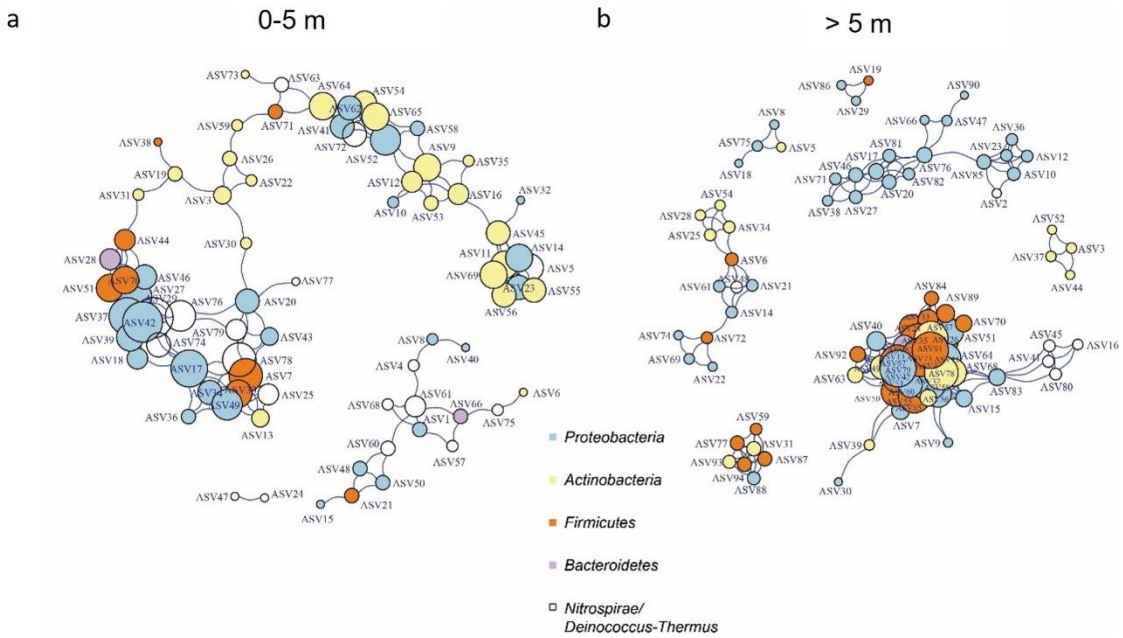

Fig. 16 Co-occurrence networks showing the correlation among bacterial at the deposit of tailings. The size of each node is proportional to its number of connections. a) Corresponds to oxidized zone (0-5m) and b) Corresponds to non-oxidized zone (> 5 m).

Interesting, peripheral modules were more abundant in the non-oxidized zone than in the oxidized one. Most of peripheral modules in the non-oxidized zone were independent (not connected to each other), whereas in the oxidized zone the main modules are interconnected by an uncultured bacterium belonging to the phylum *Actinobacteria*. This observation highlights the importance of the microbial dark matter in these artificial ecosystems. As expected *Meiothermus* (ASV 61, 78 and 5) was one of the keystone species in the oxidized zone followed by uncultured bacterium (ASV 7, 29, 42 and 69 among others) belonging mainly to the phyla *Proteobacteria*, *Firmicutes* and *Nitrospirae*. Members of the genus *Meiothermus* have been identified in the oxidized zone of Pb-Zn-Sb alkaline tailings, in fresh cooper tailings (Sun et al., 2018; Gupta et al., 2020), in shallow samples collected in a hot spring (Albuquerque et al., 2009) and in abandoned deposit of tailings with acid mine drainage (Li et al., 2014; Yang et al., 2014, Zhang et al., 2019). Despite *Spingomonas* (ASV32 and 58) and *Devosia* (ASV18) were enriched in this section, it seems that these genera are not significant in the bacterial network structure. Previous works have reported *Spingomonas* in fresh tailings derived from Pb-Zn and Cu mines and neutral cobalt and arsenic rich tailings (Chen et al., 2013; Courchesne et al., 2021; Gupta et al., 2020).

On the other hand, the non-oxidized zone seems more diverse than the oxidized one, as it was seen in the Deseq2 plot (Fig. 15), because it concentrated the keystone species in only one big module, while other six smaller peripheral modules are isolated. The bigger module host members of the genera *Desulfosporosinus* (ASV73), *Ferrimicrobium* (ASV78), *Acidithiobacillus* (ASV79), *Clostridium* (ASV91), *Sulforospirillum* (ASV46), *Lysinibacillus* (ASV24), *Paenibacillus* (ASV26), among others. Unlike this study, previous works have reported *Thiobacillus* as the most dominant genus in fresh and circum-neutral pH in the deposit of tailings (Blowes et al., 1998; Chen et al., 2013; Chung et al., 2019; Sun et al.,

2018). Nevertheless, *Thiobacillus* is not significant in the bacterial network structure despite it was dominant in the non-oxidized zone. However, members of the genera *Clostridium*, *Paenibacillus*, *Rhizobium* and *Desulfosporosinus* have been identified in fresh and neutral cobalt-arsenic and gold tailings (Courchesne et al., 2021; Liu et al., 2018 Winch et al., 2009). *Tumebacillus* has been reported as dominant genus in the initial stage (pH > 5) of an experiment of natural pyrite oxidative dissolution that simulates the acidification process in sulfidic mine tailings (Chen et al., 2014). In addition, *Acidithiobacillus* has also been found in tailings with circum-neutral pH and fresh tailings as a result of the presence of acidophilic microenvironments on the decomposing sulfide grains (Cwalina et al., 2009; Majzlan et al., 2011). In contrast, member of the genera *Desulfotomacullum, Ferrimicrobium and Sulforospirillum* have been reported mostly in acid-generating mine residues (Chen et al., 2016; Schippers et al., 2010; Winch et al., 2009).

The networking analysis also reveals a closely association between sulphate reducers, sulfide oxidizers, iron oxidizers/reducers and nitrogen fixing bacteria which suggest a mutualistic activity between them. Previous works have also reported a close interconnection between nitrogen fixing (*Bacillus* and *Lysinibacillus*) and sulfur-oxidizing bacteria. They can use sulfate and ammonia as electron donor and acceptor to remove nitrogen and sulfur simultaneously under anaerobic condition (Duan et al., 2020). On the other hand, Diaby et al., (2007) reported the association between *Leptospirillum* spp. and acidophilic iron and sulfur-oxidizing bacteria such as *Sulfobacillus* and *Acidithiobacillus ferrooxidan* in the catalysis of the oxidative dissolution of pyrite and other sulfide minerals in a porphyry copper tailings deposit.

4.2.3 Relationship between bacterial composition and geochemical characteristics

The more significant bacteria differentiating the sections determined by random forest analysis were used to stablish correlations with environmental variables using Pearson correlation and clustering analysis (Fig.17). It is worthy to mention that this study does not probe experimentally the functionality and role of these bacteria; however, based on the literature it can suggest the influence of certain genera in the biogeochemical cycle of some metals in this system. The heatmap show three main cluster of bacteria (clusters were labelled as A, B and C, Figure 17). *Leptospirillum*, *Meiothermus* and *Gemmatimonas* formed the cluster A. Cluster A could be sub-divided into 2 sub-clusters. Sub-cluster A1 consisted of *Leptospirillum*. Sub-cluster A2 consisted of *Meiothermus* and *Gemmatimonas* which were mostly detected in the oxidized zone. The cluster B consisted of *Quadrisphaera*, *Acidithiobacillus* and *Desulfosporosinus*. Cluster B could be sub-divided into 2 sub-clusters. Sub-cluster B1 consisted of *Quadrisphaera.* The sub-cluster B2 consisted of *Acidithiobacillus* and *Desulfosporosinus* which were mostly detected in the range of depth from > 5 m. Cluster C consisted of *Paenibacillus* and *Thiobacillus*. *Thiobacillus* had positive and significant correlation with Mn, Co, and pH. Besides, Pearson's correlation matrix shows an excellent correlation between Co-Mn (0.751) in the soluble fraction data (Fig. S17). However, Co concentrations did not show significant differences through the depth profile. In contrast, the Mn concentrations were significantly higher in the non-oxidized zone. Previous works have reported that *Thiobacillus ferrooxidans* and *Thiobacillus thiooxidans*

can solubilize Mn under anaerobic condition (Lodha et al., 2010). The prediction by PICRUSt2 of oxidoreductases (EC: 1.8.1.4) suggests that *Thiobacillus* could reduce Co and Mn in the presence of sulfur, solubilizing the Mn and Co associated with pyrite. On the other hand, the positive correlation between *Thiobacillus* and pH indicates that probably the dominant species in the deposit of tailings were *Thiobacillus thioparus*. They have a growth optimal pH between 6.0 to 8.0 (Kuenen et al., 1992; Gould et al., 1994).

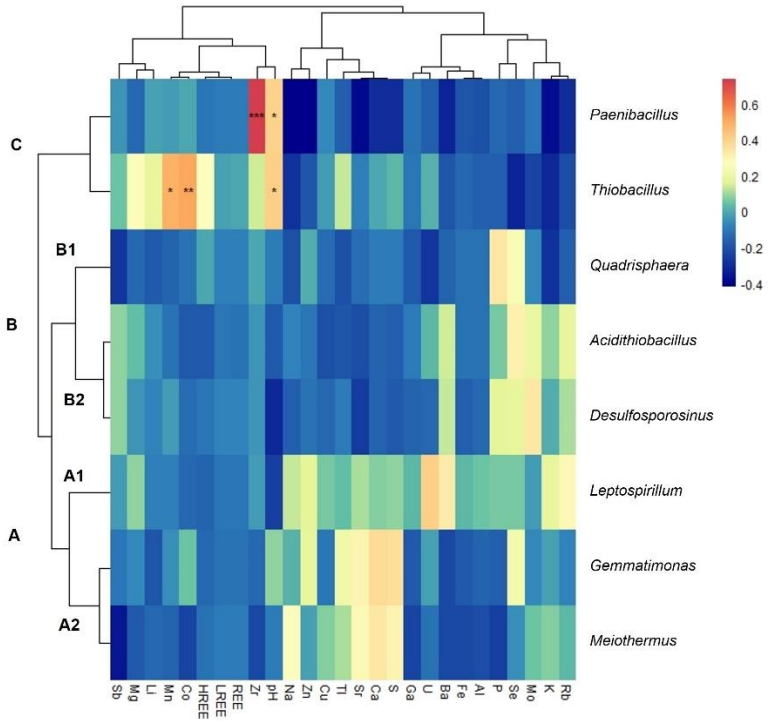

*Fig. 17 A heat map depicting the correlation of the bacterial diversity at genus level and abundances of the physicochemical parameters. Only the top 10 abundant genus are shown in this figure. Dendrograms for hierarchical cluster analysis grouping genus and environmental variables are shown at the left and at the top, respectively. Color key for the correlation values is shown on the right panel inset; positive correlations are in red, negative correlations are in blue, non-significant correlations are shown in white. The corresponding value of heatmap is the Pearson correlation coefficient where marked * indicates significances test p<0.05, marked ** indicated significance test p<0.01 and marked *** indicated significance test p<0.001.*

Additionally, random forest analysis (Fig. 18) was performed in order to determine the microorganisms that play a significant role in the analyzed depth intervals and that could be used as bioindicators of the redox conditions within the deposit of tailings. In arid climate conditions, water flow limitations make it highly complex to obtain pore water samples to determine the redox potential and dissolved oxygen content within the deposit of tailings. According to Fig. 8, it can be seen that *Meiothermus* is the genus that dominates in the first 5 m of depth and is characterized by being an aerobic microorganism with the ability to promote the oxidation of metal sulfides. This trend correlates with the oxidized zone delimited for the El Buitre deposit by González-Díaz et al., (2022). While *Thiobacillus* and *Desulfosporosinus* are the microorganisms that dominate in depths > 5 m and are found mainly under anaerobic conditions. These microorganisms can transform heavy metals into metal sulfides crystals (Su et al., 2022). *Leptospirillum* and *Quadrisphaera* appear to be

dominant in both depth intervals. *Leptospirillum* is an aerobic, acidophilic and Fe (II) oxidizing microorganism, therefore it could be present in the capillary zone or transition to anoxic conditions. This microorganism together with *Meiothermus* could accelerate the oxidation kinetics of pyrite in the oxidized zone. Whereas sulfate-reducing bacteria could be used as bioindicators of anoxic conditions within the tailings deposit, which seem to be established at depths > 5 m.

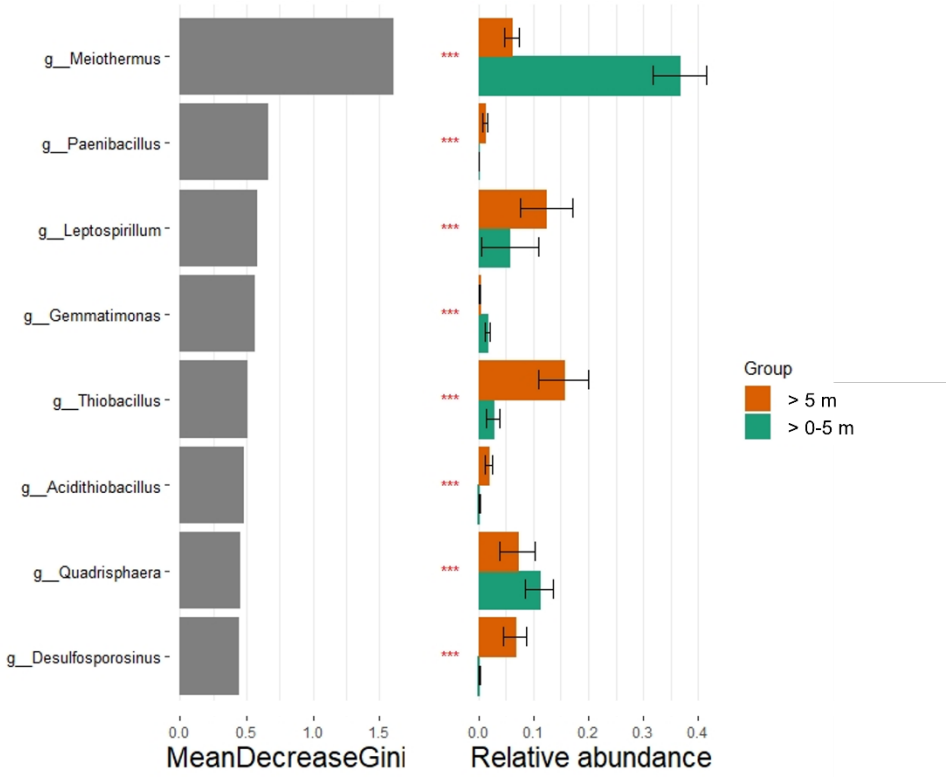

*Fig. 18 Random Forest analysis indicating the most dominant genera in the oxidized and non-oxidized zone. *** It indicates that there is a significant difference between the depth ranges studied.*

On the other hand, the most abundant KEGG pathways predicted by PICRUSt in the deposit of tailings are summarized in (Fig. 19). In general, the relative abundances of the predicted functions were similar between the oxidized and non-oxidized. The most abundant energy metabolism pathway was cysteine and methionine metabolism, follow by sulfur metabolism. Interestingly, these assimilatory sulfate reduction pathways were significantly higher in the oxidized zone, probably due to a higher concentration of bioavailable sulfate for sulfur-amino acid synthesis, if compared with the non-oxidized zone. Additionally, previous works have reported that the main response of microorganisms to heavy metals is the presence of metallothionines (proteins rich in the amino acid cysteine), which are capable of binding metals to their molecular structure and removing them from the intracellular medium (Bozo et al., 2007).

In ddition, in oligotrophic environments with high concentration of contaminating metals, bacterial chemotaxis, two component system, ABC transporters and bacterial secretion

system help bacteria to find optimum conditions for their growth and survival in this extreme environment (Gupta et al., 2020). These pathways facilitate bacterial fitness, homeostasis and competitive advantages for their environmental adaptability (Torre et al., 2012). Bacterial chemotaxis was the most abundant pathway in the deposit of tailings. In addition, two component system and bacterial chemotaxis were significantly higher in the non-oxidized zone, probably due to the change in the chemical composition through the depth profile, that is reflected in an increase in the concentration of elements such as Fe, U, Sb, Al, P, Ba and Mn compared to the oxidized zone. Finally, siderophore biosynthesis occurred in a low proportion. However, it has an important role to increase the mobility and availability of iron and other metals and translocate them intracellularly (Kumar. et al., 2017).

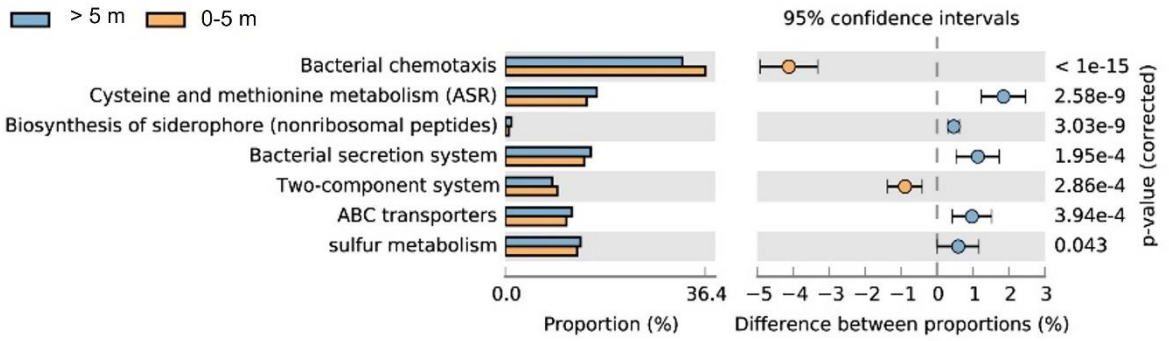

Fig. 19 At the top is shown PICRUSt function analysis. The relative abundance of the predicted functions grouped according KEGG level 3 categories of the bacterial communities in the oxidation (0-5 m) and non-oxidized zone (> 5 m) of the deposit of tailings. At the bottom is shown the biosynthesis of siderophore group nonribosomal peptides pathway.

4.2.4 Biogeochemical conceptual model

Fig. 9 summarizes the main taxa that determine the community differences between the oxidized (0-5 m) and non-oxidized zone (> 5 m), and their association with the bioavailable fraction. In addition, it depicts the synergism between the sulfur-oxidizing bacteria, sulfur-reducing bacteria, iron-oxidizing bacteria, iron-reducing bacteria and bacteria reducing other metals. *Meiothermus* and *Leptospirillum* are the genera that control the cycle of sulfur and iron in the oxidized zone, together with uncultured bacterium belonging to the phylum *Actinobacteria*. In the capillary or transition zone to the non-oxidized zone, *Acidithiobacillus* and *Leptospirillum* could control the oxidation of ferrous iron. The ferric iron ions generated could be reduced by *Meiothermus* and *Spingomonas*. Nevertheless, in the non-oxidized zone, Thiobacillus, could utilize the oxidized metallic elements e.g., Mn^{+4} in presence of sulfur, as an electron sink for their metabolism (Rastogi et al., 2010; Lodha et al., 2010). On the other hand, *Acidithiobacillus*, *Sulforospirillum* and *Tumebacillus* might represents the main source of sulfate in the non-oxidized zone. In addition, *Acidithiobacillus* could participates in the reduction of Fe^{3+} together with bacteria of the genus *Acidiphillum* in the non-oxidized zone. In the deeper sample, sulfate-reducing bacteria could favor the preservation of pyrite. This trend corresponds to the higher relative abundance of pyrite minerals reported by González-Díaz et al., (2022) at the bottom of the deposit of tailings. Additionally, sulfate-

reducing bacteria were used as bioindicators of the redox conditions within the deposit of tailings. Its significant presence in samples with depths > 5 m delimits the beginning of a possible anoxic zone.

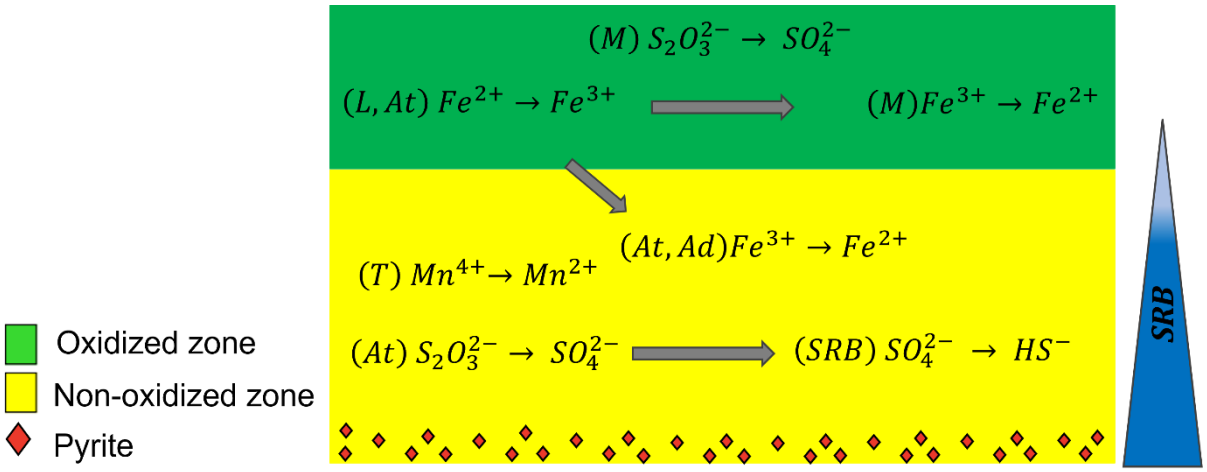

Fig. 20 Conceptual microbiological model based on the sections defined by González-Díaz et al. (2022) and in the significance taxa that determine the community differences between the oxidized (0-5m) and non-oxidized zone (> 5m). M = Meiothermus, L = Leptospirillum, At = Acidithiobacillus, Ad = Acidiphillum, T = Thiobacillus and sulfate-reducing bacteria (SRB). The triangle represents SRB as bioindicators of redox conditions within the deposit of tailings. The light blue color indicates the capillary zone or transition zone to anoxic conditions, while the dark blue color indicates fully anoxic conditions.

4.2.5 Environmental and economic implications

Successful remediation and revalorization strategies can be carried out based on a deep understanding of the functionality and distribution of the core genera and their mutualistic activity with other bacteria in the deposit of tailings (Sun et al., 2018; Chung et al., 2019).

González-Díaz et al., (2022) reported that conditions of high aridity, low water flow and alkaline pH conditions restrict the mobility of contaminating metals within the deposit of tailings El Buitre. Therefore, most of the polluting and toxic elements are associated with sulfide minerals, iron oxyhydroxides and aluminosilicates. Based on previous work, it is possible to propose remediation strategies that include several steps (White et al., 1998). First, stimulate the development of sulfur-oxidizing bacteria (*Meiothermus, Acidithiobacillus* and *Thiobacillus*) to acidify the soil by generating sulfuric acid and solubilizing toxic metals. Subsequently, perform the removal of metals from the leachate, using sulfate-reducing bacteria (*Desulfosporosinus, Desulfotomaculum* and *Thiobacillus*). These bacteria can effectively adsorb metal ions and recover them through metal sulfides precipitation by biosorption and biomineralization (Iravani and Varma, 2020). Additionally, it is possible to stimulate the removal of metals through oxidation-reduction reactions mediated by iron-oxidizing bacteria, iron- reducing bacteria and other metals. For instance, the solubility of Fe increases by reducing ferric iron to ferrous iron (McLean et al., 2002). This reaction could

occur mainly in the non-oxidized zone by *Acidithiobacillus* and *Acidiphilum*. Similarly, *Thiobacillus* can increase the solubility of Mn by reducing it from Mn^{+4} to Mn^{+2} (McLean et al., 2002). Additionally, previous works have reported remediation strategies for soils contaminated with metal relies on siderophore-mediated metal solubilization. Although primarily produced as a means of obtaining iron (e.g., *Leptospirillum*), siderophores are also able to bind other metals such as Mg^{2+}, Mn^{2+}, $Cr^{3+,}$ Ga^{3+}, among others (Hesse et al., 2018).

Finally, the restoration of the deposit with plants could be carried out taking into consideration the plant species that are currently growing on the surface and that were probably established by wind dispersal of the seeds from nearby inhabitants. In addition, the development of native plants could be stimulated by bacteria such as *Paenibacillus*, *Lysinibacillus* and *Bacillus*, characterized as plant growth-promoting bacteria (Tiwari et al., 2016).

González-Díaz et al., (2022) based on the geochemical and mineralogical characterization of El Buitre tailings deposit, proposed as future revalorization studies, the economic recovery of Fe associated with magnetite, Cu associated with chalcopyrite and pyrite, and Co incorporated within the pyrite crystal structure. Based on the microbiological characterization, in situ pyrite bioleaching strategies could be proposed for the recovery of Co and Cu. In the oxidized zone, promote the development of sulfur and iron oxidizing bacteria that dominate in this section (*Meiothermus, Leptospirillum* and *Acidithiobacillus*) through bioaugmentation technique (Branco et al., 2009). In order to stimulate the chemical alteration of pyrite and subsequent release of the Co and Cu incorporated in its crystalline structure. In contrast, in the non-oxidized zone, sulfate-reducing bacteria favor the precipitation of pyrite. However, the bioaugmentation of the genus *Acidithiobacillus* could stimulate pyrite oxidation at the bottom of the deposit of tailings. In the case of Cu and Fe associated with chalcopyrite and magnetite, it is not feasible to propose their recovery through in situ bioleaching because they are highly recalcitrant mineral, with a fairly slow dissolution kinetics that requires more advanced extraction techniques (Hong et al., 2021; Tang et al., 2019).

On the other hand, currently, studies have been developed aimed at reducing the toxicity and cost of the chemical reagents used in the magnetite flotation process for the recovery of Fe (Kim et al., 2015). An alternative is the use of indigenous bacteria found in mining waste, such as species of the genus *Paenibacillus* and *Bacillus* (Teng et al., 2018, 2021; Zhao et al., 2017) found mainly in the non-oxidized zone of the deposit of tailings. The adsorption of the bacteria to the mineral surface can induce extracellular bio-reagents production such as proteins and polysaccharides, which can act as silicate mineral depressants during magnetite flotation (Dwyer et al., 2012).

CHAPTER 5

5. SUPPLEMENTARY MATERIAL

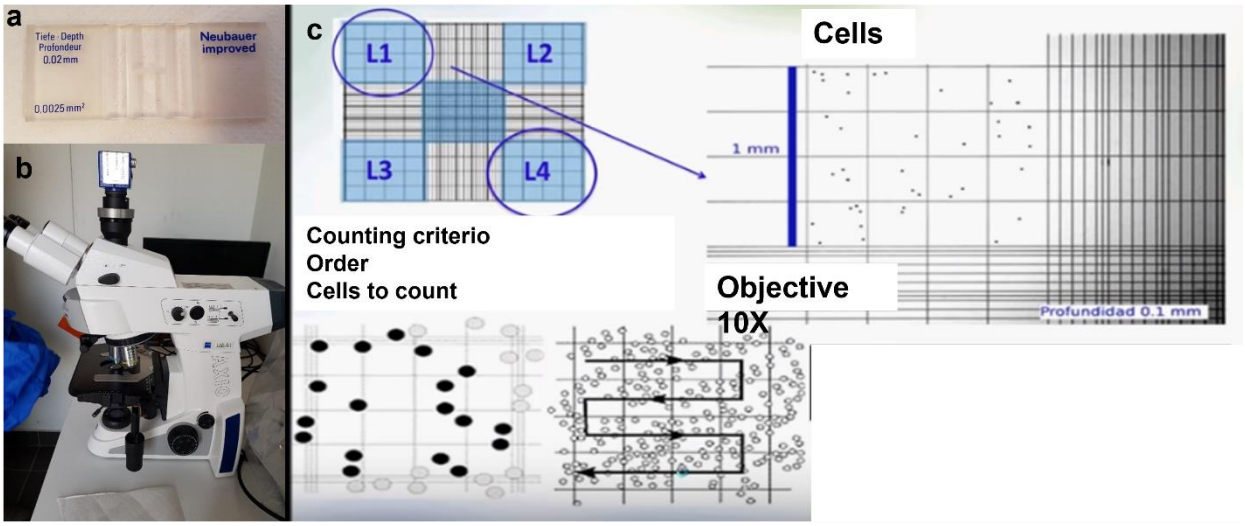

Fig. S 1 a. Neubauer cell counting chamber, b, microscope for cell counting. c. Criteria used for cell counting, counting order is indicated by the arrows and the cells are represented as points.

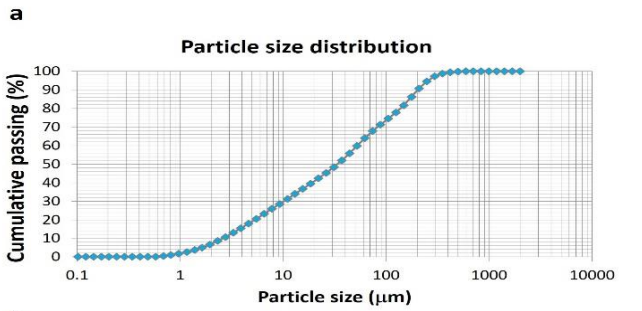

Depth range	paste pH
0-1m	7.94
1-2m	7.87
2-3m	7.91
3-4m	7.93
4-5m	7.92
8-9m	7.95
11-12m	7.78
14-18m	7.90
20-23m	7.82
34-43m	7.94
Mean	**7.90**

Fig. S 2. Physicochemical main characteristics of the deposit of tailings: a) particle size distribution of the tailings; b) oxidation reactions in fine-grained layers; c) paste pH at different depth ranges.

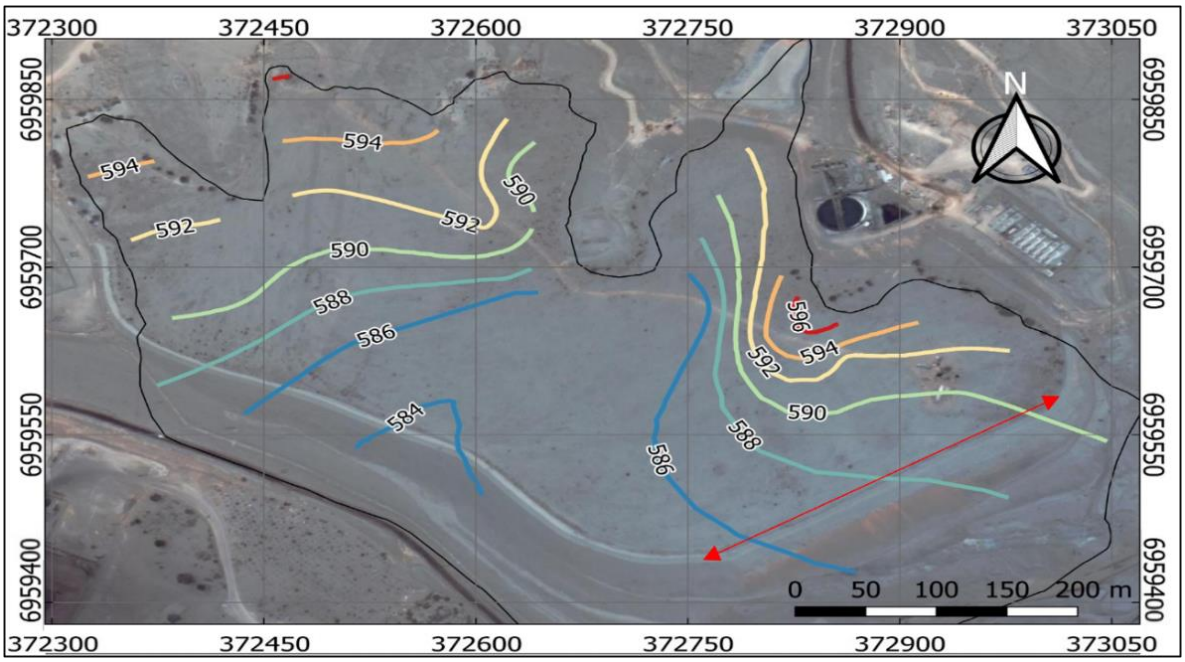

Fig. S 3 Iso piezometric map defining the "moisture horizon" within the deposit of tailings. The isopiezometric lines are reference in meters above sea level (msnm).

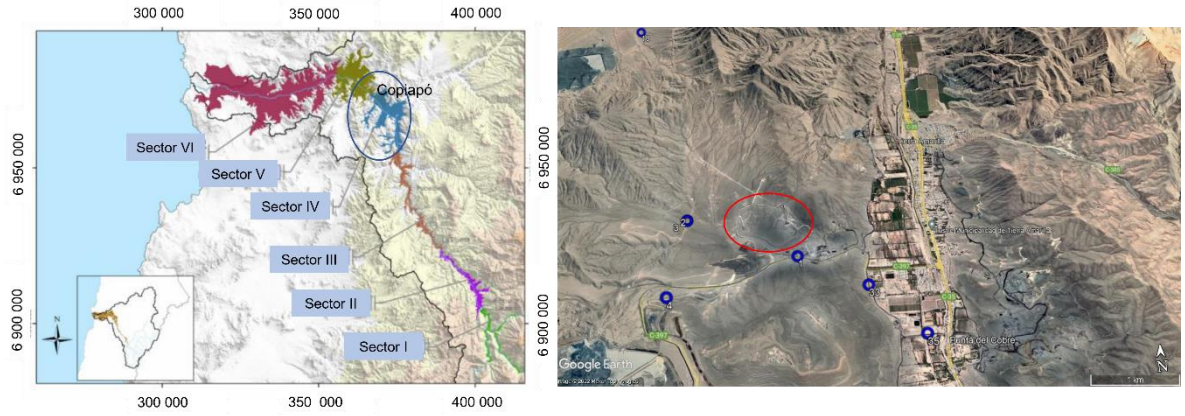

Fig. S 4 The left panel represents the unconfined Copiapó aquifer and its 6 subdivisions (modified from Compañía Contractual Minera Candelaria, 2013). El Buitre tailings deposit is located in sector IV. The right panel represents the groundwater monitoring boreholes belonging to the Compañía Contractual Minera Candelaria, located in the vicinity of El Buitre tailings deposit (highlighted in red). The depth of the boreholes (m) and the piezometric level (m) are indicated in brackets: 1 (n/i, 89), 2 (150, 89), 3 (130, 28.2), 4 (150, 44), 18 (125, 54), 33 (162, 56) and 35 (n/i). n/i: no information.

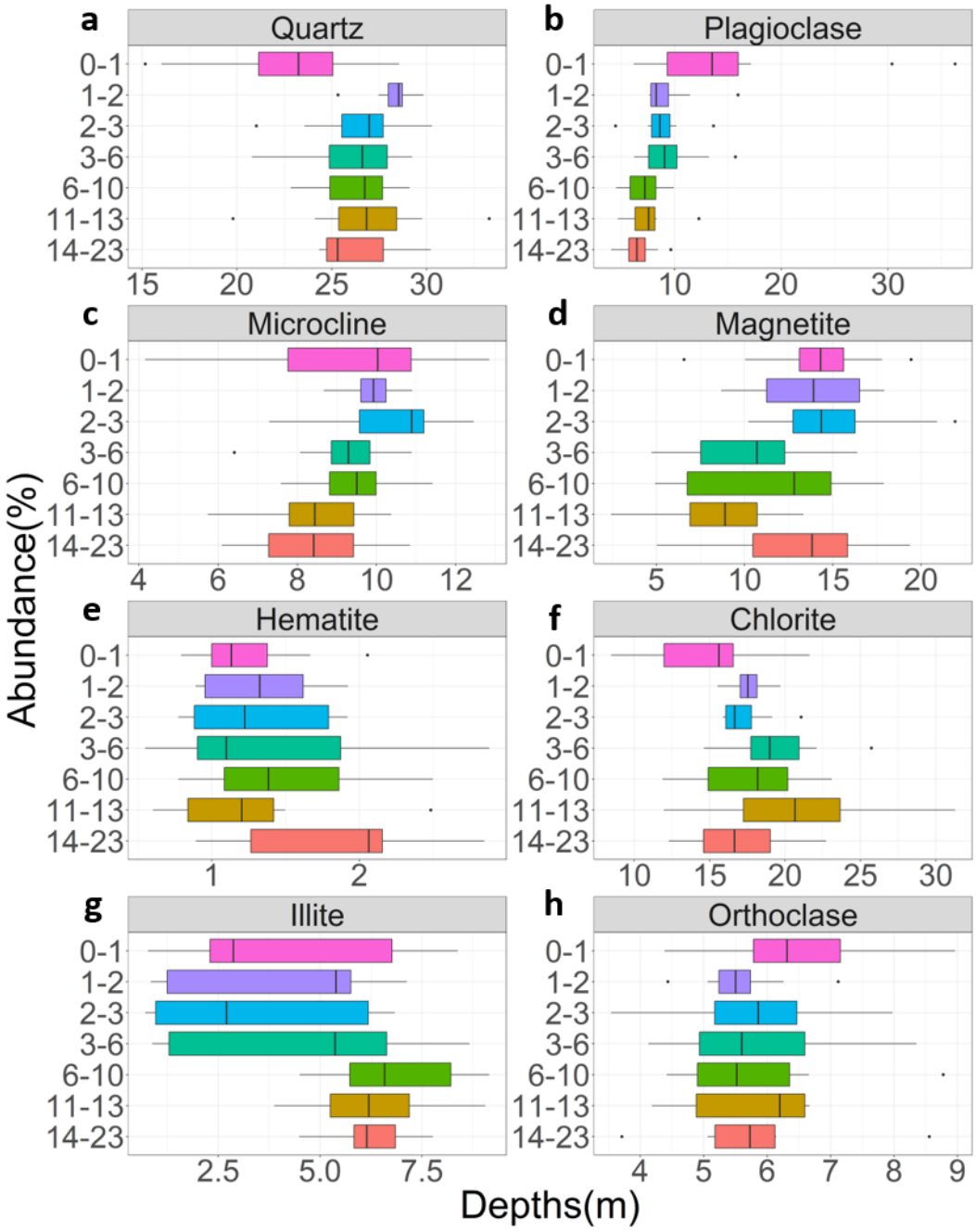

Fig. S 5. Mineralogical characterization of major minerals by XRD in samples at different depths.

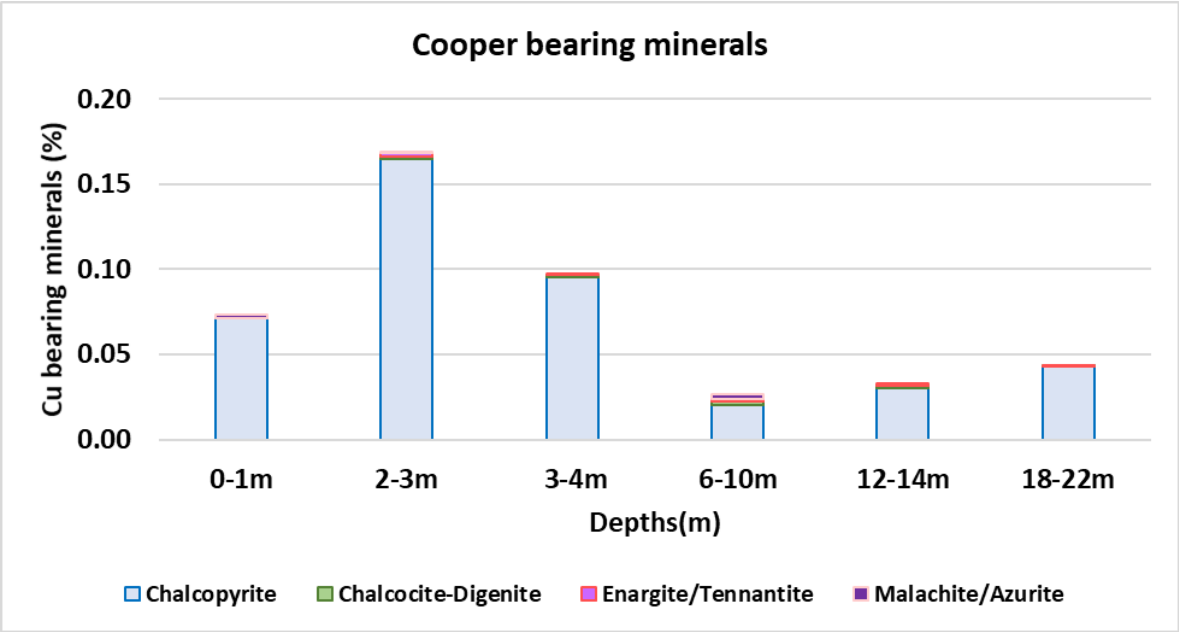

Fig. S 6 Main copper-bearing minerals in the deposit of tailings

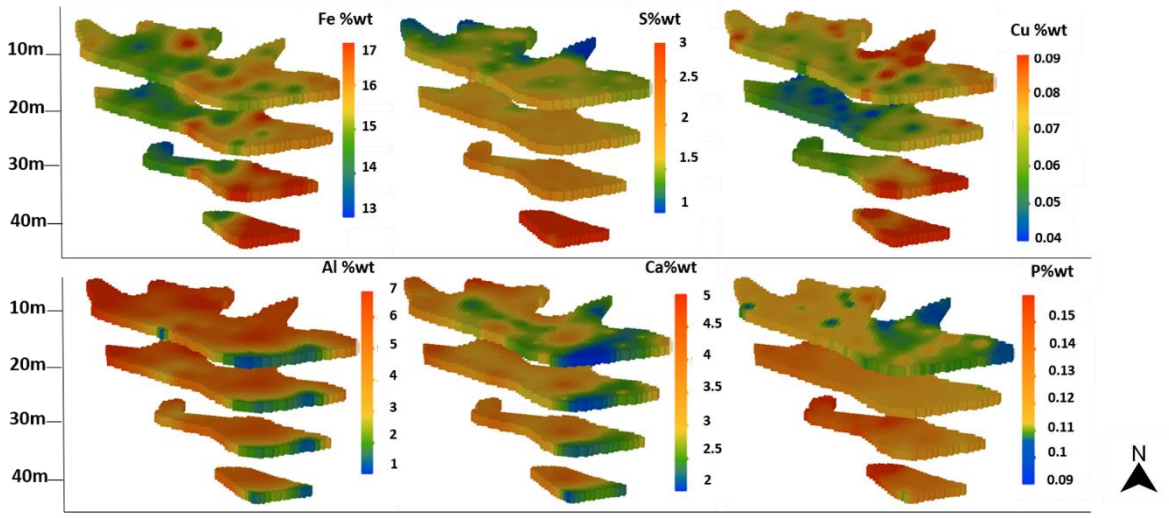

Fig. S 7 Spatial distribution of Fe, S, Cu, Al, Ca, and P grades in the deposit of tailings according to the block model

.

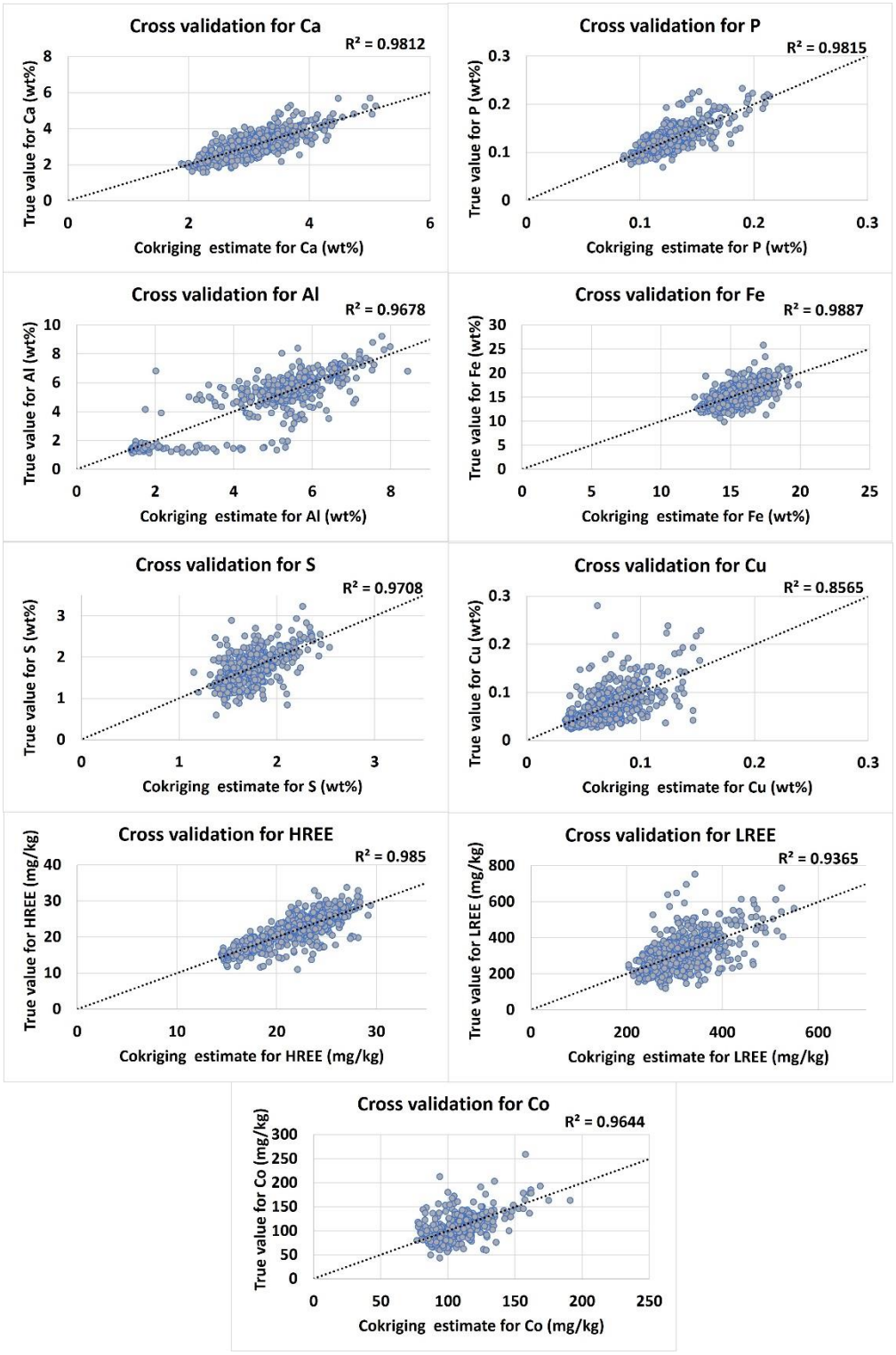

Fig. S 8 Cross validation of the geostatistical model for the main majority (Ca, P, Al, Fe and S), minority (LREE and Co) and traces (HREE) elements.

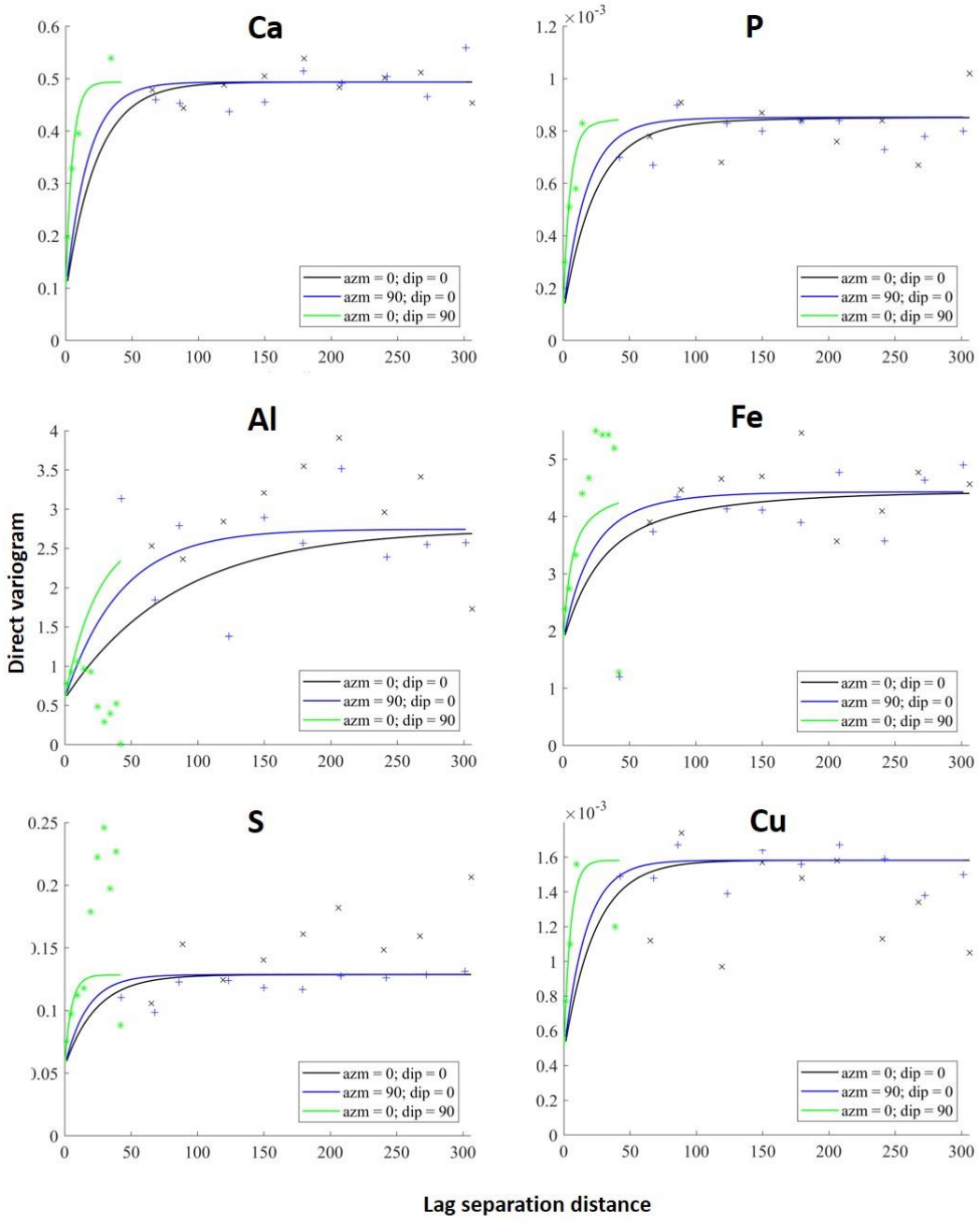

Fig. S 9 Variograms for Ca, P, Al, Fe, S and Cu models calculated omni-horizontally (black), azimuth 90°; dip=0 (blue) and vertically (green).

.

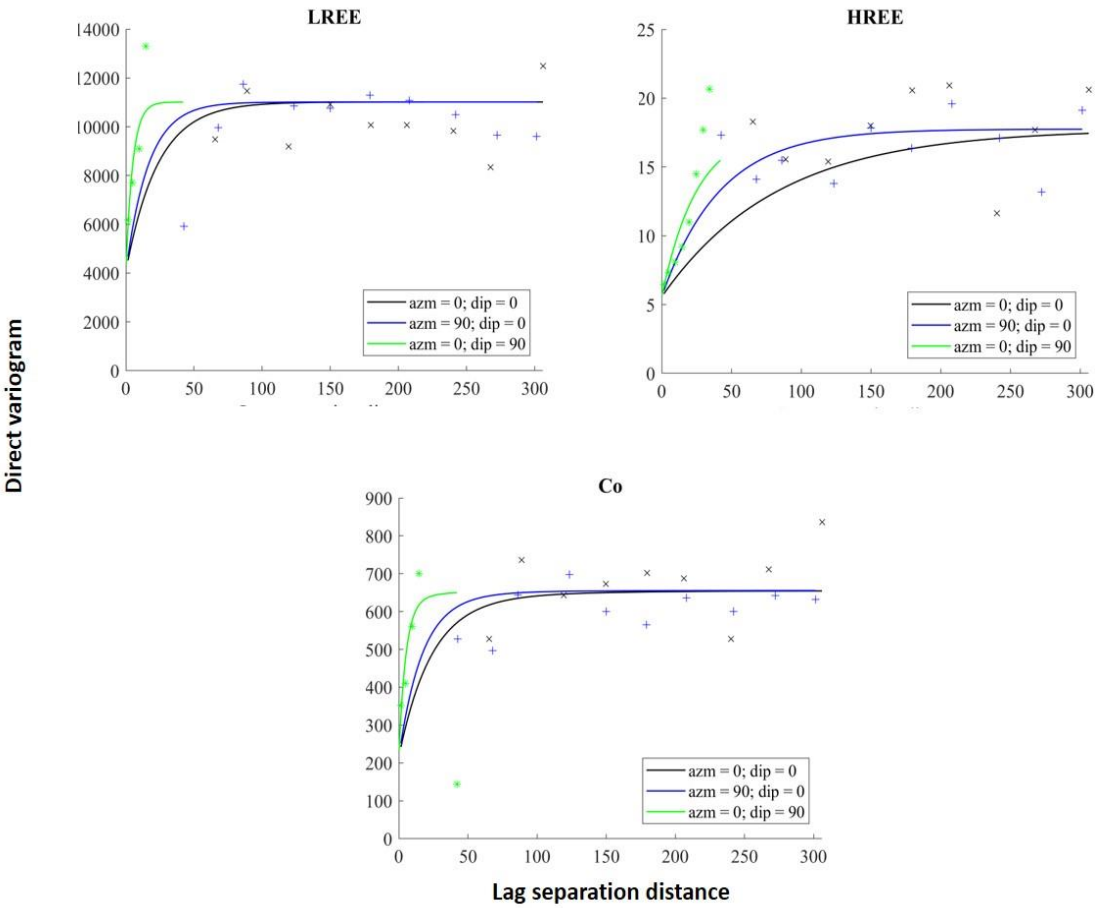

Continuation Fig. S9. Variograms for LREE, HREE and Co models calculated omni-horizontally (black) and vertically (green).

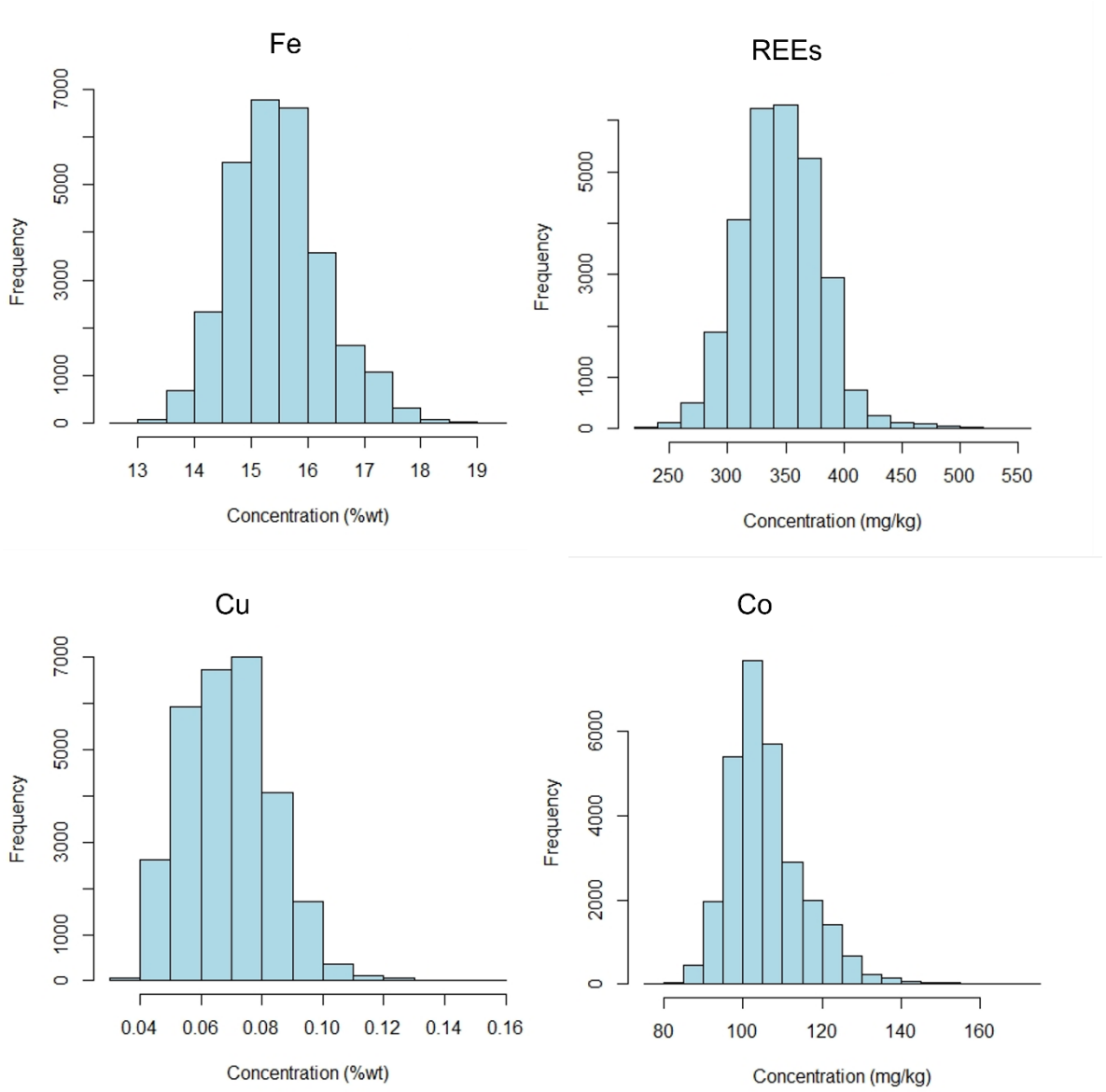

Fig. S 10 Distribution of Fe, REEs, Cu and Co concentrations according to the block model.

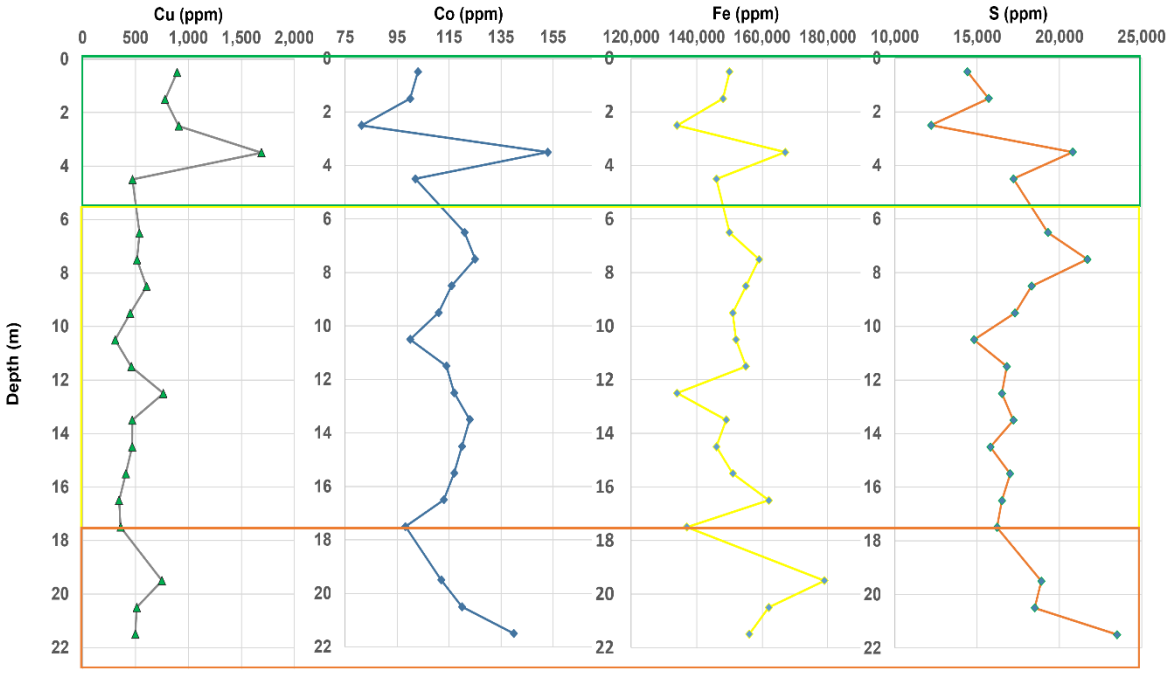

Fig. S 11 Representative trend of the boreholes Ad1, Ad2, Ad3, PB1, PB3, PB5, PB6, PB7 and the samples taken with a hand auger (M1-M8), of the concentrations of Cu, Co, Fe and S through the depth profile. The sections outlined in colors represent changes in the trend of elemental concentrations: the green rectangle up to ~ 5 m, the yellow up to ~ 17 m and the orange at > 17 m.

Depths < 5 m

	Ti	P	S	Ag	Cs	Al	As	Be	Bi	Ca	Co	Cu	Fe	Ga	Ge	K	Li	Mg	Mn	Mo	Na	Ni	Pb	Re	Sn	Th	U	V	W	Zn	LREE	HREE
Ti	1.000																															
P	0.146	1.000																														
S	-0.345	0.288	1.000																													
Ag	-0.042	0.357	0.558	1.000																												
Cs	0.457	0.078	-0.103	0.069	1.000																											
Al	0.389	-0.100	-0.141	0.020	0.368	1.000																										
As	0.035	0.083	0.498	0.407	0.195	0.031	1.000																									
Be	0.509	-0.074	-0.098	0.191	0.742	0.508	0.117	1.000																								
Bi	-0.150	0.447	0.648	0.548	0.186	-0.029	0.565	0.100	1.000																							
Ca	0.448	0.617	0.055	0.279	0.347	0.215	0.035	0.346	0.367	1.000																						
Co	-0.120	0.170	0.817	0.571	0.167	0.130	0.449	0.253	0.501	0.076	1.000																					
Cu	-0.093	-0.324	0.282	0.354	0.079	0.152	0.155	0.217	0.076	-0.281	0.392	1.000																				
Fe	-0.095	0.083	0.495	0.506	0.225	0.139	0.370	0.375	0.374	-0.028	0.675	0.280	1.000																			
Ga	0.300	0.055	0.044	0.430	0.412	0.735	0.260	0.576	0.187	0.215	0.349	0.223	0.479	1.000																		
Ge	0.320	-0.029	-0.015	0.263	0.289	0.259	0.225	0.508	0.051	0.148	0.230	0.172	0.355	0.496	1.000																	
K	0.149	-0.280	0.061	0.074	0.349	0.307	0.091	0.355	0.126	-0.137	0.160	0.305	0.275	0.310	0.181	1.000																
Li	0.272	0.086	0.127	0.198	0.770	0.255	0.257	0.733	0.403	0.367	0.289	0.142	0.343	0.349	0.317	0.476	1.000															
Mg	0.319	0.274	0.112	0.304	0.673	0.369	0.121	0.656	0.388	0.422	0.334	0.069	0.485	0.603	0.338	0.492	0.778	1.000														
Mn	0.411	0.584	0.056	0.428	0.431	0.383	0.158	0.418	0.424	0.803	0.179	-0.152	0.216	0.522	0.305	-0.040	0.418	0.591	1.000													
Mo	0.271	-0.062	0.103	0.145	0.074	0.428	0.277	0.077	0.014	0.038	0.207	0.218	0.050	0.291	0.084	0.008	-0.032	-0.094	0.174	1.000												
Na	0.470	-0.300	-0.380	-0.188	0.259	0.308	-0.183	0.552	-0.353	0.073	-0.160	0.118	-0.269	0.174	0.271	0.057	0.215	0.095	-0.036	0.016	1.000											
Ni	-0.123	0.472	0.710	0.679	0.088	0.126	0.559	0.155	0.697	0.268	0.719	0.088	0.677	0.425	0.176	-0.031	0.215	0.383	0.423	0.089	-0.320	1.000										
Pb	-0.076	0.299	0.257	0.251	0.081	-0.365	0.205	0.023	0.358	0.256	0.143	-0.054	0.118	-0.197	0.005	-0.055	0.266	0.172	0.139	-0.237	-0.115	0.223	1.000									
Re	0.217	-0.044	-0.081	0.286	0.029	0.419	0.105	0.165	-0.029	0.081	0.094	0.146	0.065	0.508	0.302	-0.002	-0.105	0.036	0.254	0.404	0.121	0.101	-0.257	1.000								
Sn	0.349	0.117	0.074	0.323	0.501	0.412	0.204	0.646	0.258	0.441	0.260	0.104	0.303	0.507	0.413	0.222	0.588	0.532	0.490	0.134	0.222	0.272	0.102	0.118	1.000							
Th	0.292	0.026	-0.056	0.054	0.344	0.431	-0.170	0.426	0.079	0.177	0.120	0.069	0.166	0.328	-0.011	0.576	0.378	0.564	0.227	-0.021	0.257	0.079	-0.064	0.030	0.292	1.000						
U	0.220	0.029	0.052	0.315	0.629	0.344	0.125	0.637	0.329	0.265	0.220	0.215	0.269	0.446	0.273	0.606	0.811	0.705	0.369	0.024	0.185	0.166	0.157	0.075	0.568	0.565	1.000					
V	0.531	0.070	-0.117	-0.130	0.589	0.088	-0.033	0.620	0.001	0.329	0.113	-0.023	0.292	0.055	0.227	0.176	0.559	0.497	0.212	-0.115	0.306	0.029	0.214	-0.240	0.391	0.344	0.337	1.000				
W	-0.071	0.119	0.358	0.363	0.148	0.004	0.477	0.173	0.429	0.165	0.281	0.175	0.293	0.130	0.051	0.176	0.434	0.192	0.180	0.202	-0.151	0.345	0.235	-0.051	0.310	0.024	0.419	0.067	1.000			
Zn	0.497	0.090	-0.197	0.173	0.510	0.416	-0.038	0.545	-0.040	0.312	0.131	0.021	0.186	0.533	0.369	0.154	0.316	0.501	0.471	0.139	0.288	0.112	-0.053	0.285	0.400	0.380	0.342	0.404	-0.100	1.000		
LREE	-0.074	-0.096	0.174	0.212	0.076	0.319	0.118	0.149	0.119	-0.293	0.349	0.218	0.444	0.495	0.119	0.375	0.060	0.276	0.011	0.174	-0.039	0.254	-0.232	0.250	0.060	0.489	0.184	-0.113	0.002	0.220	1.000	
HREE	0.448	0.245	-0.074	0.225	0.353	0.652	-0.050	0.483	0.107	0.372	0.207	-0.015	0.229	0.665	0.247	0.240	0.222	0.481	0.556	0.243	0.223	0.238	-0.201	0.389	0.415	0.622	0.350	0.193	-0.073	0.586	0.615	1.000

Depths between 5-17 m

	Ti	P	S	Ag	Al	As	Cs	Be	Bi	Ca	Co	Cu	Fe	Ga	Ge	K	Li	Mg	Mn	Mo	Na	Ni	Pb	Re	Sn	Th	U	V	W	Zn	LREE	HREE
Ti	1.000																															
P	0.512	1.000	0.492																													
S	-0.086	0.492	1.000																													
Ag	0.421	0.424	0.346	1.000																												
Al	0.629	0.373	0.053	0.223	1.000																											
As	0.357	0.625	0.592	0.319	0.293	1.000																										
Cs	0.678	0.441	-0.132	0.174	0.524	0.342	1.000																									
Be	0.592	0.102	-0.187	0.408	0.469	0.119	0.523	1.000																								
Bi	0.421	0.667	0.501	0.360	0.350	0.709	0.439	0.205	1.000																							
Ca	0.739	0.719	0.339	0.408	0.564	0.664	0.595	0.405	0.702	1.000																						
Co	0.351	0.542	0.768	0.596	0.451	0.625	0.181	0.292	0.565	0.566	1.000																					
Cu	-0.117	-0.397	-0.351	0.152	-0.270	-0.380	-0.106	0.152	-0.292	-0.360	-0.389	1.000																				
Fe	-0.121	-0.075	0.312	0.351	0.007	0.003	-0.240	0.350	0.049	-0.091	0.451	0.121	1.000																			
Ga	0.787	0.532	0.025	0.569	0.795	0.322	0.572	0.642	0.418	0.641	0.554	-0.116	0.132	1.000																		
Ge	0.362	0.127	0.016	0.329	0.327	0.154	0.153	0.482	0.165	0.313	0.313	0.070	0.299	0.493	1.000																	
K	0.176	-0.085	-0.210	0.078	0.200	-0.254	0.200	0.227	-0.033	0.018	-0.126	0.255	0.148	0.107	0.076	1.000																
Li	0.678	0.325	-0.231	0.161	0.447	0.171	0.785	0.673	0.324	0.547	0.138	0.032	-0.155	0.566	0.252	0.230	1.000															
Mg	0.764	0.547	-0.084	0.447	0.529	0.151	0.680	0.604	0.363	0.575	0.360	-0.014	0.019	0.819	0.346	0.184	0.794	1.000														
Mn	0.779	0.714	0.271	0.562	0.631	0.612	0.615	0.518	0.680	0.909	0.597	-0.209	0.026	0.794	0.410	0.116	0.568	0.689	1.000													
Mo	0.304	0.251	0.163	0.220	0.508	0.442	0.247	0.148	0.355	0.432	0.286	-0.176	0.002	0.349	0.146	0.037	0.054	0.024	0.452	1.000												
Na	0.351	-0.200	-0.345	-0.009	0.154	-0.154	0.114	0.424	-0.301	0.010	-0.048	0.097	-0.069	0.254	0.253	-0.146	0.344	0.283	0.026	-0.128	1.000											
Ni	0.342	0.636	0.692	0.673	0.458	0.556	0.167	0.310	0.556	0.512	0.886	-0.294	0.512	0.607	0.341	-0.008	0.076	0.413	0.620	0.299	-0.095	1.000										
Pb	-0.057	0.213	0.176	0.045	-0.283	0.321	0.111	-0.080	0.354	0.135	0.039	0.011	-0.003	-0.165	-0.087	-0.113	0.153	0.030	0.049	-0.038	-0.242	-0.017	1.000									
Re	0.461	0.191	0.088	0.521	0.464	0.257	0.097	0.335	0.181	0.397	0.393	-0.022	0.197	0.565	0.387	0.145	-0.016	0.221	0.509	0.429	0.080	0.463	-0.302	1.000								
Sn	0.614	0.321	0.086	0.532	0.456	0.318	0.450	0.681	0.420	0.615	0.454	-0.001	0.213	0.628	0.435	0.138	0.566	0.535	0.675	0.253	0.215	0.391	0.029	0.398	1.000							
Th	0.460	0.223	0.003	0.245	0.500	-0.046	0.434	0.339	0.224	0.376	0.265	-0.032	0.110	0.475	0.013	0.504	0.432	0.560	0.398	0.094	0.019	0.244	-0.084	0.177	0.317	1.000						
U	0.703	0.211	-0.225	0.371	0.465	0.125	0.707	0.676	0.306	0.501	0.238	0.082	-0.064	0.652	0.282	0.277	0.804	0.728	0.563	0.116	0.277	0.143	0.043	0.217	0.654	0.580	1.000					
V	0.049	-0.009	-0.057	-0.117	-0.079	-0.087	0.216	0.362	0.117	-0.017	0.003	0.110	0.431	-0.043	-0.009	0.190	0.383	0.232	-0.052	-0.191	0.102	0.024	0.299	-0.369	0.158	0.216	0.232	1.000				
W	0.260	0.118	0.110	0.125	0.125	0.326	0.177	0.231	0.256	0.249	0.152	0.018	0.031	0.099	0.009	0.018	0.274	0.091	0.268	0.190	0.087	0.065	0.194	0.024	0.396	0.071	0.262	0.170	1.000			
Zn	0.627	0.482	0.131	0.567	0.452	0.355	0.467	0.527	0.481	0.492	0.490	-0.027	0.208	0.713	0.340	0.126	0.436	0.667	0.646	0.203	0.195	0.603	0.032	0.436	0.557	0.360	0.537	0.159	0.158	1.000		
LREE	0.438	0.430	0.167	0.485	0.648	0.099	0.283	0.365	0.266	0.354	0.515	-0.156	0.281	0.715	0.241	0.203	0.249	0.548	0.505	0.313	0.023	0.564	-0.209	0.380	0.356	0.641	0.407	0.015	0.013	0.459	1.000	
HREE	0.732	0.572	0.186	0.565	0.807	0.337	0.525	0.521	0.478	0.672	0.618	-0.231	0.161	0.882	0.368	0.253	0.454	0.691	0.778	0.434	0.070	0.645	-0.185	0.562	0.585	0.670	0.611	-0.028	0.120	0.648	0.855	1.000

Fig. S 12 . Pearson's correlation for Ti, P, S, Ag, Cs, Al, As, Be, Bi, Ca, Co, Cu, Fe, Ga, Ge, K, Li, Mg Mn, Mo, Ni, Pb, Re, Sn, Th, U, W, Zn, LREE and HREE in 755 samples. The p value at level 0.05.

Depths > 17 m

	Ti	P	S	Ag	Al	As	Bi	Be	Cs	Ca	Co	Cu	Fe	Ga	Ge	K	Li	Mg	Mn	Mo	Na	Ni	Pb	Re	Sn	Th	U	V	W	Zn	HREE	LREE
Ti	1.000																															
P	0.180	1.000																														
S	-0.477	0.559	1.000																													
Ag	-0.264	0.720	0.825	1.000																												
Al	0.494	0.677	0.276	0.400	1.000																											
As	0.055	0.541	0.630	0.578	0.491	1.000																										
Bi	0.075	0.752	0.651	0.630	0.618	0.656	1.000																									
Be	-0.255	-0.113	0.268	0.191	-0.145	0.037	0.056	1.000																								
Cs	0.805	0.433	-0.211	0.002	0.678	0.073	0.307	-0.159	1.000																							
Ca	0.399	0.786	0.391	0.507	0.672	0.657	0.697	-0.213	0.472	1.000																						
Co	-0.484	0.541	0.922	0.770	0.309	0.526	0.630	0.326	-0.170	0.285	1.000																					
Cu	-0.269	-0.155	-0.010	0.120	-0.279	-0.147	-0.171	0.124	-0.232	-0.234	-0.003	1.000																				
Fe	-0.710	0.026	0.651	0.433	-0.207	0.109	0.145	0.604	-0.546	-0.202	0.680	0.092	1.000																			
Ga	0.286	0.865	0.497	0.632	0.818	0.550	0.721	0.025	0.499	0.721	0.538	-0.255	0.032	1.000																		
Ge	-0.037	0.141	0.217	0.153	0.119	0.186	0.184	0.304	-0.046	0.172	0.229	-0.079	0.241	0.166	1.000																	
K	0.262	-0.404	-0.537	-0.501	-0.148	-0.482	-0.398	-0.131	0.075	-0.320	-0.507	0.022	-0.279	-0.297	-0.090	1.000																
Li	0.772	0.435	-0.215	0.048	0.593	0.273	0.288	-0.357	0.748	0.622	-0.270	-0.198	-0.701	0.478	-0.059	0.045	1.000															
Mg	0.382	0.839	0.291	0.537	0.614	0.341	0.553	-0.204	0.542	0.702	0.275	-0.213	-0.178	0.829	0.011	-0.183	0.680	1.000														
Mn	0.506	0.786	0.335	0.514	0.726	0.576	0.648	-0.116	0.580	0.915	0.232	-0.265	-0.202	0.794	0.176	-0.207	0.692	0.787	1.000													
Mo	0.490	0.288	-0.011	0.117	0.583	0.297	0.251	-0.116	0.517	0.369	-0.017	-0.050	-0.239	0.396	0.130	0.122	0.438	0.263	0.489	1.000												
Na	0.017	-0.353	-0.324	-0.380	-0.240	-0.104	-0.342	0.056	-0.234	-0.306	-0.241	0.037	-0.162	-0.334	0.036	0.025	-0.233	-0.473	-0.382	-0.134	1.000											
Ni	-0.431	0.672	0.920	0.863	0.344	0.550	0.638	0.281	-0.158	0.395	0.919	-0.085	0.672	0.634	0.233	-0.522	-0.194	0.441	0.372	-0.030	-0.286	1.000										
Pb	-0.531	0.266	0.539	0.500	-0.072	0.282	0.267	0.187	-0.312	0.036	0.518	0.173	0.507	0.077	0.111	-0.480	-0.317	0.019	-0.057	-0.133	-0.035	0.549	1.000									
Re	0.164	0.158	0.165	0.245	0.216	0.325	0.123	0.177	0.010	0.246	0.150	-0.081	0.123	0.355	0.166	-0.012	0.040	0.159	0.335	0.235	-0.009	0.227	-0.086	1.000								
Sn	0.456	0.292	0.069	0.146	0.468	0.252	0.328	0.111	0.440	0.444	0.027	-0.093	-0.198	0.410	0.140	-0.024	0.503	0.342	0.556	0.429	-0.262	0.001	-0.217	0.192	1.000							
Th	0.157	0.473	0.181	0.258	0.442	0.002	0.409	-0.117	0.326	0.407	0.235	-0.167	-0.051	0.471	-0.088	0.219	0.183	0.443	0.377	0.139	-0.131	0.279	-0.040	0.031	0.166	1.000						
U	0.734	0.031	-0.472	-0.229	0.320	-0.072	-0.006	-0.198	0.624	0.215	-0.488	-0.065	-0.729	0.157	-0.084	0.388	0.755	0.305	0.350	0.353	-0.150	-0.496	-0.545	0.064	0.518	0.130	1.000					
V	-0.489	0.128	0.456	0.308	-0.151	0.031	0.132	0.345	-0.281	-0.023	0.462	-0.064	0.740	0.021	0.138	-0.364	-0.511	-0.051	-0.138	-0.270	-0.070	0.539	0.532	-0.074	-0.384	0.089	-0.739	1.000				
W	-0.051	0.073	0.211	0.225	0.204	0.237	0.133	0.124	-0.030	0.033	0.213	0.140	0.181	0.122	-0.022	-0.034	0.073	0.034	0.134	0.353	-0.105	0.139	0.069	0.037	0.322	-0.091	0.078	-0.110	1.000			
Zn	0.574	0.467	0.009	0.133	0.455	0.416	0.414	-0.124	0.521	0.641	-0.057	-0.131	-0.352	0.484	0.118	0.008	0.566	0.484	0.666	0.453	-0.107	0.039	-0.086	0.307	0.409	0.291	0.391	-0.213	-0.140	1.000		
HREE	0.362	0.801	0.395	0.534	0.834	0.483	0.691	-0.033	0.551	0.749	0.448	-0.255	-0.087	0.890	0.155	-0.113	0.490	0.703	0.791	0.462	-0.265	0.493	-0.010	0.326	0.438	0.668	0.269	-0.084	0.091	0.522	1.000	
LREE	-0.098	0.697	0.586	0.598	0.593	0.406	0.619	0.120	0.159	0.483	0.689	-0.129	0.302	0.759	0.140	-0.188	0.079	0.509	0.511	0.262	-0.204	0.689	0.237	0.234	0.178	0.613	-0.134	0.182	0.163	0.195	0.842	1.000

Continuation Fig. S12. Pearson's correlation for Ti, P, S, Ag, Cs, Al, As, Be, Bi, Ca, Co, Cu, Fe, Ga, Ge, K, Li, Mg Mn, Mo, Ni, Pb, Re, Sn, Th, U, W, Zn, LREE and HREE in 755 samples. The p value at level 0.05.

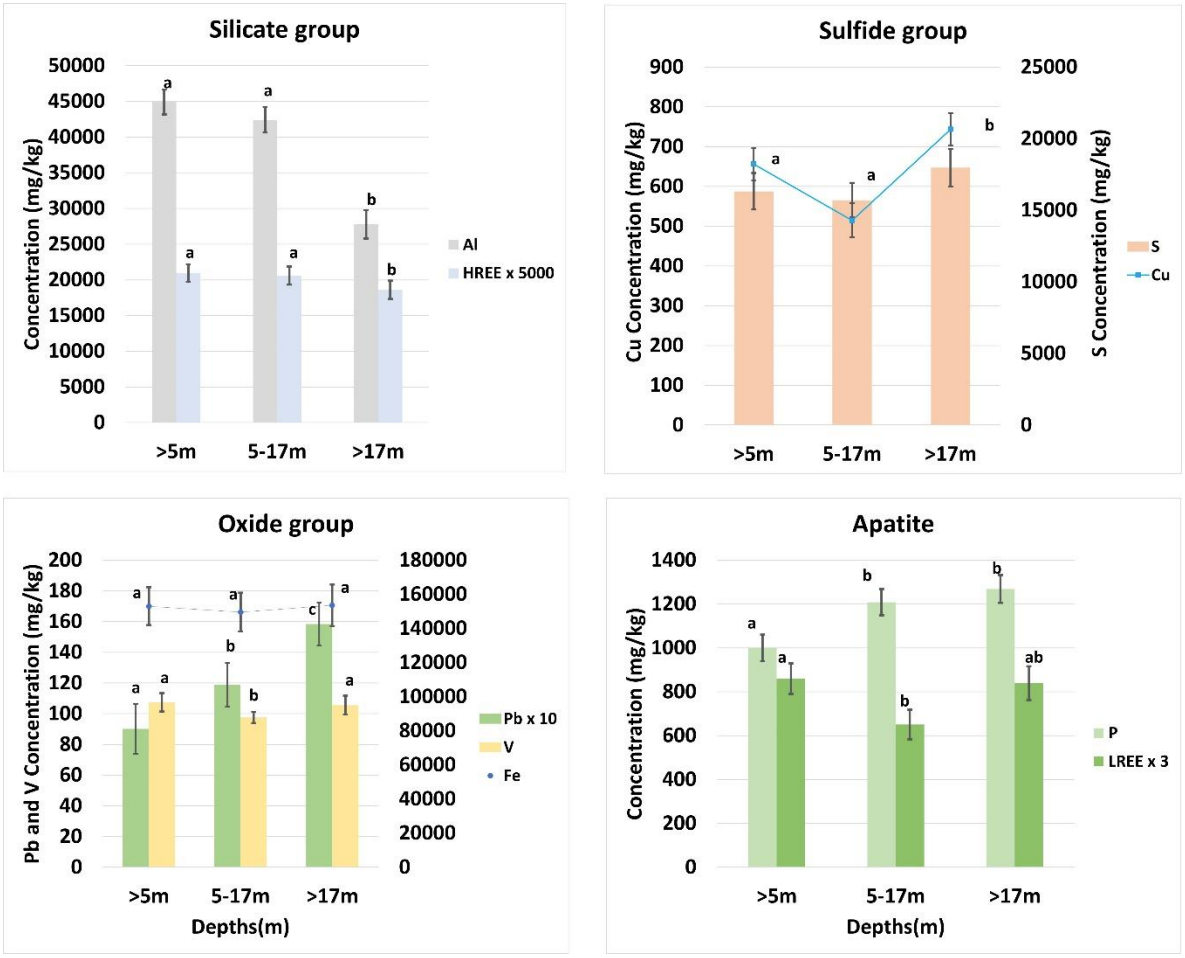

Fig. S 13 One-way ANOVA and Welch test analysis comparing the main elements grouped by the PCA at different depth intervals < 5 m (N = 195), 5-17 m (N = 202) and > 17 m (N = 191). Some elements were multiplied by integers to improve their visualization.

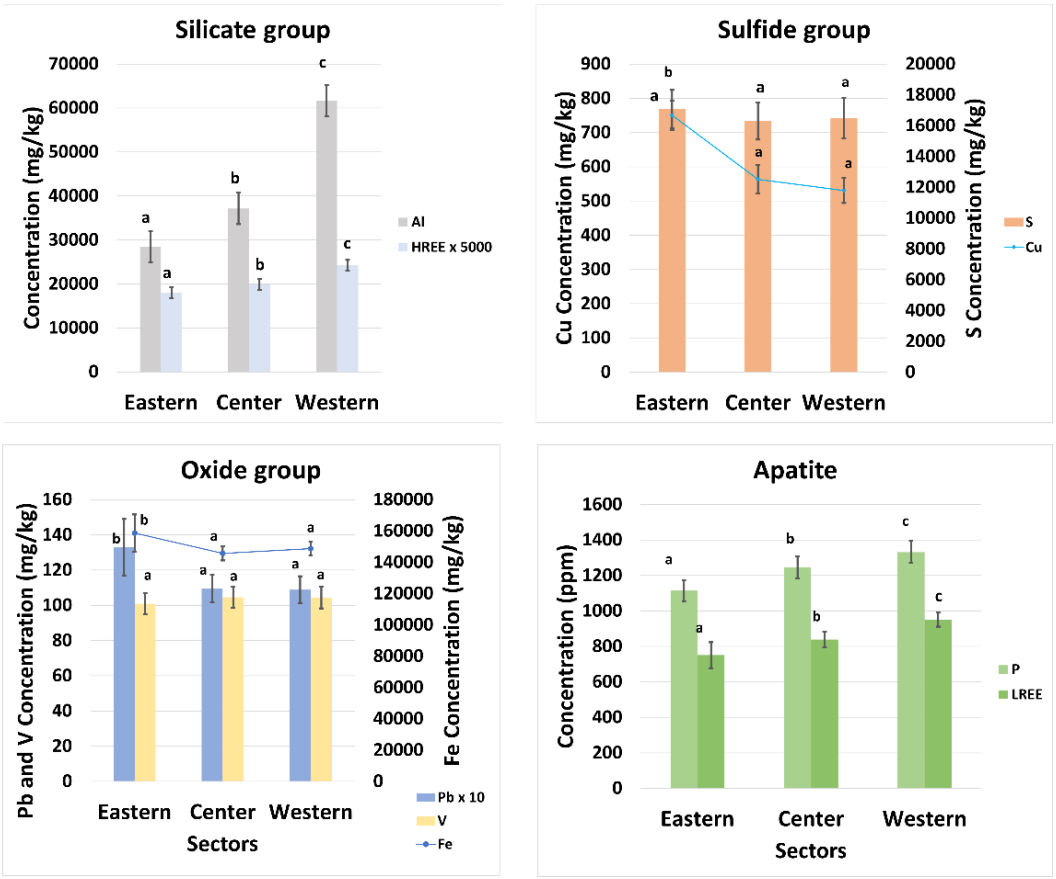

Fig. S 14 One-way ANOVA analysis and Welch test comparing the main elements grouped by the PCA at different location inside the tailing impoundment: eastern sector located near the dam (N = 180), center sector (N = 202) and western sector located in the most distal areas of the dam (N = 191). Some elements were multiplied by integers to improve their visualization.

Table S 1 Detection limits reported by Actlabs for their analytical package ICP-MS for soil samples. The coefficient of variation was less than 10 %.

Elements	Detection limit	Elements	Detection limit	Elements	Detection limit
Fe	0.01 %	In	0.1 ppm	Ba	1 ppm
Ca	0.01 %	La	0.1 ppm	Cr	0.5 ppm
Mg	0.01 %	Lu	0.1 ppm	Mn	1 ppm
Na	0.01 %	Nb	0.1 ppm	Sn	1 ppm
K	0.01 %	Nd	0.1 ppm	V	1 ppm
P	0.001 %	Pr	0.1 ppm	Zr	1 ppm
Al	0.01 %	Sb	0.1 ppm	Bi	0.02 ppm
As	0.1 ppm	Se	0.1 ppm	Cs	0.05 ppm
Be	0.1 ppm	Sm	0.1 ppm	Ag	0.05 ppm
Cd	0.1 ppm	Ta	0.1 ppm	Mo	0.1 ppm
Ce	0.1 ppm	Tb	0.1 ppm	Tl	0.05 ppm
Co	0.1 ppm	Te	0.1 ppm	Eu	0.05 ppm
Dy	0.1 ppm	Th	0.1 ppm	Hg	10 ppb
Er	0.1 ppm	Ti	0.0005%	Li	0.5 ppm
Ga	0.1 ppm	Tm	0.1 ppm	Ni	0.5 ppm
Ge	0.1 ppm	U	0.1 ppm	Pb	0.5 ppm
Gd	0.1 ppm	W	0.1 ppm	Sr	0.1 ppm
Hf	0.1 ppm	Y	0.1 ppm	Cu	0.2 ppm
Ho	0.1 ppm	Yb	0.1 ppm	Rb	0.2 ppm
Zn	0.2 ppm	Re	0.001 ppm		

Table S 2 Physicochemical treatment and main dissolved minerals in the different stages of sequential extraction (Dold and Fontboté, 2001)

Steps	Physical and chemical treatment	Main minerals dissolved
1: Water soluble fraction	1.0 g sample into 50 ml deionized water and shake for 1 h	Secondary sulfates e.g., Gypsum
2: Exchangeable fraction	1M ammonium acetate pH 4.5 shake for 2 h	Calcite and adsorbed and exchangeable ions
3: Fe (III) oxyhydroxides	0.2 M ammonium oxalate pH 3 and shake for 1h in darkness	Schwertmannite, ferrihydrite, secondary jarosite, manganese oxides.
4: Fe (III) oxides	0.2 M ammonium oxalate pH 3 heat in water bath 80 °C for 2 h	Goethite, jarosite, hematite, magnetite
5: Organics and secondary Cu sulfides	35 % hydrogen peroxide heat in water bath for 1h	Organics, covellite, chalcocite and digenite
6: Primary sulfides	Combination of potassium chlorate and hydrochloric acid, followed by 4 M nitric acid boiling	Pyrite, chalcopyrite, sphalerite, molybdenite, galena
7: Residual fraction	Digestion with nitric, perchloric, hydrofluoric and hydrochloric acid	Silicates and residual

Table S 3 Detection limits reported by AGQ Labs for their analytical package sequential extraction for soil samples

Elements	Detection limit	Elements	Detection limit
Al	0 %	Ag	0.22 ppm
Sb	2.2 ppm	Pb	0.56 ppm
As	0.08 ppm	Se	3.3 ppm
S	0.03 %	Na	0.01 %
Ba	0.74 ppm	Tl	8.2 ppm
Be	0.26 ppm	Ti	0.03 ppm
Cd	1.1 ppm	V	0.76 ppm
Ca	0.01 %	Zn	0.81 ppm
Co	1.9 ppm	Fe	0.01 %
Cu	8 ppm	Li	0.07 ppm
Cr	0.37 ppm	Mg	0.03 %
Sn	11 ppm	Mn	0.02 ppm
Sr	0.41 ppm	Mo	0.66 ppm
P	2.8 ppm	Ni	0.74 ppm

.

Table S 4. Detection limits reported by Actlabs for their analytical package ICP-MS for soil samples. The coefficient of variation was less than 10%. All detection limit in ppb.

Elements	Detection limit	Elements	Detection limit	Elements	Detection limit
Al	1000	Er	0.1	Sb	1
Ca	5000	Eu	0.1	Sc	20
Fe	100	Ga	0.5	Se	5
K	2000	Gd	0.1	Sm	0.5
Mn	50	Ge	0.1	Sn	1
Mg	1000	Hf	0.1	Sr	10
Na	3000	Hg	1	Ta	0.5
P	100	Ho	0.05	Tb	0.05
Ti	50	In	0.05	Te	1
Au	1	La	2	Th	2
Ag	0.5	Li	0.1	Tl	0.2
As	5	Lu	0.05	Tm	0.05
Ba	10	Mo	1	U	0.1
Be	1	Nb	0.5	V	50
Bi	0.5	Nd	1	W	2
Cd	0.5	Ni	5	Y	1
Ce	1	Pb	3	Yb	0.5
Co	1	Pr	0.5	Zn	10
Cs	0.5	Rb	2	Zr	1
Cu	5	Re	0.05		
Dy	0.1	S	10000		

Table S 5 Trace minerals characterized by QEMSCAN (% relative abundance) in samples at different depths (N = 12).

	Mean	DS	Mean	DS	Mean	DS	Mean	DS	Mean	DS	Mean	DS
Depths (m)	0-1		2-3		3-4		6-10		12-14		18-22	
Amphibole	0.28	0.25	0.51	0.25	0.28	0.19	0.29	0.21	0.45	0.23	0.56	0.36
Apatite	0.44	0.10	0.65	0.11	0.73	0.28	0.30	0.16	0.56	0.25	0.87	0.20
Biotite	2	1.1	2	1.10	2	1.10	2	1.10	2	1.14	2	1.30
Chalcopyrite	0.14	0.06	0.56	0.29	0.28	0.14	0.08	0.02	0.10	0.03	0.15	0.09
Dolomite-Ankerite	0.05	0.03	0.16	0.08	0.14	0.06	0.39	0.75	0.11	0.26	0.11	0.05
Epidote	0.10	0.07	0.07	0.04	0.04	0.02	0.04	0.03	0.08	0.05	0.07	0.03
Garnet	0.04	0.02	0.09	0.06	0.08	0.03	0.04	0.01	0.04	0.02	0.07	0.02
Ilmenite	0.12	0.04	0.06	0.04	0.06	0.02	0.91	1.96	0.09	0.76	0.05	0.02
Muscovite	2	0.88	2	0.90	2	0.86	2	0.87	2	0.91	2	0.95
Pyroxenes	0.19	0.11	0.17	0.05	0.11	0.06	0.38	0.62	0.12	0.21	0.13	0.06
Rutile	0.49	0.07	0.52	0.14	0.55	0.14	0.40	0.20	0.50	0.19	0.55	0.07
Sphene	0.04	0.02	0.06	0.04	0.04	0.03	0.02	0.01	0.02	0.02	0.07	0.03
Tourmaline	0.96	0.40	2	1	1	0.71	4	6	1	2	1	1

Table S 6 Univariate elements of the tailings with Min., Max., Mean, Median, standard deviation (SD) and percentiles (25, 50, 75 and 95). Major elements in percent and minor and trace elements in mg/kg, except for Hg in µg/kg. The concentrations correspond to the total digestion analysis (N = 755 samples) except for Si that was obtain using portable XRF (N = 269 samples).

	Min.	Max.	Mean	Median	SD	Percentiles			
Major						25.0	50.0	75.0	95.0
Fe	9	26	16	15	2	14	15	17	20
Al	1	10	5	5	2	4	5	6	8
Ca	2	6	3	3	1	2	3	3	4
K	1	5	2	2	0	2	2	3	3
Mg	1	5	2	2	1	2	2	3	3
Si* (XRF)	0.2	3	2	2	0.4	1	2	2	2
S	0.2	3	2	2	0.4	1	2	2	2
Na	0.3	2	0.9	0.9	0.3	0.7	0.9	1.0	1.6
Ti	0.1	1	0.3	0.3	0.1	0.2	0.3	0.3	0.3
P	0.1	0.2	0.1	0.1	0.0	0.1	0.1	0.1	0.2
Minor									
Cu	227	4290	795	647	514	433	647	990	1790
LREE	67	800	315	306	110	234	306	373	520
Ba	30	1020	112	95	70	71	95	135	221
V	62	579	108	105	29	91	106	121	150
Co	25	303	103	100	32	83	100	120	158
Trace									
Ni	28	178	79	76	22	63	76	93	121
Zr	9	128	79	81	18	66	81	93	106
Rb	13	112	65	69	19	52	69	78	95
Zn	35	196	63	60	18	50	60	71	93
Sr	20	451	57	53	38	35	53	68	93
As	1	107	38	37	12	30	37	43	59
Li	14	79	30	26	10	22	26	33	52
Ga	14	41	24	25	5	19	25	28	32
HREE	10	44	22	22	5	18	22	25	30
Pb	2	38	12	11	6	8	11	16	24
W	0.1	101	7	6	6	4	6	8	12
Th	0.7	9	3	3	1	3	3	4	5
Sn	1	18	3	2	2	2	2	3	5
Sb	0.1	19	2	2	1	1	2	3	5
Nb	0.1	12	2	2	1	2	2	3	4

Continuation Table S6

Trace	Min.	Max.	Mean	Median	SD	Percentiles		Min.	Max.
						25.0	50.0	75.0	95.0
Hf	0.3	3	2	2	1	1	2	2	3
Cs	0.8	7	2	2	1	1	2	2	3
U	0.9	3	2	2	0	2	2	2	2
Ag	0.1	4	1	1	1	1	1	1	2
Mo	0.1	4	1	1	1	1	1	1	2
Ge	0.1	2	0.6	0.6	0.4	0.3	0.6	0.8	1
Bi	0.1	4	0.6	0.6	0.3	0.4	0.6	0.7	1
Tl	0.1	0.8	0.3	0.3	0.1	0.2	0.3	0.3	0.5
Ta	0.1	1	0.2	0.2	0.1	0.1	0.2	0.2	0.3
Te	0.1	0.6	0.2	0.2	0.1	0.2	0.2	0.3	0.4
In	0.1	0.3	0.1	0.1	0.0	0.1	0.1	0.1	0.2
Re	0.001	0.017	0.004	0.004	0.002	0.002	0.004	0.005	0.007
Hg*	10	1280	277	230	187	150	235	380	640
Cd	<DL	<DL	<DL	<DL	<DL	<DL	<DL	<DL	<DL
Ba	<DL	<DL	<DL	<DL	<DL	<DL	<DL	<DL	<DL
Cr	<DL	<DL	<DL	<DL	<DL	<DL	<DL	<DL	<DL
Nb	<DL	<DL	<DL	<DL	<DL	<DL	<DL	<DL	<DL
Sb	<DL	<DL	<DL	<DL	<DL	<DL	<DL	<DL	<DL
Se	<DL	<DL	<DL	<DL	<DL	<DL	<DL	<DL	<DL

<DL = below detection limit

Table S 7 Results of the sequential extraction corresponding to the average of boreholes Ad2, B-04 and B-13. The values are expressed in mmol/ kg. Elements below the detection limit are indicated as <DL. Step 1: water soluble fraction. Step 2: exchangeable fraction, Step 3: Fe (III) oxyhydroxides, Step 4: Fe (III) oxides, Step 5: Organics and secondary Cu-sulfides, Step 6: Primary sulfides and Step 7: residual fraction.

Steps	1	2	3	4	5	6	7
Depth (m)			Mean ±SD				
Manganese		Carbonates					
1	<DL	7 ± 1.5	1 ± 0.1	0.4 ± 0.0	1 ± 0.1	3 ± 0.1	7 ± 0.1
3	<DL	9 ± 2.7	2 ± 0.5	0.4 ± 0.1	1 ± 0.3	3 ± 0.1	7 ± 0.4
9	<DL	10 ± 0.1	2 ± 0.1	0.5 ± 0.1	2 ± 0.2	3 ± 0.7	7 ± 0.3
15	<DL	11 ± 0.1	2 ± 0.1	0.5 ± 0.1	2 ± 0.1	3 ± 0.5	6 ± 1.0
21	<DL	12 ± 1.2	3 ± 1.3	0.6 ± 0.2	2 ± 0.1	4 ± 0.4	7 ± 1.2
35	<DL	13 ± 1.5	2 ± 0.1	0.5 ± 0.1	2 ± 0.3	5 ± 0.6	7 ± 0.5
Arsenic						Primary sulfide	
1	<DL	<DL	0.2 ± 0.0	<DL	<DL	0.3 ± 0.0	<DL
3	<DL	<DL	<DL	<DL	<DL	0.3 ± 0.0	<DL
9	<DL	<DL	<DL	<DL	<DL	0.4 ± 0.1	<DL
15	<DL	<DL	0.2 ± 0.0	<DL	<DL	0.4 ± 0.0	<DL
21	<DL	<DL	0.2 ± 0.1	<DL	<DL	0.5 ± 0.2	<DL
35	<DL	<DL	0.2 ± 0.0	<DL	<DL	0.5 ± 0.0	<DL
Cobalt					Secondary sulfide	Primary sulfide	
1	<DL	0.2 ± 0.04	0.2 ± 0.1	<DL	1.1 ± 0.1	0.3 ± 0.1	0.1 ± .03
3	<DL	0.1 ± 0.02	0.1 ± 0.05	<DL	1.1 ± 0.04	0.5 ± 0.04	0.2 ± .04
9	<DL	0.1 ± 0.03	0.1 ± 0.01	<DL	1.3 ± 0.1	0.4 ± 0.2	0.2 ± 0.001
15	<DL	0.2 ± 0.01	0.2 ± 0.04	<DL	1.5 ± 0.1	0.2 ± 0.02	0.1 ± 0.01
21	<DL	0.2 ± 0.04	0.3 ± 0.2	<DL	1.3 ± 0.02	0.5 ± 0.1	0.1 ± 0.04
35	<DL	0.3 ± 0.14	0.2 ± 0.1	<DL	2.0 ± 0.3	0.7 ± 0.4	0.2 ± 0.04
Chromium							Silicates
1	<DL	<DL	<DL	<DL	<DL	0.5 ± 0.2	1.3 ± 0.2
3	<DL	<DL	<DL	<DL	<DL	0.5 ± 0.2	1.9 ± 0.4
9	<DL	<DL	<DL	<DL	<DL	0.2 ± 0.0	0.8 ± 0.2
15	<DL	<DL	<DL	<DL	<DL	0.3 ± 0.1	0.6 ± 0.1
21	<DL	<DL	<DL	<DL	<DL	0.3 ± 0.2	1.0 ± 0.3
35	<DL	<DL	<DL	<DL	<DL	0.2 ± 0.0	0.3 ± 0.1

Continuation Table S7

Steps	1	2	3	4	5	6	7	7

Depth (M)			Mean ±SD				
Nickel					Secondary sulfide	Primary sulfide	
1	<DL	<DL	0.12 ± 0.02	<DL	0.58 ± 0.01	0.41 ± 0.09	0.78 ± 0.23
3	<DL	<DL	0.11 ± 0.02	<DL	0.58 ± 0.08	0.49 ± 0.11	1.15 ± 0.12
9	<DL	<DL	0.11 ± 0.01	<DL	0.90 ± 0.07	0.40 ± 0.06	0.83 ± 0.12
15	<DL	<DL	<DL	<DL	0.85 ± 0.03	0.31 ± 0.10	0.53 ± 0.03
21	<DL	0.10 ± 0.02	0.21 ± 0.16	<DL	0.96 ± 0.01	0.53 ± 0.13	0.82 ± 0.27
35	<DL	0.12 ± 0.01	0.15 ± 0.02	<DL	1.14 ± 0.10	0.57 ± 0.11	0.65 ± 0.13
Vanadium							Silicates
1	<DL	<DL	<DL	<DL	<DL	0.3± 0.0	2 ± 0.5
3	<DL	<DL	<DL	<DL	<DL	0.3 ± 0.0	2 ± 0.1
9	<DL	<DL	<DL	<DL	<DL	0.3 ± 0.1	2 ± 0.1
15	<DL	<DL	<DL	<DL	<DL	0.4 ± 0.1	1 ± 0.3
21	<DL	<DL	<DL	<DL	<DL	0.4 ± 0.0	2 ± 0.2
35	<DL	<DL	<DL	<DL	<DL	0.5 ± 0.0	1 ± 0.1

Table S 8 Saturation index of gypsum in the water-soluble fraction, along the depth profile. This index was calculated by PHREEQC 3.6.2-15100.

Boreholes	Depth (m)	Gypsum
Ad-02	1	3.18
	3	3.28
	9	3.04
	15	3.07
	21	3.55
	35	3.36
B-04	1	3.32
	3	3.37
	9	3.01
	15	3.20
	21	3.15
	35	3.43
B-13	1	2.96
	3	3.20
	9	3.08
	15	3.00
	21	3.15
	35	3.20

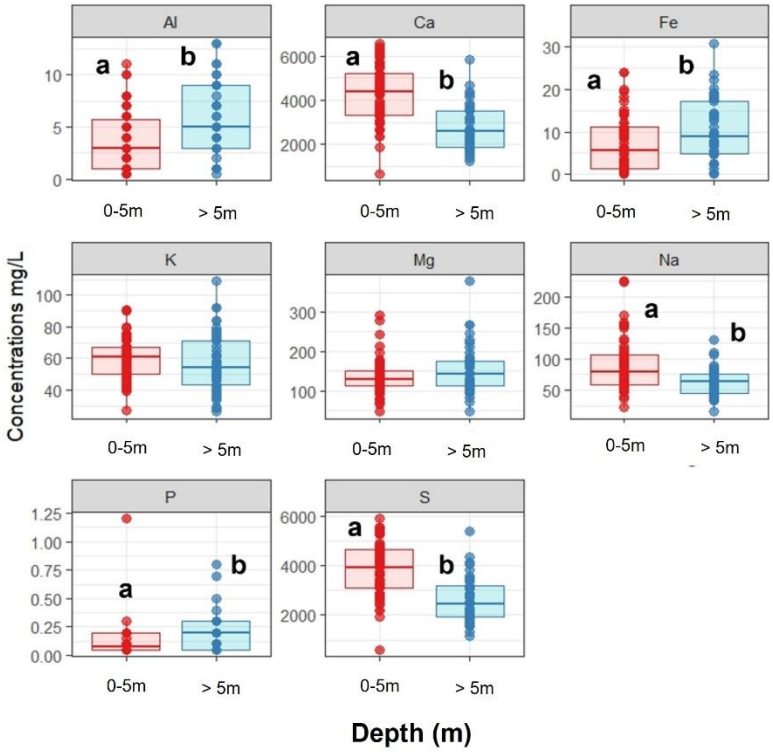

Fig. S 15. One-way Anova analysis comparing the major elements in the soluble fraction at different depth intervals from 0 to 5 m (N = 52) and >5 m (N = 41). Different letters indicate that there is a significant difference in the elemental concentrations at a certain depth. On the contrary, the same letters indicate that there are no significant differences.

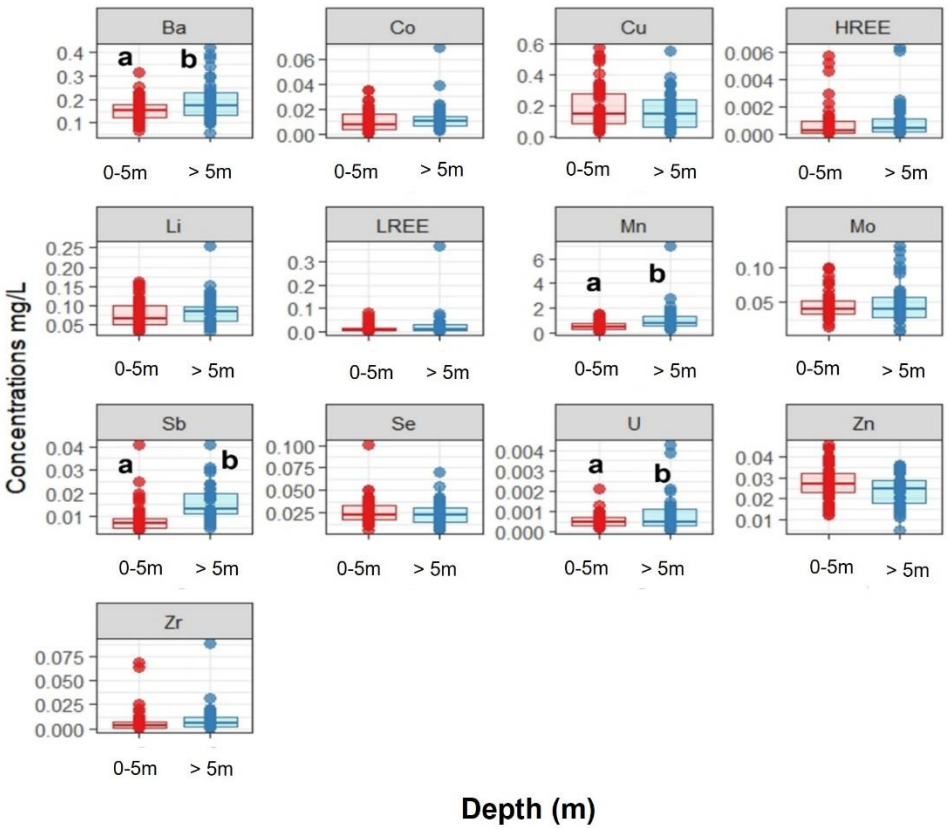

Fig. S 16. One-way Anova analysis comparing the minor elements in the soluble fraction at different depth intervals from 0 to 5 m (N = 52) and >5m (N = 41). Different letters indicate that there is a significant difference in the elemental concentrations at a certain depth. On the contrary, the same letters indicate that there are no significant differences.

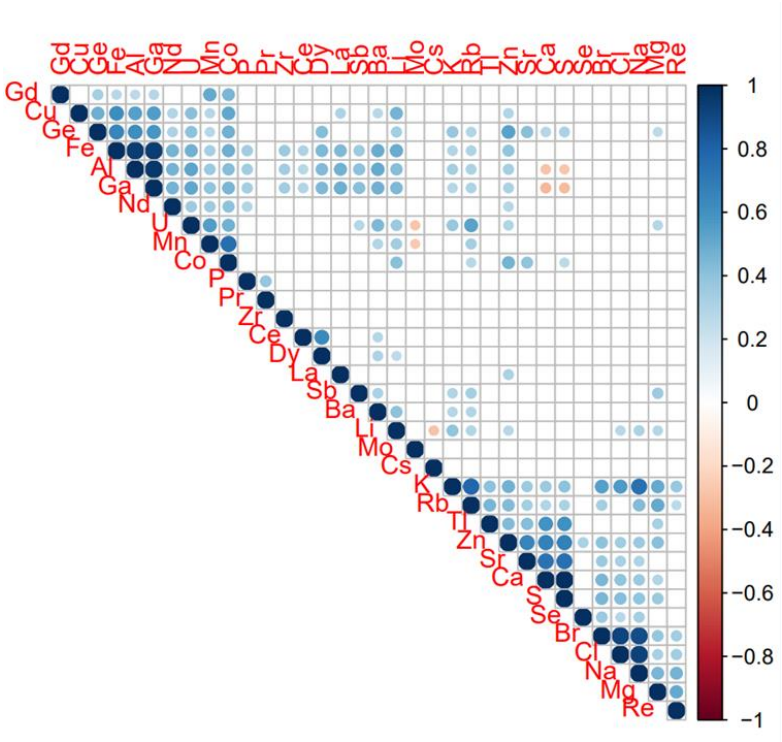

Fig. S 17 Pearson's correlation matrix for Gd, Cu, Ge, Fe, Al, Ga, Nd, U, Mn, Co, P, Pr, Zr, Ce, Dy, La, Sb, Ba, Li, Mo, Cs, K, Rb, Tl, Zn, Sr, Ca, S, Se, Na, Mg and Re in 98 samples. The p value at level 0.05.

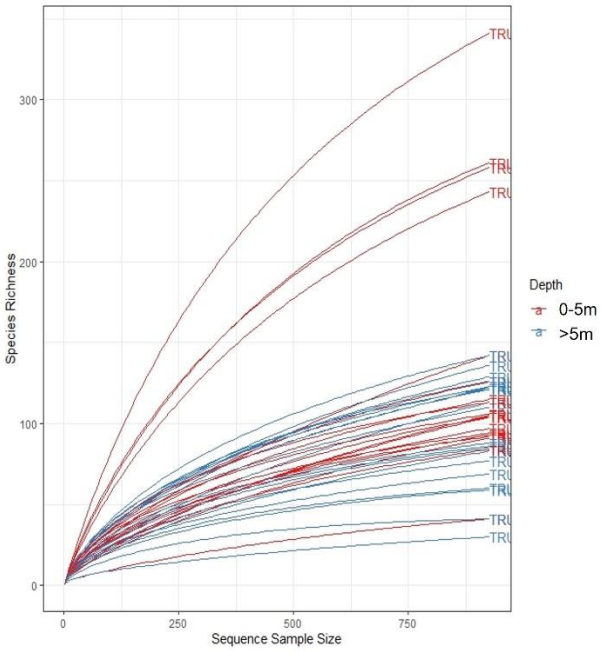

Fig. S 18 Rarefaction curves for sampling of tailings dam depicting the observed species. The x- axis represents the number of sequences sampled while the y-axis represents estimated species richness detected.

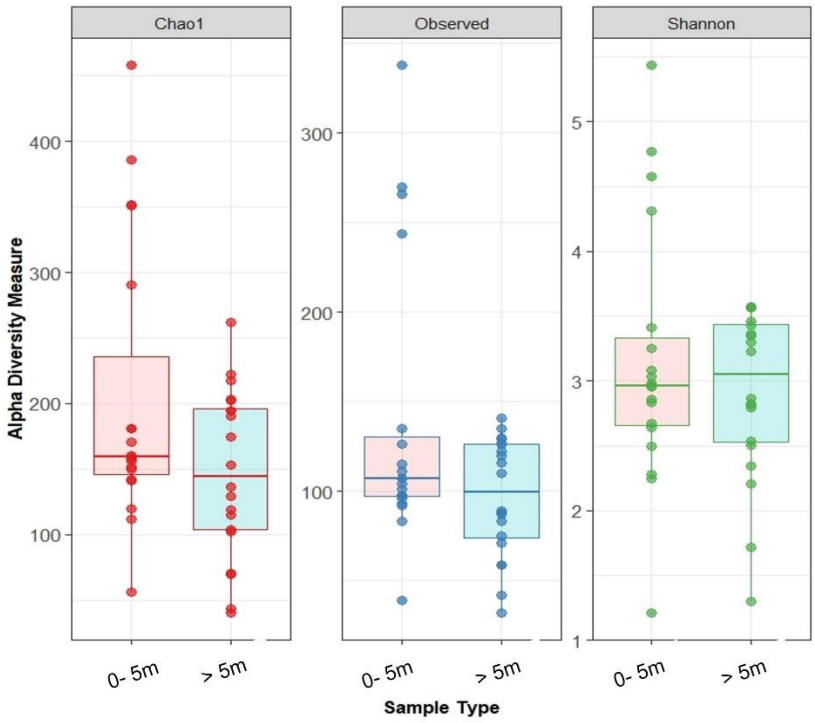

Fig. S 19 Alpha diversity measures (observed, Chao1 and Shannon diversity index) along the depth profile (0-5m (N=52) and > 5m (N=41)).

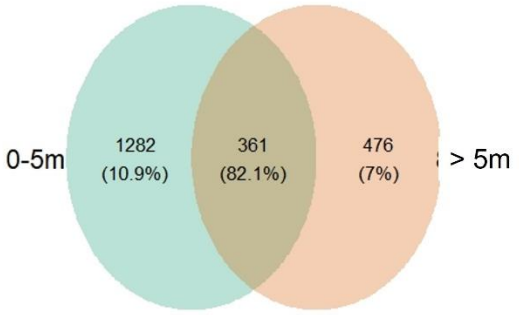

Fig. S 20 Venn diagram showing the distribution of bacterial OTUs between the range of depth studied in the tailing dam. The intersection represents the number of taxa shared between the ranges of depths evaluated. The blue and pink sections represent taxa unique to each depth range.

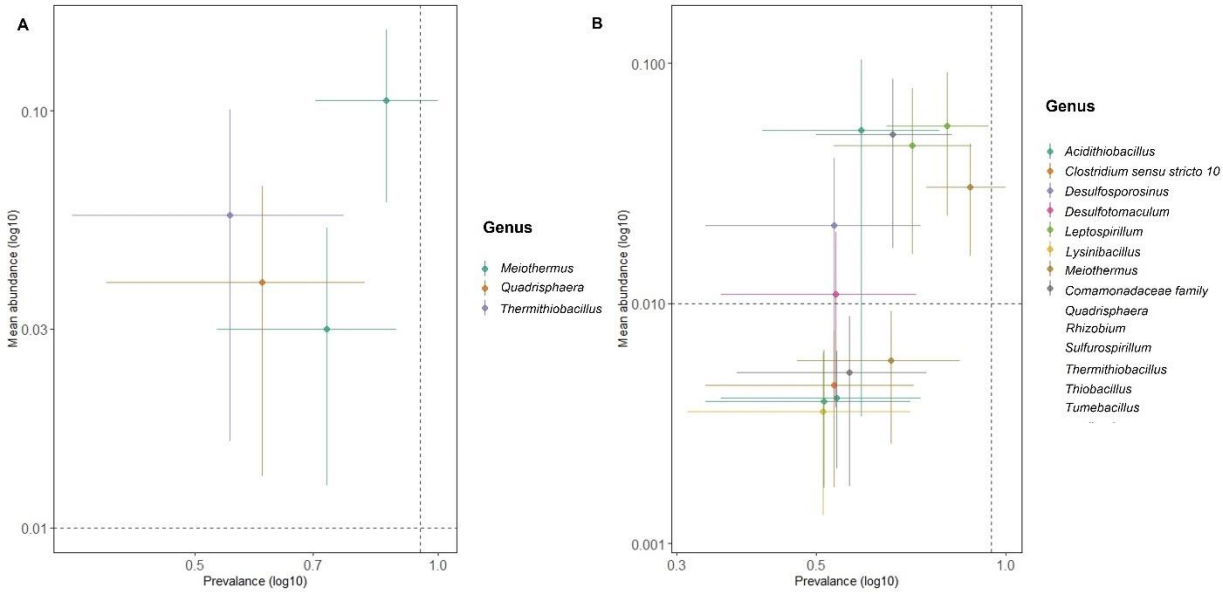

Fig. S 21 Prevalence and abundance at the genus level in the range depth from 0-5m (a) and >5m (b)

CHAPTER 6

6. GENERAL CONCLUSIONS AND FUTURE INSIGHTS

6.1 GENERAL CONCLUSIONS

Based on the findings of the present study, the general conclusions should include the following considerations:

The deposit of tailings presents a slight chemical stratification observed with the geochemical analysis of total rock and bioavailable fraction. It is characterized by layers with different geochemical and mineralogical characteristics (found at the bottom of this deposit of tailings), that are unaffected by the limited supergene weathering processes. These differences are most probably due to a different origin of the ore material processed in the mineral processing plant. Whether it comes from a different section of the ore deposit with slightly different mineralogical characteristics (hydrothermal alteration zones, veins, etc.) or from a different mine located in the vicinity of the deposit of tailings. Nevertheless, despite the presence of slight stratifications within the deposit of tailings, from a reprocessing perspective, the geochemistry and mineralogy of the tailings is quite homogeneous, and it exhibits similar grades for potentially valuable elements (i.e., Fe, Cu, and Co) along the depth and horizontal profiles. Simplifying its exploration and exploitation for future revalorization studies that could focus on the recovery of Fe by magnetic separation. Process that in turn could favor the concentration of Cu and Co in the purification stages of the magnetic concentrate. In contrast, the recovery of REE as a by-product is improbable due to their double association, with apatite and aluminosilicate minerals.

The chemical stratification of the bioavailable fraction generated variations in the structure of the microbial communities that inhabit the tailings dam. Nevertheless, biomass and species richness remain practically constant with depth. Similarly, the difference between the oxidized and no-oxidized zone clearly influences the diversity of species. The predicted functional profile of the bacterial communities was similar along the depth profile. This indicates that bacteria develop similar survival strategies within the deposit of tailings. However, the small variations could be associated with the enrichment of Fe, Al, Ba, Sb and Mn at the bottom of the deposit of tailings, increasing the percentage of relative abundance of bacterial chemotaxis and two component system pathways as defense mechanisms against these variations in the chemical composition. On the other hand, the biogeochemical cycle of the chemical elements within the deposit of tailings is controlled by the mutualistic activity of different microbial consortia: *Meiothermus* and an uncultured bacterium belonging to the phylum *Actinobacteria* dominate in the oxidized zone. While *Thiobacillus, Desulfosporosinus, Desulfotomaculum, Acidithiobacillus, Leptospirillum, Acidiphilum, Tumebacillus, Sulforospirillum, Paenibacillus, Lysinibacillus* and *Rhizobium* dominate in the reductive zone. Besides, based on the functionality, distribution and mutualistic activity among the microorganisms, capabilities can provide a direction for the management of the deposit of tailings and maximize their potential for revalorization.

6.2. FUTURE INSIGHTS

Based on the findings of the present study, the future research should include the following considerations:

The relative homogeneity of the grades within the deposit of tailings opens the possibility of restructuring the initial sampling mesh. Geostatistical studies are needed to evaluate the possibility of decreasing the number and density of boreholes while maintaining a robust and representative characterization of the deposit. This could drastically reduce the exploration cost of this marginally profitable secondary deposit.

Also, the present study has shown how limited the weathering and enrichment/depletion processes are in this type of neutral paste-pH deposit of tailings in an arid climate. However, this slow mineral weathering cannot be neglected and robust hydrogeochemical models are needed to better understand the formation and evolution of these deposit of tailings stored (or to be stored) for decades. This information is essential to anticipate their long-term chemical stability and/or their possible generation of bigger and deeper oxidation zones within older deposits.

In addition, based on the characterization of the microbial communities that inhabit the deposit of tailings, future studies should consider the following:

The characterization of the microbial communities within the deposit of tailings, their functionality, distribution, and mutualistic activity among the microorganisms are key to evaluating future in situ strategies for the revalorization and restoration of the deposit of tailings. However, it is suggested to make deeper predictions of the metabolic capabilities of microorganisms, determining the genes involved in their metabolic functions. Additionally, the revalorization and restoration strategies of these systems require an economic feasibility study.

On the other hand, future studies should consider the application of native bacteria from the deposit of tailings, for ex situ biotechnological applications of valuable elements associated with recalcitrant minerals, for instance iron recovery from magnetite by bio-flotation processes.

Finally, due to the high cost of metagenomic analysis, geostatistical studies could also be used to determine the density of samples to be analyzed to achieve a representative characterization of microbial communities. Furthermore, geostatistical modeling in microbiology is not widely used and could be a handy tool to visualize and better understand the distribution of microbial communities within deposit of tailings.

BIBLIOGRAPHY

Abraitis, P.K., Pattrick, R.A.D, Vaughan, D.J., 2004. Variations in the compositional, textural and electrical properties of natural pyrite: A review. International Journal of Mineral Processing 74(1–4):41–59. https://doi.org/10.1016/j.minpro.2003.09.002

Ahmadi, A., Khezri, M., Abdollahzadeh, A.A., Askari, M., 2015. Bioleaching of copper, nickel and cobalt from the low grade sulfidic tailings of Golgohar Iron Mine, Iran. Hydrometallurgy 154, 1e8. https://doi.org/10.1016/j.hydromet.2015.03.006.

Al, T.A., Blowes, D.W., 1996. Storm-water hydrograph sepa- ration of run off from a mine-tailings impoundment formed by thickened tailings discharge at Kidd Creek, Timmins, Ontario. *Journal of Hydrology*. 180, 55–78.

Albuquerque, L., Ferreira, C., Tomaz, D., Tiago, I., Veríssimo, A., da Costa, M. S., and Nobre, M. F., 2009. Meiothermus rufus sp. nov., a new slightly thermophilic red-pigmented species and emended description of the genus Meiothermus. *Systematic and Applied Microbiology*, *32*(5), 306–313. https://doi.org/10.1016/j.syapm.2009.05.002

Anawar, H. M., 2015. Sustainable rehabilitation of mining waste and acid mine drainage using geochemistry, mine type, mineralogy, texture, ore extraction and climate knowledge. *Journal of Environmental Management*, *158*, 111–121. https://doi.org/10.1016/j.jenvman.2015.04.045

Araya, N., Kraslawski, A., Cisternas, L.A., 2020. Towards mine tailings valorization: Recovery of critical materials from Chilean mine tailings. Journal of Cleaner Production 263:121555. https://doi.org/10.1016/j.jclepro.2020.121555

Araya, N., Ramírez, Y., Kraslawski, A., Cisternas, L., 2021. Feasibility of re-processing mine tailings to obtain critical raw materials using real options analysis. Journal of Environmental Management 284:112060. https://doi.org/10.1016/j.jenvman.2021.112060

Barton, M. D., 2014. Iron Oxide(-Cu-Au-REE-P-Ag-U-Co) Systems. In *Treatise on Geochemistry: Second Edition* (2nd ed., Vol. 13). Elsevier Ltd. https://doi.org/10.1016/B978-0-08-095975-7.01123-2

Bea, S. A., Ayora, C., Carrera, J., Saaltink, M. W., and Dold, B.,2010. Geochemical and environmental controls on the genesis of soluble efflorescent salts in Coastal Mine Deposit of tailingsDeposit of tailings: A discussion based on reactive transport modeling. *Journal of Contaminant Hydrology*, *111*(1–4), 65–82. https://doi.org/10.1016/j.jconhyd.2009.12.005

Beck D., Foster J.A., 2014. Machine learning techniques accurately classify microbial communities by bacterial vaginosis characteristics. PLoS ONE; 9(2):87830.

Benner, S. G., Gould, W. D., & Blowes, D. W., 2000. Microbial populations associated with the generation and treatment of acid mine drainage. *Chemical Geology*, *169*(3–4), 435–448. https://doi.org/10.1016/S0009-2541(00)00219-9

Blowes, D., Jambor, J., Hanton-Fong, C., Lortie, L., and Gould, W., 1998. Geochemical, mineralogical and microbiological characterization of a sulphide-bearing carbonate-rich gold-mine tailings impoundment, Joutel, Quebec. *Applied Geochemistry*, *13*(6), 687–705. https://doi.org/10.1016/S0883-2927(98)00009-2

Blowes, D.W., Ptacek, C.J., Jambor, J.L., Weisener, C.G., 2003. The Geochemistry of Acid Mine Drainage. Treatise on Geochemistry, 9:149–204. https://doi.org/10.1016/B0-08-043751-6/09137-4

Blowes, David W., Reardon, E. J., Jambor, J. L., and Cherry, J. A.,1991. The formation and potential importance of cemented layers in inactive sulfide mine tailings. *Geochimica et Cosmochimica Acta*, *55*(4), 965–978. https://doi.org/10.1016/0016-7037(91)90155-X

Bosecker, K., 1997. Bioleaching: Metal solubilization by microorganisms. *FEMS Microbiology Reviews*, *20*(3–4), 591–604. https://doi.org/10.1016/S0168-6445(97)00036-3

Bozo, L., Fernández, M., López, M., Reyes, R., Suárez, P., 2007. Biomarcadores de contaminación química en comunidades microbianas. Interciencia, 32(1), 8-13. http://ve.scielo.org/scielo.php?script=sci_arttext&pid=S0378-84420070001000004&lng=es&tlng=es.

Branco, R., Francisco, R., Chung, A. P. & Morais, P. V., 2009. Identification of an aox system that requires cytochrome c in the highly arsenic-resistant bacterium Ochrobactrum tritici SCII24T. Appl. Environ. Microbiol. 75, 5141–5147.

Buch, A.C., Niemeyer, J.C., Marques, E.D., Silva-Filho, E.V., 2021. Ecological risk assessment of trace metals in soils affected by mine tailings. Journal of Hazardous Materials 403:123852. https://doi.org/10.1016/j.jhazmat.2020.123852

Caporaso, J. G., Lauber, C. L., Walters, W. A., Berg-Lyons, D., Lozupone, C. A., Turnbaugh, P. J., Fierer, N., and Knight, R., 2011. Global patterns of 16S rRNA diversity at a depth of millions of sequences per sample. *Proceedings of the National Academy of Sciences of the United States of America*, *108*(SUPPL. 1), 4516–4522. https://doi.org/10.1073/pnas.1000080107

Caraballo, M.A., Serna, A., Macías, F., Pérez-López, R., Ruiz-Cánovas, C., Richter, P., Becerra-Herrera, M., 2018. Uncertainty in the measurement of toxic metals mobility in mining/mineral wastes by standardized BCR®SEP. Journal of Hazardous Materials 360:587–593. https://doi.org/10.1016/j.jhazmat.2018.08.046

Ceniceros-Gómez, A.E., Macías-Macías, K.Y., de la Cruz-Moreno, J.E., Gutiérrez-Ruiz, M.E., Martínez-Jardines, L.G., 2018. Characterization of mining tailings in México for the possible recovery of strategic elements. Journal of South American Earth Sciences 88:72–79. https://doi.org/10.1016/j.jsames.2018.08.013

Chen, L. xing, Li, J. tian, Chen, Y. ting, Huang, L. nan, Hua, Z. shuang, Hu, M., and Shu, W. sheng., 2013. Shifts in microbial community composition and function in the acidification of a lead/zinc mine tailings. *Environmental Microbiology*, *15*(9), 2431–2444. https://doi.org/10.1111/1462-2920.12114

Chen, Y., Li, J., Chen, L., Hua, Z., Huang, L., Liu, J., Xu, B., Liao, B. and Shu, W., 2014. Biogeochemical processes governing natural pyrite oxidation and release of acid metalliferous drainage. Environmental Science and Technology. 48: 5537-5545. http://dxdoi.org/10.1021/es500154z

Chen, L., Huang, L., Méndez-García, C., Kuang, J., Hua, Z., Liu, J. and Shu, W., 2016. Microbial communities, processes and functions in acid mine drainage ecosystems. Biotechnology 2016, 38:150–158. http://dx.doi.org/10.1016/j.copbio.2016.01.013

Chojnacka, K., 2010. Biosorption and bioaccumulation - the prospects for practical applications. *Environment International*, *36*(3), 299–307. https://doi.org/10.1016/j.envint.2009.12.001

Chung, A. P., Coimbra, C., Farias, P., Francisco, R., Branco, R., Simão, F. V., Gomes, E., Pereira, A., Vila, M. C., Fiúza, A., Mortensen, M. S., Sørensen, S. J., and Morais, P. V., 2019. Tailings microbial community profile and prediction of its functionality in basins of tungsten mine. *Scientific Reports*, *9*(1), 1–13. https://doi.org/10.1038/s41598-019-55706-6

Cleaver, A.E, Jamieson, H.E., Rickwood, C.J., Huntsman, P., 2021. Tailings dust characterization and impacts on surface water chemistry at an abandoned Zn-Pb-Cu-Au-Ag deposit. Journal Applied Geochemistry 128:104927. https://doi.org/10.1016/j.apgeochem.2021.104927

Compañía Contractual Minera Candelaria, 2013. Expediente de Evaluación de Impacto Ambiental proyecto Candelaria 2030-Continuidad Operacional. Región de Atacama, Chile. https://seia.sea.gob.cl/documentos/documento.php?idDocumento=2128574336

Compañía Minera del Pacífico, 2020. Memoria anual 2020. 31(3):177. https://doi.org/10.5944/reop.vol.31.num.3.2020.29271

Courchesne, B., Schindler, M., & Mykytczuk, N. C. S., 2021. Relationships Between the Microbial Composition and the Geochemistry and Mineralogy of the Cobalt-Bearing Legacy Mine Tailings in Northeastern Ontario. *Frontiers in Microbiology*, *12*(September), 1–19. https://doi.org/10.3389/fmicb.2021.660190

Cwalina, B., Pacholewska, M., Sozańska, M., and Cabala, J., 2009. Microenvironments determining growth of acidophilic bacteria in Zn-Pb flotation tailings of neutral reaction. *Environment Protection Engineering*, *35*(2), 113–121.

Daily metal prices, 2022. https://www.dailymetalprice.com/metalprices.php?c=fe&u=kg&d=1. Accessed 02-24-2022.

Deditius, A.P., Utsunomiya, S., Reich, M., Kesler, S.E., Ewing, R.C., Hough, R., Walshe, J., 2011. Trace metal nanoparticles in pyrite. Ore Geology Reviews 42(1):32–46. https://doi.org/10.1016/j.oregeorev.2011.03.003

Deutsch, C., Journel, A., 1997. GSLIB: Geostatistical Software Library and User's Guide. Oxford University Press, New York, pp. 369 (ISBN-13: 978-0195100150).

Diaby, N., Dold, B., Pfeifer, H. R., Holliger, C., Johnson, D. B., and Hallberg, K. B., 2007. Microbial communities in a porphyry copper tailings impoundment and their impact on the geochemical dynamics of the mine waste. *Environmental Microbiology*, *9*(2), 298–307. https://doi.org/10.1111/j.1462-2920.2006.01138.x

Dino, G.A., Mehta, N., Rossetti, P., Ajmone-Marsan, F., De Luca D.A., 2018. Sustainable approach towards extractive waste management: Two case studies from Italy. Resources Policy 59:33–43. https://doi.org/10.1016/j.resourpol.2018.07.009

Dold, B., Fontboté, L., 2001. Element cycling and secondary mineralogy in porphyry copper tailings as a function of climate, primary mineralogy, and mineral processing. Journal of Geochemical Exploration 74(1–3): 3–55. https://doi.org/10.1016/S0375-6742(01)00174-1

Dold, B., Fontboté, L., 2002. A mineralogical and geochemical study of element mobility in sulfide mine tailings of Fe oxide Cu - Au deposits from the Punta del Cobre belt, northern Chile. Chemical Geology 189(3–4):135–163. https://doi.org/10.1016/S0009-2541(02)00044-X

Dold, B., 2007. Biogeochemical processes in mine tailings with special focus on marine shore deposit of tailingsdeposit of tailings and their remediation. *Biohydrometallury: From the Single Cell to the Environment*, *20–21*(January 2007), 177–185. https://doi.org/10.4028/www.scientific.net/AMR.20-21.177

Dold, B., Blowes, D. W., Dickhout, R., Spangenberg, J. E., and Pfeifer, H. R., 2005. Low molecular weight carboxylic acids in oxidizing porphyry copper tailings. *Environmental Science and Technology*, *39*(8), 2515–2521. https://doi.org/10.1021/es040082h

Dold, B. and Spangenberg, J. E., 2005. Sulfur speciation and stable isotope trends of water-soluble sulfates in mine tailings profiles. *Environmental Science and Technology*, *39*(15), 5650–5656. https://doi.org/10.1021/es040093a

Duan, J., Sun, J., Ji, M., Ma, Y., Cui, Z., Tian, Ru., Xu, P., Sun, W., and Yuan, X. 2020. Indicatory bacteria and chemical composition related to sulfur distribution in the river-lake systems. Microbiological Research 236: 126453. https://doi.org/10.1016/j.micres.2020.126453

Dwyer, R., Bruckard, W.J., Rea, S. Holmes, R.J., 2012. Bioflotation and bioflocculation review: microorganisms relevant for mineral beneficiation, Miner Process Extractive Metall. (Trans Inst Miner Metall C) 121 65–71.

Emenike, C. U., Jayanthi, B., Agamuthu, P., & Fauziah, S. H., 2018. Biotransformation and removal of heavy metals: A review of phytoremediation and microbial remediation assessment on contaminated soil. *Environmental Reviews*, *26*(2), 156–168. https://doi.org/10.1139/er-2017-0045

European Comission, 2017. Critical Raw Materials and the Circular Economy. Background report. In Report EUR 28832 EN. https://doi.org/10.2760/378123

Falagán, C., Grail, B.M., Johnson, D.B., 2017. New approaches for extracting and recovering metals from mine tailings. Minerals Engineering 106:71–78. https://doi.org/10.1016/j.mineng.2016.10.008

Fein, J. B., Daughney, C. J., Yee, N., & Davis, T. A., 1997. A chemical equilibrium model for metal adsorption onto bacterial surfaces. *Geochimica et Cosmochimica Acta*, *61*(16), 3319–3328. https://doi.org/10.1016/S0016-7037(97)00166-X

Flemming, H. C., and Wingender, J., 2010. The biofilm matrix. *Nature Reviews Microbiology*, *8*(9), 623–633. https://doi.org/10.1038/nrmicro2415

Frankel, R. B., 2003. Biologically Induced Mineralization by Bacteria. *Reviews in Mineralogy and Geochemistry*, *54*(1), 95–114. https://doi.org/10.2113/0540095

Franks, D. M., Stringer, M., Torres-Cruz, L. A., Baker, E., Valenta, R., Thygesen, K., Matthews, A., Howchin, J., & Barrie, S., 2021. Tailings facility disclosures reveal stability risks. *Scientific Reports*, *11*(1), 1–7. https://doi.org/10.1038/s41598-021-84897-0

Gao, D., Liu, L., Liang, H., & Wu, W. M., 2011. Aerobic granular sludge: Characterization, mechanism of granulation and application to wastewater treatment. *Critical Reviews in Biotechnology*, *31*(2), 137–152. https://doi.org/10.3109/07388551.2010.497961

Gao, X., Jiang, L., Mao, Y., Yao, B., & Jiang, P., 2021. Progress, Challenges, and Perspectives of Bioleaching for Recovering Heavy Metals from Mine Tailings. *Adsorption Science and Technology*, *2021*. https://doi.org/10.1155/2021/9941979

Gupta, A., Dutta, A., Panigrahi, M. K., & Sar, P., 2020. Geomicrobiology of Mine Tailings from Malanjkhand Copper Project, India. *Geomicrobiology Journal*, *38*(2), 97–114. https://doi.org/10.1080/01490451.2020.1817197

González-Díaz, E., García, S., Soto, F., Navarro, F., Townley, B. and Caraballo, M.A., 2022. Geochemical, mineralogical and geostatistical modelling of an IOCG tailings deposit (El Buitre, Chile): implications for environmental safety and economic potential. Journal of geochemical exploration in Review.

Gould W. D., BeÂchard G., and Lortie L., 1994. The nature and role of microorganisms in the tailings environment. In Environmental Geochemistry of Sulfide Mine-wastes, ed. J. L. Jambor and D. W. Blowes, pp. 185±199. Mineralogical Association of Canada, Short Course Handbook.

Hallberg, K. B., & Johnson, D. B., 2003. Novel acidophiles isolated from moderately acidic mine drainage waters. *Hydrometallurgy*, *71*(1–2), 139–148. https://doi.org/10.1016/S0304-386X(03)00150-6

Hällström, L. P. B., Alakangas, L., & Martinsson, O., 2018. Geochemical characterization of W, Cu and F skarn tailings at Yxsjöberg, Sweden. *Journal of Geochemical Exploration*, *194*(March), 266–279. https://doi.org/10.1016/j.gexplo.2018.09.001

Heikkinen, P.M., Räisänen, M.L., 2008. Mineralogical and geochemical alteration of Hitura sulphide mine tailings with emphasis on nickel mobility and retention. Journal of Geochemical Exploration 97(1):1–20. https://doi.org/10.1016/j.gexplo.2007.09.001

Henne, A., Craw, D., Gagen, E. J., & Southam, G., 2019. Bacterially-mediated supergene alteration and redistribution of copper in mineralised rocks at the Salobo IOCG deposit, Brazil. *Ore Geology Reviews*, *115*(November), 103210. https://doi.org/10.1016/j.oregeorev.2019.103210

Henne, A., Craw, D., Gagen, E. J., & Southam, G., 2020. Experimental simulations of bacterially-mediated magnetite oxidation and observations on ferricrete formation at the Salobo IOCG mine, Brazil. *Applied Geochemistry*, *118*(January), 104628. https://doi.org/10.1016/j.apgeochem.2020.104628

Hennebel, T., Boon, N., Maes, S., and Lenz, M., 2015. Biotechnologies for critical raw material recovery from primary and secondary sources: R&D priorities and future perspectives. *New Biotechnology*, *32*(1), 121–127. https://doi.org/10.1016/j.nbt.2013.08.004

Henderson, R.D., 2018. Minera Valle Central Operations Rancagua, Region VI, Chile. 43–101 Technical report. pp. 118. http://www.amerigoresources.com/_resources/ Technical_Report_March_2019.pdf (Accessed 2/20/2021).

Hites, R.A., 2019. Correcting for Censored Environmental Measurements. Environmental Science and Technology 53(19):11059–11060. https://doi.org/10.1021/acs.est.9b05042

Hesse, E., O'Brien, S., Tromas, N., Bayer, F., Luján, A.M., Veen, E.M., Hodgson, D.J., Buckling, A., 2018. Ecological selection of siderophore producing microbial taxa in response to heavy metal contamination. Ecol. Lett. 21 (1), 117−127.

Hong, M., Huang, X., Gan, X., Qiu, G., Wang, J., 2021.The use of pyrite to control redox potential to enhance chalcopyrite bioleaching in the presence of *Leptospirillum ferriphilum*. Minerals Engineering 172: 107145. https://doi.org/10.1016/j.mineng.2021.107145

Hou, D., He, J., Lü, C., Ren, L., Fan, Q., Wang, J., Xie, Z., 2013. Distribution characteristics and potential ecological risk assessment of heavy metals (Cu, Pb, Zn, Cd) in water and sediments from Lake Dalinouer, China. Ecotoxicology and Environmental Safety 93: 135–144. http://dx.doi.org/10.1016/j.ecoenv.2013.03.012

Irani, S. and Varma, R., 2020. Bacteria in Heavy Metal Remediation and Nanoparticle Biosynthesis. ACS Sustainable Chem. Eng. 8, 14, 5395–5409. https://doi.org/10.1021/acssuschemeng.0c00292

Jandová, J., Lisá, K., Vu, H., & Vranka, F., 2005. Separation of copper and cobalt-nickel sulphide concentrates during processing of manganese deep ocean nodules. *Hydrometallurgy*, *77*(1–2), 75–79. https://doi.org/10.1016/j.hydromet.2004.10.011

Johnson, D. B., and Hallberg, K. B., 2003. The microbiology of acidic mine waters. *Research in Microbiology*, *154*(7), 466–473. https://doi.org/10.1016/S0923-2508(03)00114-1

Kang, X., Gan, Y., Chen, R., Zhang, C., 2021. Sustainable eco-friendly bricks from slate tailings through geopolymerization: synthesis and characterization analysis. Construction and Building Materials 278:122337. https://doi.org/10.1016/j.conbuildmat.2021.122337

Karimi, B., Dequiedt, S., Terrat, S., Jolivet, C., Arrouays, D., Wincker, P., Cruaud, C., Bispo, A., Chemidlin Prévost-Bouré, N., and Ranjard, L., 2019. Biogeography of Soil Bacterial Networks along a Gradient of Cropping Intensity. *Scientific Reports*, *9*(1), 1–10. https://doi.org/10.1038/s41598-019-40422-y

Kim, G., Park, K., Choi, J., Gomez-Flores, A., Han, Y., Choi, S. Q., & Kim, H., 2015. Bioflotation of malachite using different growth phases of Rhodococcus opacus: Effect of bacterial shape on detachment by shear flow. *International Journal of Mineral Processing*, *143*, 98–104. https://doi.org/10.1016/j.minpro.2015.09.012

Korehi, H., Blöthe, M., & Schippers, A., 2014. Microbial diversity at the moderate acidic stage in three different sulfidic mine tailings dumps generating acid mine drainage. *Research in Microbiology*, *165*(9), 713–718. https://doi.org/10.1016/j.resmic.2014.08.007

Kovács, E., Dubbin, W. E., and Tamás, J., 2006. Influence of hydrology on heavy metal speciation and mobility in a Pb-Zn mine tailing. *Environmental Pollution*, *141*(2), 310–320. https://doi.org/10.1016/j.envpol.2005.08.043

Kokkola, M., 1986. Jätealueen soijatutkimus. Outokumpu Oy Report 061/2124/02b/ MK/1986. pp. 83. http://tupa.gtk.fi/raportti/arkisto/061_2124_02b_mk_86.pdf

Krishna, R.S., Shaikh, F., Mishra, J., Lazorenko, G., Kasprzhitskii, A., 2021. Mine tailings-based geopolymers: Properties, applications and industrial prospects. Ceramics International 47(13): 17826-17843. https://doi.org/10.1016/j.ceramint.2021.03.180

Kuenen J. G., Robertson L. A. and Tuovinen O. H., 1992. The genus Thiobacillus, Thiomicrospira, and Thiosphaera. In The Prokaryotes, ed. A. Balows, H. G. Truper, M. Dworkin, W. Harder and K. H. Schleifer, 2nd ed., Vol. 3, pp. 2638±2657.

Kumar, V., Menon, S., Agarwal, H., Gopalakrishnan, D., 2017. Characterization and optimization of bacterium isolated from soil samples for the production of siderophores. Resour. Efficient Technol. 3 (4), 434–439.

Lindsay, M. B. J., Blowes, D. W., Condon, P. D., and Ptacek, C. J., 2009a. Managing pore-water quality in mine tailings by inducing microbial sulfate reduction. *Environmental Science and Technology*, *43*(18), 7086–7091. https://doi.org/10.1021/es901524z

Lindsay, M. B. J., Condon, P. D., Jambor, J. L., Lear, K. G., Blowes, D. W., and Ptacek, C. J., 2009b. Mineralogical, geochemical, and microbial investigation of a sulfide-rich deposit of tailings characterized by neutral drainage. *Applied Geochemistry*, *24*(12), 2212–2221. https://doi.org/10.1016/j.apgeochem.2009.09.012

Lam, E.J., Montofré, I.L., Álvarez, F.A., Gaete, N.F., Poblete, D.A., Rojas, R.J., 2020. Methodology to prioritize chilean tailings selection, according to their potential risks. International

Journal of Environmental Research and Public Health 17(11):3948. https://doi.org/10.3390/ijerph17113948

Lam, E.J., Montofré, Í.L., Ramírez, Y., 2021. Mine tailings phytoremediation in arid and semiarid environments. In Phytorestoration of Abandoned Mining and Oil Drilling Sites 2021:115-116. https://doi.org/10.1016/b978-0-12-821200-4.00012-1

Le Hécho, I., Pecheyran, C., Charles, S., Monperrus, M., Pavageau, M.-P., Casiot, C., Potin-Gautier, M., Leblanc, M., & Donard, O. F. X., 2003. Biogeochemical cycle and speciation of As and Cr in an acid mine environment : The case of Carnoulès Creek, France. *Journal de Physique IV*. https://doi.org/10.1051/jp4:20030406

Liang, X., Wei, G., Xiong, J., Tan, F., He, H., Qu, C., Yin, H., Zhu, J., Zhu, R., Qin, Z., Zhang, J., 2017. Adsorption isotherm, mechanism, and geometry of Pb(II) on magnetites substituted with transition metals. Chemical Geology 470:132–140. https://doi.org/10.1016/j.chemgeo.2017.09.003

Li, X., Huang, L., Bond, P. L., Lu, Y., & Vink, S., 2014. Bacterial diversity in response to direct revegetation in the Pb-Zn-Cu tailings under subtropical and semi-arid conditions. *Ecological Engineering*, *68*, 233–240. https://doi.org/10.1016/j.ecoleng.2014.03.044

Li, X., Zhang, Q. and Yang, B., 2020. Co-precipitation with CaCO3 to remove heavy metals and significantly reduce the moisture content of filter residue. Chemosphere 239: 124660. https://doi.org/10.1016/j.chemosphere.2019.124660

Lindsay, M.B.J., Blowes, D.W., Condon, P.D., Ptacek, C.J., 2009a. Managing pore-water quality in mine tailings by inducing microbial sulfate reduction. Environmental Science and Technology 43(18):7086–7091. https://doi.org/10.1021/es901524z

Lindsay, M.B.J., Condon, P.D., Jambor, J.L., Lear, K.G., Blowes, D.W., Ptacek, C.J., 2009b. Mineralogical, geochemical, and microbial investigation of a sulfide-rich tailings deposit characterized by neutral drainage. Journal Applied Geochemistry 24(12):2212–2221. https://doi.org/10.1016/j.apgeochem.2009.09.012

Liu, Jian li, Yao, J., Wang, F., Min, N., Gu, J. hai, Li, Z. fu, Sunahara, G., Duran, R., Solevic-Knudsen, T., Hudson-Edwards, K. A., & Alakangas, L., 2019. Bacterial diversity in typical abandoned multi-contaminated nonferrous metal(loid) tailings during natural attenuation. In *Environmental Pollution* (Vol. 247). https://doi.org/10.1016/j.envpol.2018.12.045

Liu, Jinxian, Li, C., Jing, J., Zhao, P., Luo, Z., Cao, M., Ma, Z., Jia, T., & Chai, B., 2018. Ecological patterns and adaptability of bacterial communities in alkaline copper mine drainage. *Water Research*, *133*, 99–109. https://doi.org/10.1016/j.watres.2018.01.014

LME, 2022. London metal exchange: LME cobalt and copper [WWW Document]. URL. https://www.lme.com/en/Metals/Accessed 02/24/2022.

Lodha, B., Badhane, R., Srivastava, S., and Killedar, D., 2010. Biokinetics of thiobacillus thiooxidans form manganese bioleching. International Journal of Environment and Pollution. Volume 43, (1-3): 274-286. DOI: 10.1504/IJEP.2010.035930

Lottermoser, B.G., 2010. Mine Wastes (third edition): Characterization, treatment and environmental impacts, Mine Wastes (Third Edition): Characterization. Treatment and Environmental Impacts. https://doi.org/10.1007/978-3-642-12419-8.

Majzlan, J., Lalinská, B., Chovan, M., Bläß, U., Brecht, B., Göttlicher, J., Steininger, R., Hug, K., Ziegler, S., & Gescher, J., 2011. A mineralogical, geochemical, and microbiogical assessment of the antimony- and arsenic-rich neutral mine drainage tailings near Pezinok, Slovakia. *American Mineralogist*, *96*(1), 1–13. https://doi.org/10.2138/am.2011.3556

Management, T., 2016. *LPSDP-TailingsHandbook. September*. https://www.industry.gov.au/sites/default/files/2019-04/lpsdp-tailings-management-handbook-english.pdf

Marescotti, P., Azzali, E., Servida, D., Carbone, C., Grieco, G., de Capitani, L., Lucchetti, G., 2010. Mineralogical and geochemical spatial analyses of a waste-rock dump at the Libiola Fe-Cu sulphide mine (Eastern Liguria, Italy). Environmental Earth Sciences 61(1):187–199. https://doi.org/10.1007/s12665-009-0335-7

Marschik, R., Fontboté, L., 2001. The Punta del Cobre formation, Punta del Cobre-Candelaria area, Northern Chile. Journal of South American Earth Sciences 14(4):401–433. https://doi.org/10.1016/S0895-9811(01)00036-0

McLean, J. and Beveridge, T., 2002. Interactions of Bacteria and Environmental Metals, Fine-grained Mineral Development, and Bioremediation Strategies. Huang, P., Bollag, J. and Senesi, N. Interactions between Soil Particles and Microorganisms. Impact on the Terrestrial Ecosystem. IUPAC Series on Analytical and Physical Chemistry of Environmental Systems, Vol. 8, 227-262.

Medina Tripodi, E. E., Gamboa Rueda, J. A., Aguirre Céspedes, C., Delgado Vega, J., and Collao Gómez, C., 2019. Characterization and geostatistical modelling of contaminants and added value metals from an abandoned Cu–Au tailing dam in Taltal (Chile). *Journal of South American Earth Sciences*, *93*(April), 183–202. https://doi.org/10.1016/j.jsames.2019.05.001

Mineralprices.com, 2022. Rare earth metals [WWW Document]. URL. http:// mineralprices.com/rare-earth-metals/. Accessed 02-24-2022.

Ministerio de obras públicas de Chile, 2020. Dirección General de Aguas, Chile. https://snia.mop.gob.cl/BNAConsultas/reportes

Ministerio Secretaría General de la Presidencia de Chile, 2002. Decreto 46. Norma de emisión de residuos líquidos a aguas subterráneas. http://bcn.cl/2eq80

Moncur, M.C., Ptacek, C.J., Blowes, D.W., Jambor, J.L., 2005. Release, transport and attenuation of metals from an old tailings impoundment. Journal Applied Geochemistry 20(3):639–659. https://doi.org/10.1016/j.apgeochem.2004.09.019

Moran-Palacios, H., Ortega-Fernandez, F., Lopez-Castaño, R., Alvarez-Cabal, J.V., 2019. The Potential of Iron Ore Tailings as Secondary Deposits of Rare Earths. Applied Sciences 9(14): 2913. https://doi.org/10.3390/app9142913

Mudd, G.M., Jowitt, S.M., 2018. Global Resource Assessments of Primary Metals: An Optimistic Reality Check. *Nat Resour Res* **27,** 229–240. https://doi.org/10.1007/s11053-017-9349-0

Mudd, G.M., Weng, Z., Jowitt, S.M., Turnbull, I.D., Graedel, T.E., 2013. Quantifying the recoverable resources of by-product metals: the case of cobalt. Ore Geol. Rev. 55, 87–98.

Mulenshi, J., Khavari, P., Chehreh Chelgani, S., Rosenkranz, J., 2019. Characterization and beneficiation options for tungsten recovery from Yxsj¨oberg historical ore tailings. Processes 7, 895. https://doi.org/10.3390/pr7120895.

Mulenshi, J., Gilbricht, S., Chehreh Chelgani, S., Rosenkranz, J., 2021. Systematic characterization of historical tailings for possible remediation and recovery of critical metals and minerals – The Yxsj¨oberg case. Journal of Geochemical Exploration 226: 106777. https://doi.org/10.1016/j.gexplo.2021.106777

Narayanan, K. B., and Sakthivel, N., 2010. Biological synthesis of metal nanoparticles by microbes. *Advances in Colloid and Interface Science*, *156*(1–2), 1–13. https://doi.org/10.1016/j.cis.2010.02.001

Narayanan, M., Devarajan, N., He, Z., Kandasamy, S., Ashokkumar, V., Raja, R., and Carvalho, I. S., 2020. Assessment of microbial diversity and enumeration of metal tolerant autochthonous bacteria from tailings of magnesite and bauxite mines. *Materials Today: Proceedings*, *33*, 4391–4401. https://doi.org/10.1016/j.matpr.2020.07.652

Oyarzun, R., Rodríguez, M., Pincheira, M., Doblas, M., Helle, S., 1999. The Candelaria (Cu-Fe-Au) and Punta del Cobre (Cu-Fe) deposits (Copiapo, Chile): A case for extension-related granitoid emplacement and mineralization processes? Mineralium Deposita 34(8):799–801. https://doi.org/10.1007/s001260050241

Onyedika, G.O., Achusim-Udenko, A.C., Nwoko, C.I.A., Ogwuegbu, M.O.C., 2012. Chemistry, processes and problems of complex ores utilization: hydrometallurgical options. Int. J. Chem. Sci. 10, 112e130.

Paktunc, D., Kingston, D., Pratt, A., McMullen, J., 2006. Distribution of gold in pyrite and in products of its transformation resulting from roasting of refractory gold ore. Canad Mineral 44(1): 213–227. https://doi.org/10.2113/gscanmin.44.1.213

Pan, H., Zhou, G., Cheng, Z., Yang, R., He, L., Zeng, D., & Sun, B., 2014. Advances in geochemical survey of mine tailings project in China. *Journal of Geochemical Exploration*, *139*, 193–200. https://doi.org/10.1016/j.gexplo.2013.07.012

Parbhakar-Fox, A., Glen, J., Raimondo, B., 2018. A Geometallurgical Approach to Tailings Management: An Example from the Savage River Fe-Ore Mine, Western Tasmania. Minerals 8, 454; doi:10.3390/min8100454

Parviainen, A., 2009. Tailings mineralogy and geochemistry at the abandoned Haveri Au–Cu mine, SW Finland. Mine Water Environ. 28 (4), 291–304.

Parviainen, A., Soto, F., Caraballo, M.A., 2020. Revalorization of Haveri Au-Cu mine tailings (SW Finland) for potential reprocessing. Journal of Geochemical Exploration 218:106614. https://doi.org/10.1016/j.gexplo.2020.106614

Pereira, L. B., Vicentini, R., & Ottoboni, L. M. M., 2014. Changes in the bacterial community of soil from a neutral mine drainage channel. *PLoS ONE*, *9*(5). https://doi.org/10.1371/journal.pone.0096605

Petrunic, B.M., Al, T.A., 2005. Mineral/water interactions in tailings from a tungsten mine, Mount Pleasant, New Brunswick. Geochimica et Cosmochimica Acta 69(10):2469–2483. https://doi.org/10.1016/j.gca.2004.10.031

Rastogi, S. O., Parag A. Vaishampayan Gary L. Andersen, and Larry D Steler, R. K. S., 2010. Thiobacillus.pdf. *Soil Microbiology*, *59*, 94–108. https://doi.org/10.1007/s00248-009-9598-5

Romero, F. M., Armienta, M. A., Gutiérrez, M. E., & Villaseñor, G., 2008. Factores geológicos y climáticos que determinan la peligrosidad y el impacto ambiental de jales mineros. *Revista Internacional de Contaminacion Ambiental*, *24*(2), 43–54.

Schippers, A., Breuker, A., Blazejak, A., Bosecker, K., Kock, D., Wright, T., 2010. The biogeochemistry and microbiology of sulfidic mine waste and bioleaching dumps and heaps, and novel Fe (II)-oxidizing bacteria. Hydrometallurgy 104: 342-350. http://10.1016/j.hydromet.2010.01.012

Schippers A, Hedrich S, Vasters J, Drobe M, Sand W, Willscher S., 2014. Biomining: metal recovery from ores with microorganisms. Adv Biochem Eng Biotechnol.;141:1-47. doi: 10.1007/10_2013_216. PMID: 23793914.

Schultze-Lam, S., Fortin, D., Davis, B. S., and Beveridge, T. J., 1996. Mineralization of bacterial surfaces. *Chemical Geology*, *132*(1-4 SPEC. ISS.), 171–181. https://doi.org/10.1016/s0009-2541(96)00053-8

Sernageomin, 2020a. Catastro de Depósitos de Relaves En Chile. Servicio Nacional de Geología y Minería de Chile. https://www.sernageomin.cl/datos-publicos-deposito-de-relaves/. Accessed 17 May 2021

Sernageomin, 2020b. Datos de Geoquímica de Depósitos de Relaves En Chile. Servicio Nacional de Geología y Minería de Chile. https://www.sernageomin.cl/datos-publicos-deposito-de-relaves/. Accessed 20 June 2021

Sillitoe, R. H., 2003. Iron oxide-copper-gold deposits: An Andean view. *Mineralium Deposita*, *38*(7), 787–812. https://doi.org/10.1007/s00126-003-0379-7

Sistema de información integral de Riego, 2020. Mapa de Evapotranspiración. Comisión nacional de riego, Chile. https://esiir.cnr.gob.cl/exp/ficha.php. Accessed 15 August 2021.

Smuda, J., Dold, B., Spangenberg, J. E., Friese, K., Kobek, M. R., Bustos, C. A., and Pfeifer, H. R., 2014. Element cycling during the transition from alkaline to acidic environment in an active porphyry copper tailings impoundment, Chuquicamata, Chile. *Journal of Geochemical Exploration*, *140*, 23–40. https://doi.org/10.1016/j.gexplo.2014.01.013

Soto, F., Garrido, M., Diaz, G., Silva, C., 2017. Rapid Multivariate Resource Assessment. Geomin-mineplanning. 5th International Seminar on Geology for the Mining Industry, Santiago

Su, W., 2009. Economic and Policy Analysis of China's Rare Earth Industry. China Financ. Econ. Publ House, Beijing.

Su, Z., Li, X., Xi, Y., Xie, T., Liu, Y., Liu, B., Liu, H., Xu, W., Zhang, C., 2022. Microbe-mediated transformation of metal sulfides: Mechanisms and environmental significance.Science of The Total Environment 825:153767. https://doi.org/10.1016/j.scitotenv.2022.153767

Sun, W., Xiao, E., Häggblom, M., Krumins, V., Dong, Y., Sun, X., Li, F., Wang, Q., Li, B., & Yan, B., 2018. Bacterial Survival Strategies in an Alkaline Tailing Site and the Physiological Mechanisms of Dominant Phylotypes As Revealed by Metagenomic Analyses. *Environmental Science and Technology*, *52*(22), 13370–13380. https://doi.org/10.1021/acs.est.8b03853

Tang, C., Li, K., Ni, W.and Fan, D., 2019. Recovering Iron from Iron Ore Tailings and Preparing Concrete Composite Admixtures. Minerals 2019, 9: 232. https://10.3390/min9040232

Teng, Q., Feng, Y., and Li, H., 2018. Effects of silicate-bacteria pretreatment on desiliconization of magnesite by reverse flotation. *Colloids and Surfaces A: Physicochemical and Engineering Aspects*, *544*(February), 60–67. https://doi.org/10.1016/j.colsurfa.2018.02.022

Teng, Q., Wen, Q., Yang, Z., and Liu, S., 2021. Evaluation of the biological flotation reagent obtained from Paenibacillus amylolyticus in magnetite and phlogopite flotation system. *Colloids and Surfaces A: Physicochemical and Engineering Aspects*, *610*(November 2020), 125930. https://doi.org/10.1016/j.colsurfa.2020.125930

Tiwari, S., Lata, C., Chauhan, P.S., Nautiyal, C.S., 2016. Pseudomonas putida attunes morphophysiological, biochemical and molecular responses in Cicer arietinum L. during drought stress and recovery. Plant Physiol. Biochem. 99, 108–117.

Torre, C., Zaja, R., Loncar, J., Smital, T., Focardi, S., & Corsi, I., 2012. Interaction of ABC transport proteins with toxic metals at the level of gene and transport activity in the PLHC-1 fish cell line. *Chemico-Biological Interactions*, *198*(1–3), 9–17. https://doi.org/10.1016/j.cbi.2012.04.008

Tremblay, G. A., and Hogan, C. M., 2000. *MEND Manual Volume 5–Treatment*. *5*, 187.

USGS, 2000. Open-File report OFR01-041. Coastal and Marine Geology Program website. https://pubs.usgs.gov/of/2001/of01-041/htmldocs/methods.htm. Accessed 16 June 2021

Wang, L., Li, Y., Wang, H., Cui, X., Wang, X., Lu, A., Wang, X., Wang, C., Gan, D., 2017. Weathering behavior and metal mobility of tailings under an extremely arid climate at Jinchuan Cu-Ni sulfide deposit, Western China. Journal of Geochemical Exploration 173:1–12. https://doi.org/10.1016/j.gexplo.2016.11.009

White, D. C., Flemming, C.A., Leung, K.T., Macnaughton, S.J., 1998. In situ microbial ecology for quantitative appraisal, monitoring, and risk assessment of pollution remediation in soils, the subsurface, the rhizosphere and in biofilms. Journal of Microbiological Methods 32: 2: 93-105.

Winch, S., Mills, H., Kostka, J., Fortin, D., and Lean, D., 2009. Identication of sulfate-reducing bacteria in methylmercury contaminated mine tailings by analysis of SSU rRNA genes. FEMS Microbiol Ecol 68 (2009) 94–107. https://10.1111/j.1574-6941.2009.00658.x

Xiao, E., Krumins, V., Dong, Y., Xiao, T., Ning, Z., Xiao, Q., and Sun, W., 2016. Microbial diversity and community structure in an antimony-rich tailings dump. *Applied Microbiology and Biotechnology*, *100*(17), 7751–7763. https://doi.org/10.1007/s00253-016-7598-1

Yang, M., Liang, X., Ma, L., Huang, J., He, H., Zhu, J., 2019. Adsorption of REEs on kaolinite and halloysite: A link to the REEs distribution on clays in the weathering crust of granite. Chemical Geology 525: 210–217. https://doi.org/10.1016/j.chemgeo.2019.07.024

Yang, Y., Li, Y., & Sun, Q. Y., 2014. Archaeal and bacterial communities in acid mine drainage from metal-rich abandoned tailing ponds, Tongling, China. *Transactions of Nonferrous Metals Society of China (English Edition)*, *24*(10), 3332–3342. https://doi.org/10.1016/S1003-6326(14)63474-9

Yuan, X. W., Xie, X. H., Fan, F. X., Zhu, W. X., Liu, N., & Liu, J. S., 2013. Effects of mutation on a new strain Leptospirillum ferriphilum YXW and bioleaching of gold ore. *Transactions of Nonferrous Metals Society of China (English Edition)*, *23*(9), 2751–2758. https://doi.org/10.1016/S1003-6326(13)62793-4

Zhang, X., Tang, S., Wang, M., Sun, W., Xie, Y., Peng, H., Zhong, A., Liu, H., Zhang, X., Yu, H., Giesy, J. P., & Hecker, M., 2019. Acid mine drainage affects the diversity and metal resistance gene profile of sediment bacterial community along a river. *Chemosphere*, *217*, 790–799. https://doi.org/10.1016/j.chemosphere.2018.10.210

Zhang, N., Tang, B., Liu, X., 2021. Cementitious activity of iron ore tailings and its utilization in cementitious materials, bricks and concrete. Construction and Building Materials 288:123022. https://doi.org/10.1016/j.conbuildmat.2021.123022

Zhao, J., Wu, W., Zhang, X., Zhu, M., & Tan, W., 2017. Characteristics of bio-desilication and bio-flotation of Paenibacillus mucilaginosus BM-4 on aluminosilicate minerals. *International Journal of Mineral Processing*, *168*, 40–47. https://doi.org/10.1016/j.minpro.2017.09.002

ANNEXES

ANNEXED A. PUBLICATION AND CONFERENCE ABSTRACTS RESULTING FROM THIS THESIS

Research papers

Erika González-Díaz, Sebastián García, Fabián Soto, Felipe Navarro, Brian Townley, Manuel A. Caraballo. 2022. Geochemical, mineralogical and geostatistical modelling of an IOCG deposit of tailings (El Buitre, Chile): implications for environmental safety and economic potential. Journal of Geochemical Exploration. Current status: Accepted.

Erika González-Díaz, Brian Townley, Manuel Caraballo, Julio Castillo. 2022. Genomic and geochemical characterization of alkaline tailing deposit (El Buitre, Chile): implications for tailings restoration and revalorization (In preparation).

Conference abstracts

Manuel A. Caraballo, Brina Townley, Byron Riquelme, Erika Y. González-Díaz**,** Sebastián García Cárdenas, Patricio Martínez, Rolando Moraga. 2019. Evaluation of the presence and spatial distribution of critical raw materials in Los Buitres and San José tailings deposit, Punta del Cobre district, Atacama, Chile. Oral presentation, Goldschmidt Congress, Barcelona, Spain.

Karen Kotthoff, Brian Townley, Manuel Caraballo, Erika González, Byron Riquelme, Sebastián García and Patricio Martínez. 2019. Mineralogy of contrasting tailing deposits in Chile and relation to source deposits: potential for recovery of valuables. Poster presentation, Goldschmidt Congress, Barcelona, Spain.

Manuel Caraballo, Brian Townley, Erika González, Byron Riquelme. Identificación, cuantificación y extracción (Bio) tecnológica de minerales/elementos de valor contenidos en depósitos de relaves. Estado del Arte. 2017. Oral presentation, Summit de Relaves Mineros: Los Yacimientos del Futuro, Santiago, Chile.

ANNEXED B. PUBLICATION AND CONFERENCES FROM CAUQUENES DEPOSIT OF TAILINGS

In this section, publications and conferences related to the Cauquenes tailings dam are presented, which was initially considered as an objective of the herein presented investigation. However, after its geochemical, microbiological, and mineralogical characterization, it was discarded due to its low concentrations in strategic critical elements other than Cu and Mo.

Research papers

Sebastian Garcia-Cardenas; Erika Gonzalez-Diaz; Lorena Camus; Roberto Collao; Manuel Caraballo Monge; Brian Townley; Annika Parviainen. 2021. Improving and diversifying mine tailings revalorization through detailed mineralogical and geochemical analysis at a current tailings recovery plant. (Submitted to journal).

Conference abstracts

Sebastián García Cardenas, Manuel A. Caraballo, Brian Townley, Byron Riquelme, Erika Y. González-Díaz, Roberto Collao, Juan Chinchón. 2019. Critical raw materials enrichment processes associated with tailings processing at the Cauquenes deposit of tailings plant. Poster presentation, Goldschmidt Congress, Barcelona, Spain.

Erika Y. González-Díaz, Sebastián García-Cardenas, Byron Riquelme, Manuel A. Caraballo, Brian Townley, Roberto Collao, Patricio Martínez, Felipe, Noriega. 2018. Evaluación de procesos hidrológicos que afectan la distribución espacial de elementos críticos estratégicos en el depósito de relaves de Cauquenes, Chile. Oral presentation, XV Congreso Geológico Chileno. Concepción, Chile.

Erika Y. González-Díaz, Sebastián García-Cardenas, Byron Riquelme, Manuel A. Caraballo, Brian Townley, Roberto Collao, Patricio Martínez, Felipe, Noriega. 2018. Evaluation of hydrological processes that affect the spatial distribution of strategic critical elements in the deposit of tailings of Cauquenes, Chile. Poster presentation, Procemin Geomet, Santiago, Chile.

Byron Riquelme, Erika Y. Gonzalez-Diaz, Sebastián Garcia-Cardenas, Manuel A. Caraballo, Brian Townley, Roberto Collao, Patricio Martínez, Felipe Noriega. 2018. Estrategias de caracterización y explotación de tranques de relave provenientes de minería de pórfidos cupríferos. Oral presentation, XV Congreso Geológico Chileno, Concepción, Chile.

Manuel A. Caraballo, Brian Townley, Erika Y. González-Díaz, Sebastián García-Cárdenas, Byron Riquelme, Roberto Collao, Patricio Martínez, Felipe Noriega. 2018. Geochemical and mineralogical characterization of Cauquenes porphyry copper tailings: moving from a mining residue to a new Cu and Mo ore deposit. Oral presentation, XIII Latin American Symposium on Environmental & Analytical Chemistry (LASEAC), La Serena, Chile.

Manuel A. Caraballo, Brian Townley, Erika Y. González-Díaz, Byron Riquelme, Sebastián García Cárdenas, Roberto Collao, Patricio Martínez, Felipe Noriega. 2018. Evaluation of the presence and spatial distribution of critical raw materials in the Cauquenes porphyry copper tailings. Oral presentation, 28h Goldschmidt Conference, Boston, USA